AN EXPERIMENTAL STUDY OF FRICTIONAL PHENOMENA AROUND THE PIN JOINTS OF PLATES USING MOIRE INTERFEROMETRY

by

Duksung Joh

Dissertation submitted to the faculty of the

Virginia Polytechnic Institute and State University

in partial fulfillment of the requirements for the degree of

DOCTOR OF PHILOSOPHY

in

Engineering Mechanics

APPROVED:

Daniel Post, Chairman

R. Czarnek

C. T. Herakovich

W. E. Kohler

J. N. R[illegible]y

D. P. Telionis

December, 1986

Blacksburg, Virginia

AN EXPERIMENTAL STUDY OF FRICTIONAL PHENOMENA AROUND THE PIN JOINTS OF PLATES USING MOIRÉ INTERFEROMETRY

by

Duksung Joh

(ABSTRACT)

Although contact problems with friction have received considerable attention in recent years, analytical as well as experimental limitations have tended to obscure some of their essential features. All the experimental techniques employed in the past lacked either required sensitivity or adequate spatial resolution for local measurements of deformation near the contact surface. Further, most techniques also did not allow the use of prototype material which is crucial for investigation of contact stress problems with friction. In the present study, a relatively new experimental method, which has been developed at VPI & SU, is employed: high-sensitivity moiré interferometry. Using a clearance pin-joint model made of prototype structural material, Aluminum 7071-T6, studies on frictional phenomena between the pin and plate are conducted to provide a comprehensive treatment of the following subjects: slip-stick phenomena, variation of contact zone, distribution of frictional force at the contact region, effects of frictional shear stress on stress concentration, and identification of slip amplitude. Experimental techniques and algorithms of analysis necessary for the research are further developed. The results showed

a strong influence of friction, including significant differences in the load-increasing and load-decreasing phases.

ACKNOWLEDGEMENTS

The author wishes to express his sincere appreciation to his committee chairman, Professor D. Post, for his support and encouragement during the course of the author's academic and research endeavors at Virginia Polytechnic Institute and State University. Professor Post has unselfishly shared with the author his intuition and originality of a genius. In addition, the author wishes to express:

- his thanks to Alan Kushner and Office of Naval Research under Grant N00014-84-K-0552.
- his sincere thanks to Dr. R. Czarnek for his overall support and enlightening discussions.
- his appreciation to his committee members for their participation.
- his thanks to Dr. L. C. Burton for his assistance.
- his thanks to Mr. R. Loyd for his help with data acquisition.
- his appreciation to Mrs. Peggy Epperly for typing the manuscript.
- his love and appreciation to his wife, whose encouragement and understanding provided the strength required for his effort.

TABLE OF CONTENTS

LIST OF FIGURES

CHAPTER I

INTRODUCTION

1.1 Motivation and Survey of Previous Research

Many contact problems with friction have received considerable attention in recent years [1-36]. They abound in engineering practice, e.g., in bearings, pinned or bolted joints, turbine blade root connections, etc. [1,8-11]. A systematic study of the physical interactions in frictional contact zones is increasingly being required for safety and longevity in sophisticated engineering design. However, the challenge being presented to investigators by the complex mechanism of friction is becoming more acute due to the lack of suitable techniques, both experimental and analytical [1,7,15].

Frictional shear stresses at the interface between two bodies in contact are known to cause wear and fatigue crack initiation [2,5,35, 36]. Above all, in a mechanical or structural element which is subject to small-amplitude oscillating slip a damaging effect arises on the fatigue life of the components [31]. This effect is related to the phenomenon known as fretting. Fretting is defined as a process caused by friction occurring at the contact surfaces under a normal load when the surfaces experience cyclic tangential relative motions of small amplitude.

Fretting fatigue occurring in multi-component structures and systems which are subjected to vibration or cyclic loading is so likely that the fatigue behavior of such assemblages can be said to be

entirely determined by the response of the contacting surfaces to fretting [12,29]. Some researchers have reported cases in which fretting has a devastating effect on the total fatigue life of the components, reducing by as much as 90 percent the crack initiation period; in many cases this represents most of the predicted fatigue life [1,9,13].

However, there have been fervent controversies about the mechanism of fretting fatigue failure over the last quarter of a century [2,5,16]. Among many theories postulated, the abrasive pit-digging hypothesis [9,10] and the friction-generated cyclic-stress fretting hypothesis [3,6,22,35] have been the two main branches in the disputes. Supporting evidence has been presented to show that under various circumstances each of the two mechanisms is active and significant in fretting damage, whereas by the notable advances recently achieved in fracture mechanics, it has become generally understood that the major factor in the initiation of fatigue cracks by fretting is the alternating shear stress occasioned by cyclic loading or oscillation [2,27,36].

The mechanism of frictional phenomena is so complicated that it cannot be described in a simple manner. The coefficient of friction may vary according to the surface roughness and molecular adhesion between the mating parts [7]. It may also be influenced by surface contamination, and even by the magnitude of normal load [26]. With all these complications it is not surprising that the laws of friction are empirical, and the effects of friction at the contact zone, including the consequences of non-constant friction coefficients and slip-stick effects, must be determined by physical measurements. Experimental

methods found in the literature, however, have not been adequate to determine the details of local deformations in slip-stick zones, since they could not satisfy indispensable requirements, such as high sensitivity and the use of prototype materials. Due to these experimental difficulties, the majority of the experimental investigations into the frictional phenomena have been focused on the observation of the fractured or damaged surface resulting from friction rather than on the observation of the frictional stress mechanism in the process prior to damage.

One of the typical examples of failure caused by fretting damage can be found in the pin joints of plates. Many researchers have approached the pin-joint problem analytically as well as experimentally [37-52]. In numerous investigations, however, either the friction at the interface has been ignored, or the coefficient of friction has been assumed to be constant. Most numerical analyses have neglected the elasticity of the pin by assuming that it is perfectly rigid, while others have assumed a cosinusoidal radial-stress distribution at the contact region between the pin and the plate.

Many experimentalists attempted to verify the validity of these assumptions or to extend the knowledge of the frictional influence on the strength of pinned joints of plates using various methods. Strain gages were used to obtain the stress concentration factors around pin-loaded holes, and developed to be widely applied as a powerful means to measure the strain even at the high-strain gradient regions. Photoelasticity has been the most popular technique in the experiments for the pin joint problems [38,41,43,44,46,50]. Oplinger et al. [39]

studied the strain and deformation field in pin-loaded composite plates using the moiré method. Wilkinson and Rowlands [47] investigated the frictional behavior of mechanical joints in wood using coarse moiré method and correlated the results to numerical prediction.

Each of these experimental methods employed so far has certain limitations, however. Electric strain gages have very high sensitivity but inadequate spatial resolution for measuring the localized deformations at the contact zone. They give only pointwise discontinuous information of the deformation field averaged over the gage area. Photoelasticity has a relatively low sensitivity. Further, because it requires models made of photoelastic materials, it does not allow studies on models of prototype structural materials. It must be noted that the true stress states at the frictional interface cannot be known without using the structural material, since material properties and conditions at the contact surface are crucial factors in contact stress problems. The grid method has been applied with rubber models under very large deformations [49]; it also precludes the use of prototype structural materials. Geometrical moiré has been considered suitable for measuring the displacement between the two surfaces of contact, because it can be used with prototype materials, and can give whole-field information about the deformation field. However, it requires large deformation as well, since the grating frequency is limited to about 40 ℓ/mm (1,000 ℓ/in.). This is equivalent to a sensitivity of 25 μm per fringe order. This sensitivity is of the same order as the maximum displacement to be measured in most contact problems. Geometrical moiré is thus too coarse for this particular

application. To summarize, none of the above methods combine the requirements of high sensitivity and the capability of testing real materials for successful experimental analyses of contact stress problems.

On the other hand, Sproles and Duquette succeeded in achieving high resolution and sensitivity in measuring slip in a fretting experiment [34]. A pair of diffraction gratings were attached to the fretting specimens, and the slip was measured at a point by a photoresistor. The sensitivity of measurements was 1.9 μm. However, their technique was lacking the spatial resolution which is needed for detecting the distribution of slip variation at the contact region.

Ruiz, Post, and Czarnek [56] applied a more advanced method to the investigation of the frictional phenomena occurring at the turbine blade root connection. They measured distributions of slip, opening and closure along the contacting boundary with such a high sensitivity as a fraction of μm. It was the first application of high-sensitivity moiré interferometry to the frictional problem. High-sensitivity moiré interferometry [54,55] is an optical technique that yields whole-field contour maps (or fringe patterns) of in-plane displacement components, U and V. The sensitivity of this method is 0.417 μm per fringe order (16.4 μin./fringe order), which is in the sub-wavelength range of light. High-sensitivity moiré interferometry offers unique potential for the study of many types of two-body problems [53].

Specimen alignment with the loading frame is another question raised by the characteristics of the friction problems of this kind. A slight misalignment of the specimen, which is admissible in most

other experiments, would produce significantly erroneous results caused by the torsional friction around the pin. So far this detrimental friction inherent in the experimental system of pin joints has been neglected by investigators due to the relatively low sensitivity of techniques employed. Development of a new technique with high sensitivity, however, necessitates designing of a special loading frame which is compatible with such a high sensitivity.

1.2 Objectives of the Present Research

Although contact problems with friction have received considerable attention in recent years, analytical as well as experimental difficulties have tended to stagnate the development of a powerful means to look into the phenomena due to the extreme complexity inherent in frictional problems. Some assumptions and approximations were used in all numerical or analytical techniques in order to simplify the complicated two-body problem so that it may be solved. Many alternative techniques for experimental investigations were presented to find the clue to the solution for frictional phenomena. Key factors were dissected from the problem assisted by the keen observations of many investigators. However, it is a unique characteristic of friction problems that a small variation in geometrical configuration or material combinations in friction pairs can cause amplified differences in the results due to nonlinearities of frictional properties of materials. In order to understand the mechanism of friction and its correlation to failures of mechanical or structural components, it is first imperative to justify or correct the assumptions and approximations

employed in the past analyses by a reasonably accurate experimental investigation.

The present study will discuss major difficulties and limitations with the study of frictional behavior of solids, and will be directed toward the development of new techniques for the analysis of two-dimensional contact problems. A relatively new technique, high-sensitivity moiré interferometry, will be applied to this two body contact problem. High-sensitivity moiré interferometry has been used as a rigorous tool of experimental analyses for stress or strain fields in structures made of advanced modern engineering materials. It is another major advantage of this method that any solid material can be used in the test. An application of this versatile technique to friction problems of pin joints will be presented, and some preliminary research work will be used as a basis for the analysis in this study.

Many experimental investigations found in the literature are based on the observations of contact surfaces on a micromechanics scale. A scanning electron microscope has been used to investigate the damaged interface after the surface failure. The results obtained by post-failure observations of micromechanics have provided an invaluable foundation for the understanding of frictional phenomena. On the other hand, many prudent studies have been conducted on a macromechanical scale on the same subject. Numerous numerical analyses have been conducted ever since the advent of highly sophisticated computers, while many experimentalists have applied various methods to their experiments either to broaden their understanding of contact stresses or to verify the assumptions employed in numerical analyses.

Despite this unprecedented progress made in two scales of mechanics there is still a grey area left to be enlightened by a more elaborate investigation. It may be between the micromechanics of material science and the assumption of continuum mechanics. The study on effects of friction in this intermediate area between the two poorly interrelated fields is urgently needed. The demand for more convincing evidence to explain the complicated roles of friction is acute due to the development of advanced modern engineering materials and increasing applications to structures. Of course, a breakthrough can be found empirically first. It may be achieved only by the development of suitable experimental techniques. As mentioned earlier, existing techniques could not satisfy the requirements of high sensitivity and spatial resolution, and of the use of test specimens made of real structural materials. Based on these preliminary observations, the needs for substantiating the behavior of friction motivated the following study.

The first objective involves the design of the loading apparatus. An application of high-sensitivity moiré interferometry for the two-body friction problem is another subject to study. The procedure and the characteristics of the experiment are to be described in detail.

The next objective is to find a method for data reduction. As observed in the fringe patterns obtained from the experiments of friction problems, highly localized frictional effects are characterized by changes of fringe curvatures near the contact boundary. Conventional methods of analysis for moiré patterns cannot be applied to the fringe patterns showing highly localized frictional effects. These methods

will be modified to cope with the problems in the analysis of the data involving contact stresses. The final objective is the interpretation of the reduced data. Relative displacements will be measured along the pin/plate boundary. Strains will be calculated from the measured displacement data, and then stresses will be calculated using the plane-stress constitutive equations. Shear and normal stresses thus determined along the periphery of the hole will be used to define the contact region developed with increments of load. Slip-amplitude distribution within the contact region will be another contribution made by the present study for the elucidation of the fretting mechanism. Slip-stick regions will also be determined. Finally effects of the frictional shear stress on the stress concentration will be compared between the loading and unloading phases.

These objectives will be discussed in detail in the following chapters. In Chapter II, the experimental techniques are described. A new idea for the design of a loading frame is presented. An application of moiré interferometry to two-body contact problems is detailed. Chapter III contains the development of a new method for data reduction. Use of the digitizing board to read the data from the fringe patterns and semi-automatic coordinate transformations into r - θ system are discussed. A modified algorithm of data analysis for moiré fringe patterns is introduced in this chapter. In Chapter IV, stress fields are discussed in cylindrical coordinates. Effects of friction on stress distributions are examined in conjunction with the load levels. The contact region at each load level is determined. Variations of stress concentration factor during the loading and unloading phases

are discussed in this chapter. Slip-stick phenomena are measured and discussed in Chapter V. Slip amplitudes are measured with the sensitivity of sub-micron level. The summations and conclusions are made in Chapter VI with recommendations for future works.

CHAPTER II

EXPERIMENT

2.1 Introduction

While high-sensitivity moire interferometry is very effective for displacement measurements in continuous bodies, special difficulties arise with two-body problems. The application of a specimen grating for one-body and two-body problems is illustrated in Figure 2. As shown in Figure 2.1a, a drop of uncured resin is pressed between the mirrorized grating mold and the specimen until it is cured. The phase grating with a highly reflective surface is replicated on to the specimen when the mold has been taken off. However, for the pin-joint specimens, where the main objective is to observe the frictional phenomena at the contacting interface, this replication process raises some troublesome questions. In this case the clearance between the pin and the plate is filled with the resin during the process of curing, as shown in Figure 2.1b. The resin entrapped in the clearance may change the frictional properties of the specimen material significantly at the interface.

An alternative to this method is to transfer the grating to the two bodies of the specimen separately. Since the contacting boundary can be kept from being contaminated by the resin material, this method allows the true study of the friction mechanism of real specimen materials. However, this immediately raises a question of alignment of the two separate gratings on the pin and the plate. The two bodies

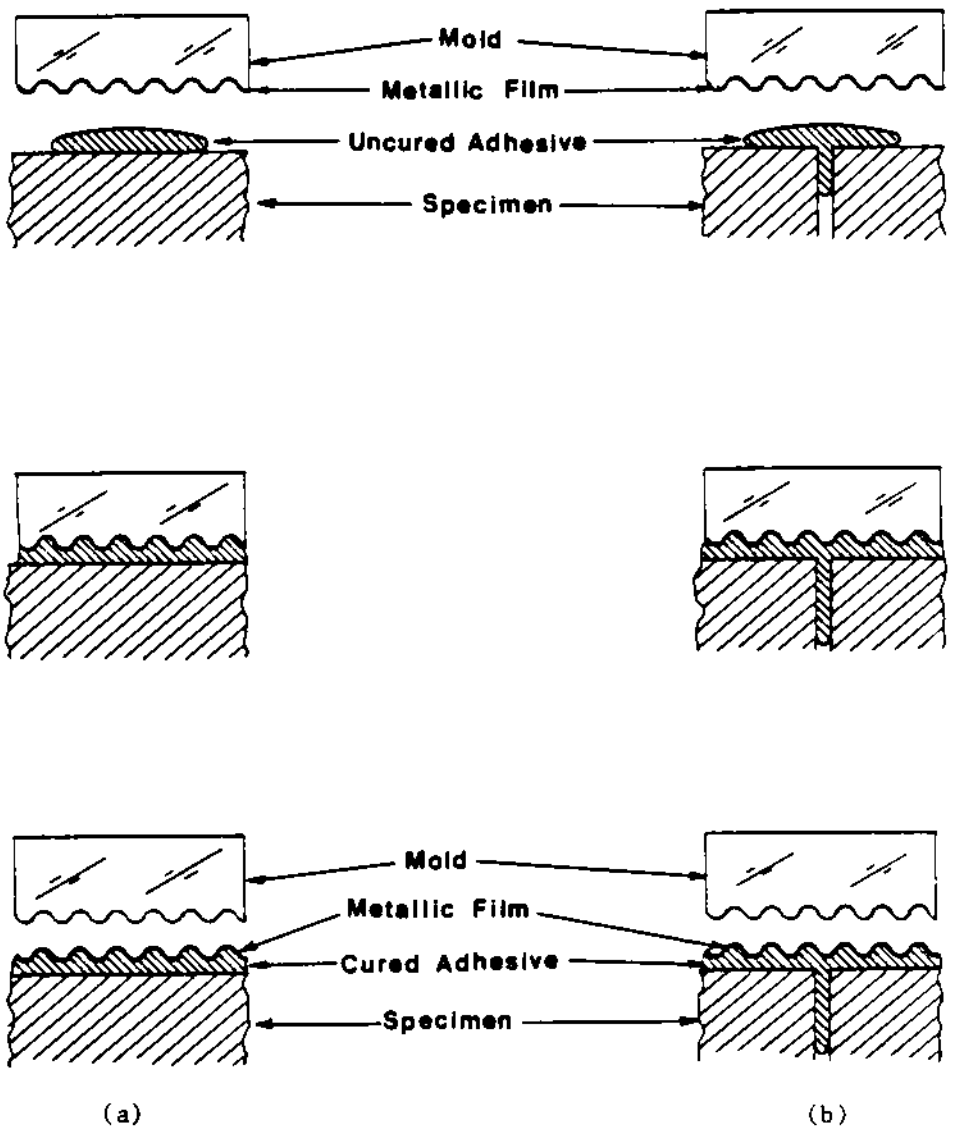

Figure 2.1 Replication technique to form a high-frequency high reflectance grating (a) on a continuous-body specimen, (b) on a two-body specimen.

must be kept in contact at least at a point to secure the continuous information across the contacting interface. It is not difficult to align the two gratings before the specimen is loaded. When the specimen is loaded, however, this alignment may be disturbed because a perfect alignment of the specimen in the loading frame is practically impossible. In tests using pin and plate specimens even the slightest misalignment would be a serious problem, considering the high sensitivity of the present technique. When the specimen is reoriented in the loading direction to realign it, the plate specimen will be subjected to rotation relative to the pin fixed in the loading fixture. This would cause additional friction at the contact region, increasing uncertainty of the experimental data. This problem necessitates the use of a special loading device.

In this chapter the geometry and material of the specimen is briefly discussed first. Then a special design of the loading frame is considered. After the optics of the experimental technique is explained, the procedure of the experiment is specified.

2.2 Geometry and Material of the Specimen

The experiment involves a thin, pin-loaded plate under a uniform in-plane load, as shown in Figure 2.2. The pin was given an undercut to ensure the plane stress at the contacting boundary for two dimensional analysis of the plate. The pin has a stiff three-dimensional geometry. As specified in Figure 2.3, the clearance between the pin and the hole of the plate is 0.001 inch.

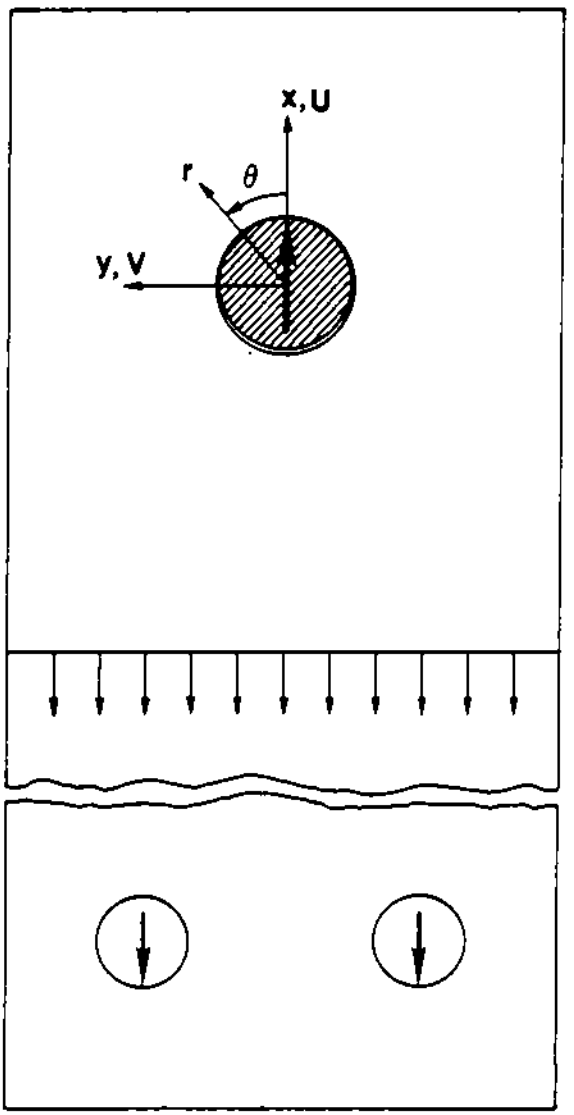

Figure 2.2 A thin plate restrained by a pin and subjected to a uniform, in-plane load.

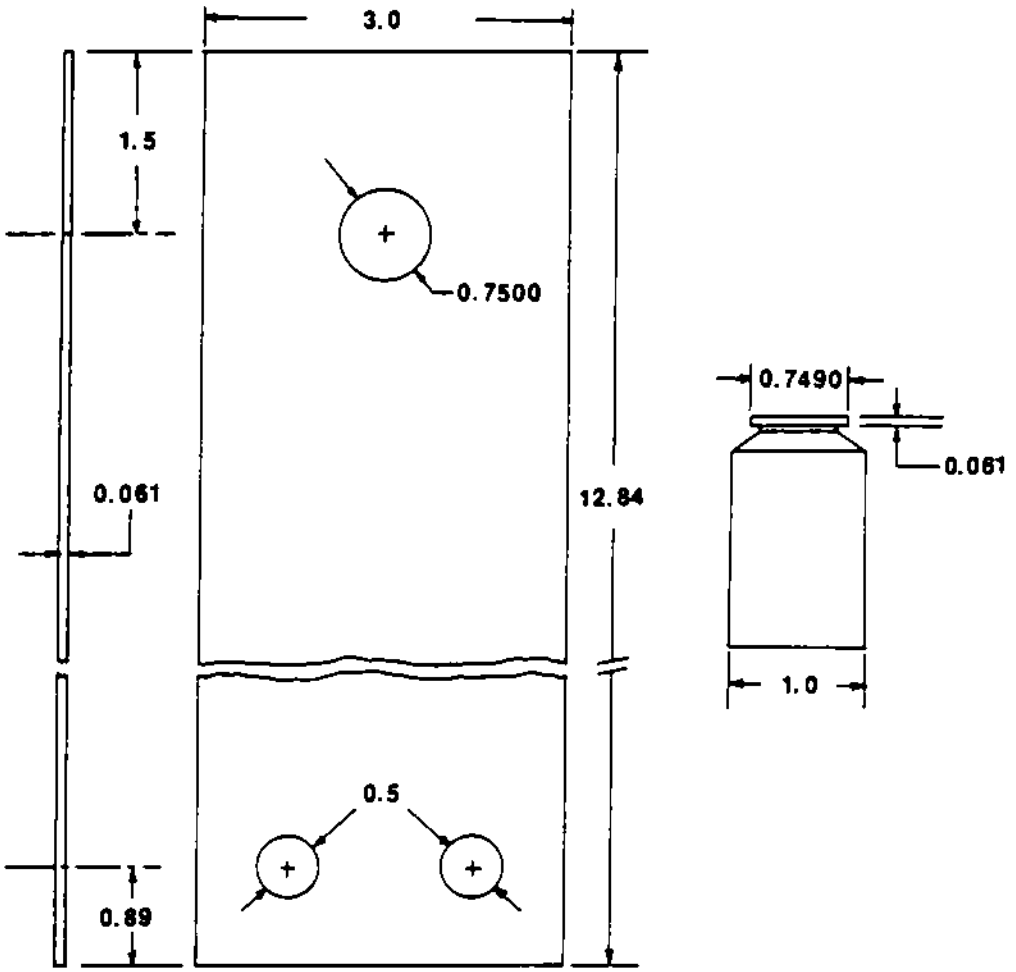

Figure 2.3 Geometry of a finite plate and a single pin specimen; specimen material is Aluminum 7075-T6. The pin is clearance fitted into the hole of the plate.

In the present study both the pin and the plate are made of Aluminum 7075-T6. Aluminum 7075-T6 is one of the most popular structural materials applied in aerospace engineering. This material shows a large elastic elongation which is a favorable advantage for the application of high-sensitivity moiré interferometry. It also has a large coefficient of friction compared to other metals such that the structure made of this material is prone to fretting damage. In the experiment, however, this detrimental condition of Aluminum 7075-T6 becomes another advantage for a good sample material to be used in the test for the frictional effects.

2.3 Loading Frame

The test specimen and the loading fixtures are shown in Figure 2.4. The pin is clearance fitted to the hole of the plate specimen. Specimen gratings are replicated on the pin and on the plate around the hole within the area of 1.5 in^2. These specimen gratings are aligned with the optical setup of moiré interferometry at zero-load level. When the load is applied, the plate specimen would be reoriented into the loading direction if the alignment had not been perfect. By this rotation of the plate specimen, the carrier pattern will be added to the load induced fringe pattern, but it can be subtracted by adjusting the whole structure of the loading frame to the optical arrangement. The problem involved here is the friction induced by the rotation of the plate with respect to the pin. Since this friction is not related to the deformation of the specimen, it must be avoided. Prabhakaran [46] used a specially devised fixture to load the pin in his experiment, obstructing a small portion of the area around the pin.

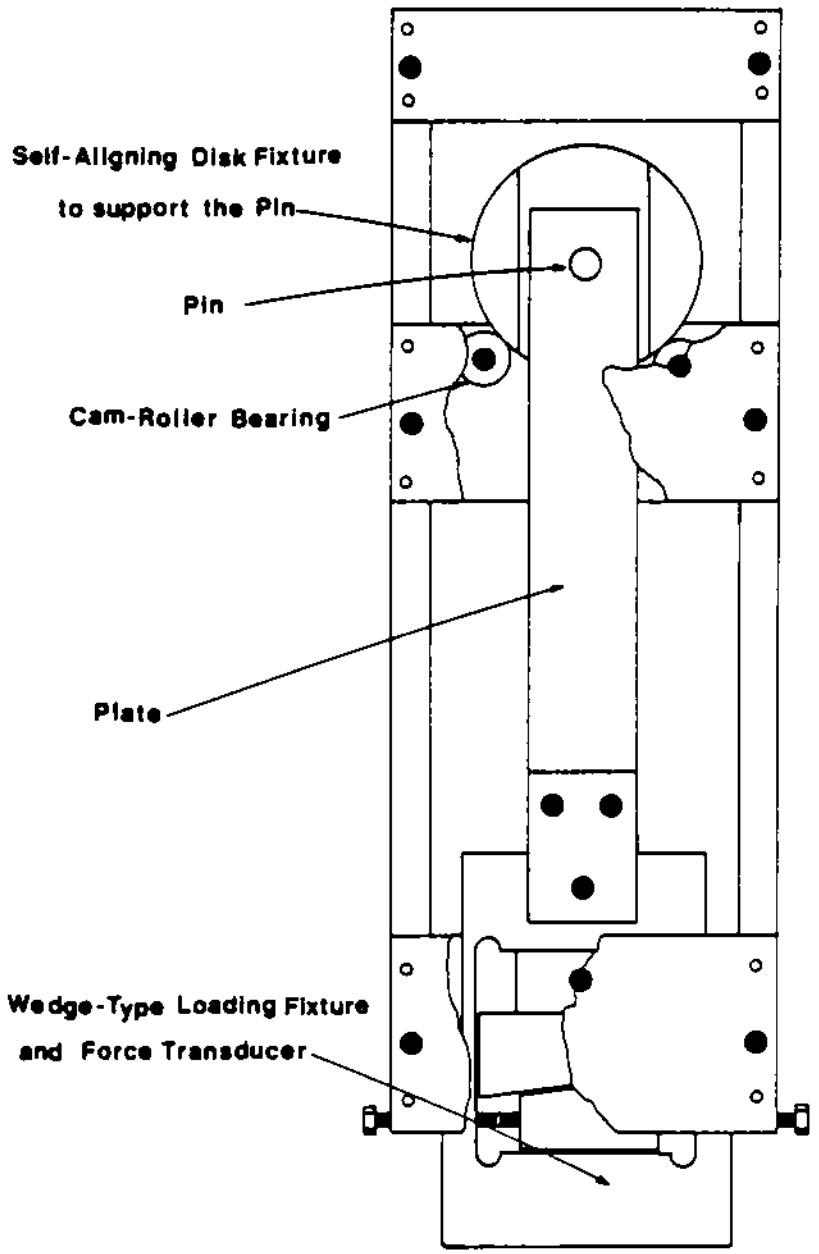

Figure 2.4 Schematic diagram of loading frame: Detrimental friction at the pin/plate boundary caused by aligning of the loading fixture elements are removed by supporting the disk fixture with cam-roller bearings.

In the present study the pin is fixed in a massive circular disk fixture made of cold rolled steel. This fixture is then supported by a pair of cam-roller bearings to remove the rotational constraint of the pin. By this configuration the relative rigid-body rotation between the pin and the plate can be avoided while still allowing a full-field view around the hole.

One may be concerned about the bending of the pin. If the pin bends, the reliability of the data in the resulting fringe patterns would be questionable. The bending of the pin may be influenced by the thickness of the plate and the load. However, the neck of the pin is very stiff (Figure 2.3), the pin specimen is fixed in the sturdy disk fixture by press fitting, and this disk fixture is designed with its central plane coincident with the central plane of the plate. To confirm this argument, the stresses calculated for the contact region were integrated to compare with corresponding applied loads. The results will be shown in Figure 4.14. The equilibrium balance was very good, indicating uniform stresses through the thickness of the plate, therefore precluding bending of the pin.

2.4 Moiré Interferometry

Moiré interferometry is a whole-field optical method using coherent light to measure in-plane displacements [54]. Briefly, a high frequency crossed-line diffraction grating is replicated on the specimen surface using a special mold, as illustrated in Figure 2.1. The result is a thin--usually less than 25 μm (0.001 in.) thick--

reflective phase grating firmly adhered to the specimen, deforming together with the specimen surface. The specimen grating is observed in an optical arrangement illustrated in Figure 2.5. Two beams of light, illuminating the specimen grating at angles α and $-\alpha$, form a virtual reference grating. Its frequency is $f = (2 \sin \alpha)/\lambda$, where λ is the wavelength of the light. This reference grating interacts with the specimen grating to form the interference pattern recorded in the camera. When the reference grating lines are perpendicular to the x axis, the pattern is a contour map of the x-displacement field governed by the relationship

$$U = \frac{1}{f} N_x \tag{2.1}$$

where U is the x component of the in-plane displacement at any point of the specimen surface, and N_x is the fringe order at that point.

In this work, a crossed-line grating was applied in the x-y plane with lines perpendicular to the x and y axes. When the reference grating lines were perpendicular to the y axis, in-plane displacements V were obtained from fringe orders N_y by

$$V = \frac{1}{f} N_y \tag{2.2}$$

The frequency f was 2,400 ℓ/mm (60,960 ℓ/in.). An argon-ion laser was used at wavelength 0.514 μm (20.3 μin.) and 100 mW power. The optical arrangement used in these experiments had two additional mirrors which produced a virtual reference grating perpendicular to that of Figure 2.5. Individual patterns of N_x or N_y were obtained by blocking the light of the alternate virtual reference grating.

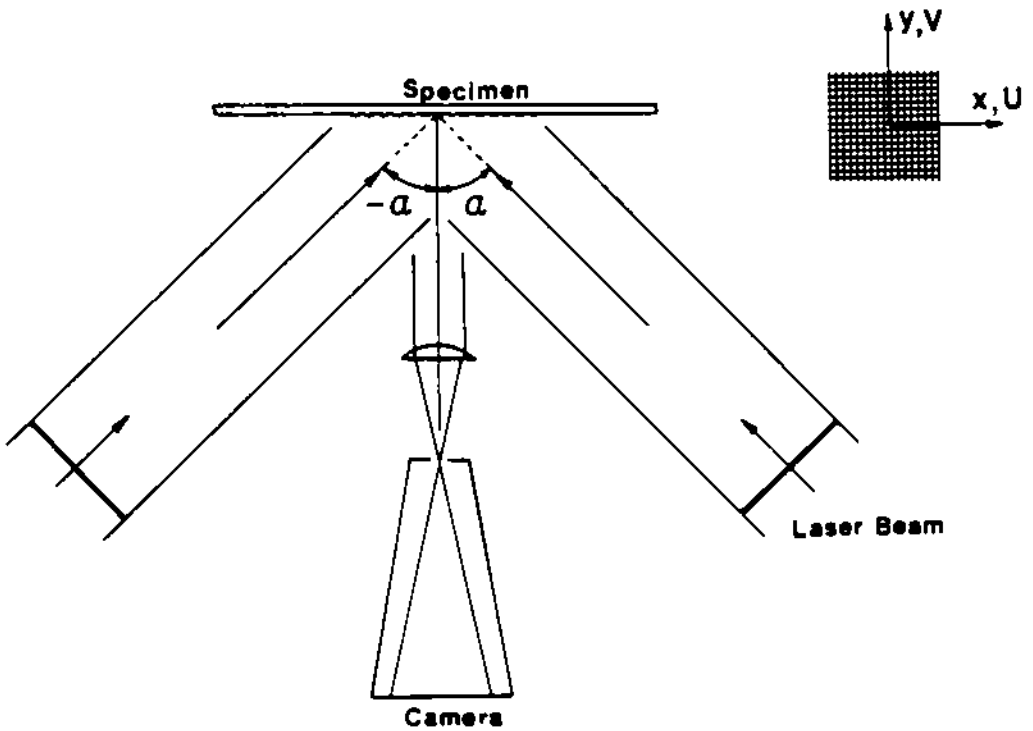

Figure 2.5 Optical arrangement for moiré interferometry.

2.5 Loading History

What is pursued in this research is the effect of friction at the contact region along the pin/plate boundary. To avoid nonsteady surface conditions during the incipient running-in period, the specimen is given preliminary cyclic loadings before the test. The loading history is shown in Figure 2.6. The dots on the last cycle represent loads for which whole-field moiré interferometry data are taken. The load was increased up to 1,980 lb. and unloaded to zero. Fringe patterns of U and V displacements were taken at 17 points in the last loading cycle. One of the typical fringe patterns is shown in Figure 2.7. At the contact region the fringe pattern shows some irregularities on the pin and on the plate. These are due to the contact stresses caused by the asperities on the contact surfaces.

Loading Sequence	Loads in Increasing Phase (lb)	Loading Sequence	Loads in Decreasing Phase (lb)
1	20	9	1,980
2	230	10	1,800
3	660	11	1,600
4	1,040	12	1,440
5	1,240	13	1,210
6	1,460	14	1,070
7	1,670	15	630
8	1,840	16	210
9	1,980	17	40

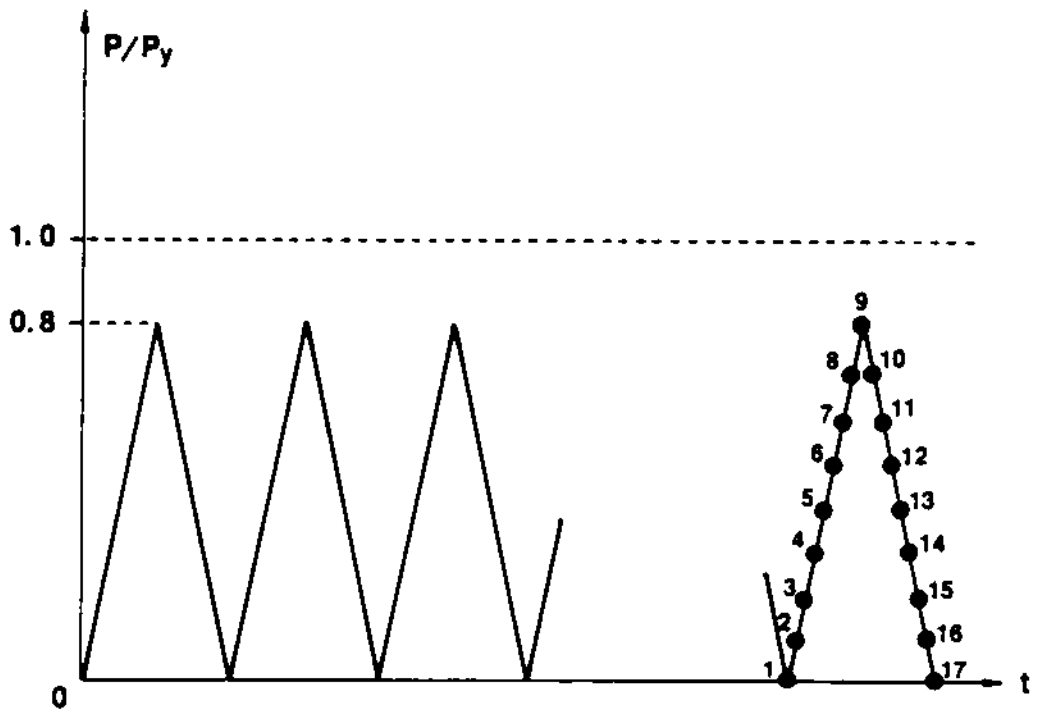

Figure 2.6 Loading history: The dots on the last cycle represent loads for which the whole-field moiré-interferometry data were taken. P_y is the predicted failure load.

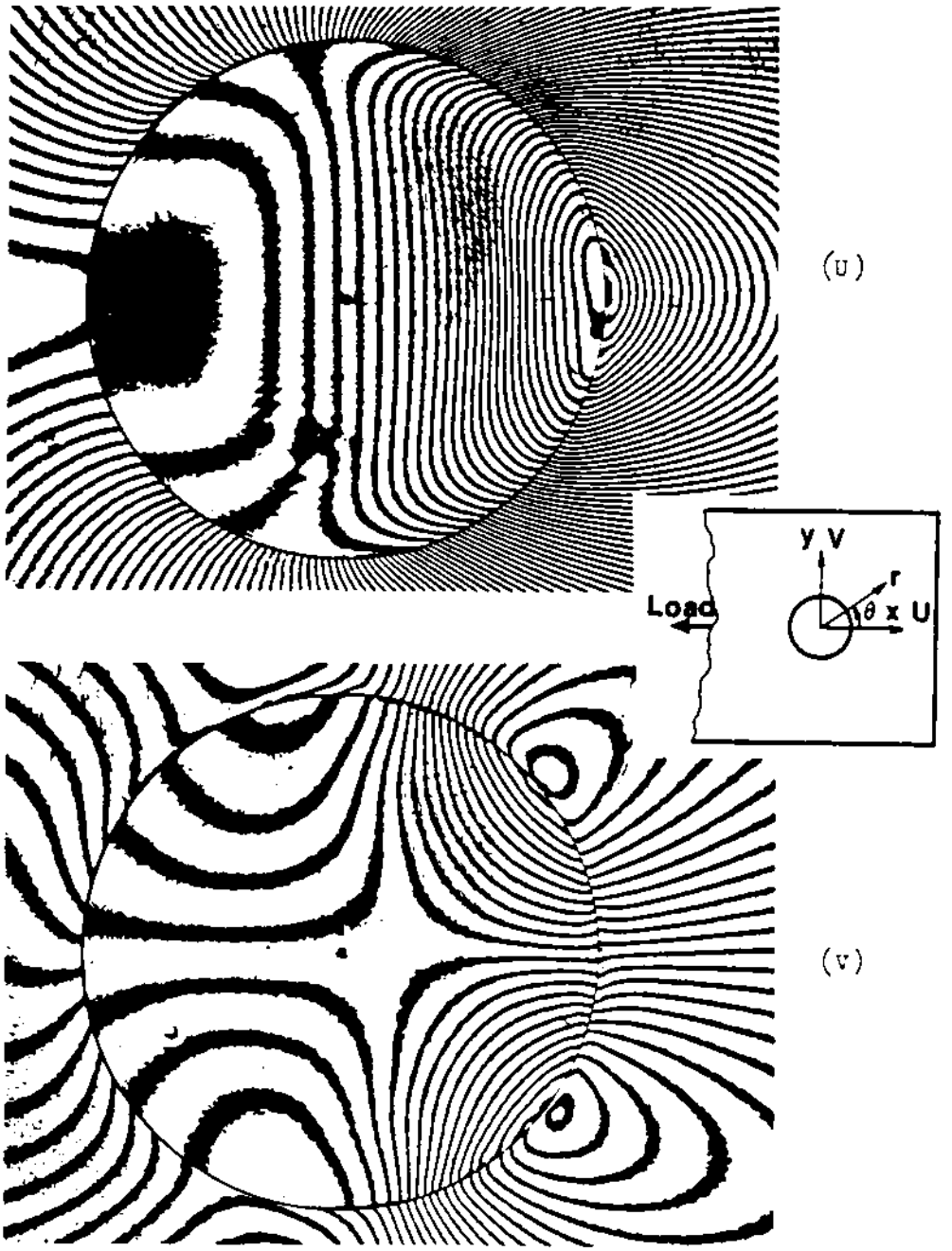

Figure 2.7 U and V-fringe patterns for load number 15.

CHAPTER III

DATA ACQUISITION AND ANALYSIS

3.1 Introduction

As might have been implied by the high sensitivity of moiré interferometry and the number of load levels at which the pictures are taken, there is a huge number of data points to be analyzed. For displacement analysis, these include the N_x and N_y fringe orders and x and y coordinates of the points along the inner and outer circular boundary at all the load levels. For the strain analysis another set of the same number of data points are needed. Furthermore, in the analyses of friction problems, all the physical properties and quantities involved are expressed in the coordinate system where the two coordinate axes are perpendicular and tangential to the contact boundary, respectively. Therefore, all the data obtained in x and y coordinate system must be transformed into a cylindrical coordinate system. Coordinate transformations on such a huge quantity of data necessitate the use of an appropriate data acquisition system.

In the fringe patterns of Figure 2.7, it is observed that changes of curvature appear in the fringes near the contact boundary. When the curvatures of the fringes are relatively large with respect to the density of fringes, conventional methods of moiré analysis cannot be applied. For the two-body contact problems with highly localized frictional effects, a new algorithm of moiré analysis must be developed.

3.2 Data Acquisition System

This system consists of a digitizing tablet, a cursor, and a micro-computer. There are built-in electromagnetic fields in the former two components, by which the coordinates of the data points are measured with a sensitivity of 0.001 in. Using enlarged pictures of the fringe patterns and the magnifying lens attached to the cursor, the data points are easily located and digitized by the system with sufficiently good accuracy. These raw data are transferred to the micro-computer, in which the x-y coordinate system is transformed into the $r - \theta$ coordinate system by the computer software made by the user.

3.3 A New Algorithm of Moiré Analysis

At the contact zone, frictional shear stress causes the curvature of moiré fringes to change abruptly near the boundary. To calculate for these high-gradient strains at the pin-plate boundary, a new scheme must be devised to reflect these localized effects in the analysis.

First, virtual fringes are drawn tangentially to the fringes at the boundary, as represented by the dashed lines in Figure 3.1. A practical procedure of doing this is as follows: First step is to read the data on the fringe at the boundary point. Then the cursor is put tangentially to the fringe at that point, and any other point on that cursor line is located and digitized. The two data points registered in the system will be used to define the virtual fringe, as represented in Figure 3.1.

The chord length ΔD_y between the points A_1 and A_2 can be expressed as

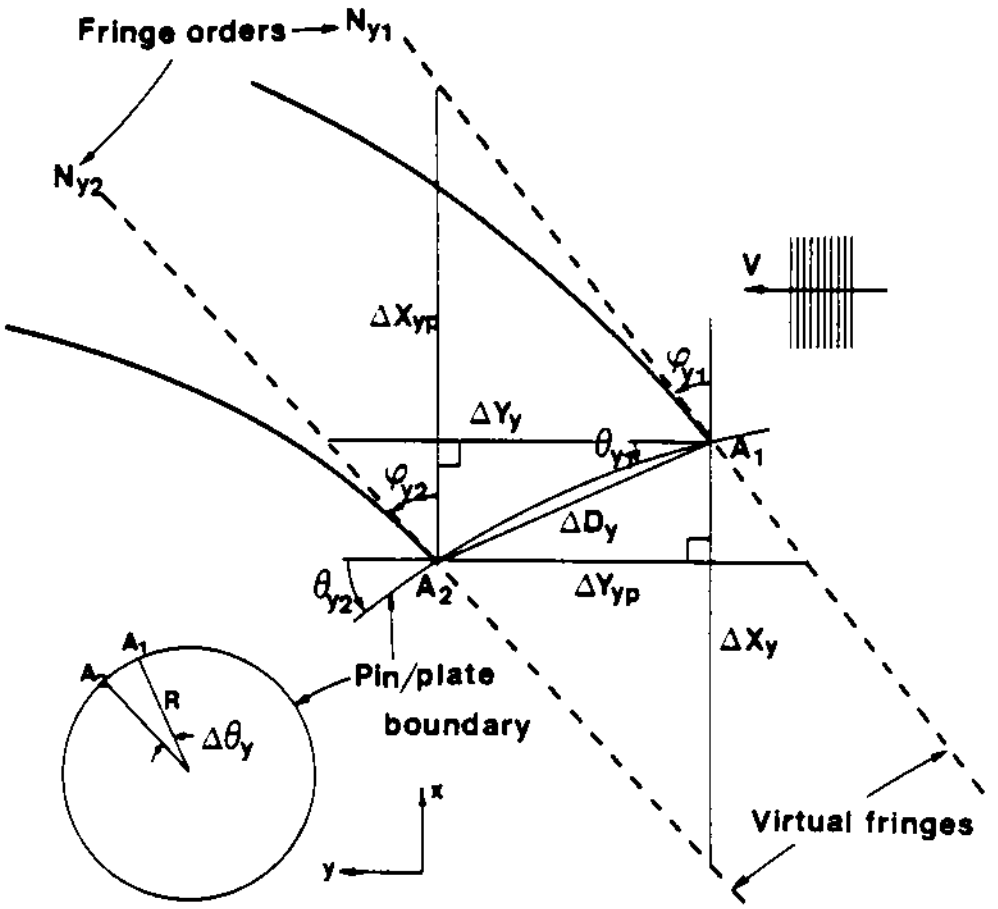

Figure 3.1 Schematic illustration of the new method of moiré analysis using virtual fringes which are tangential to the original ones.

$$\Delta D_y \cong R\Delta\theta_y \tag{3.1}$$

when $\Delta\theta_y$ is very small. Subscript y indicates the V-displacement pattern from which the data are extracted, and R is the radius of the hole. Assuming that ΔD_y is small, angles θ_{y_1} and θ_{y_2} can be averaged over this arc length. Thus,

$$\theta_y \equiv \frac{\theta_{y_1} + \theta_{y_2}}{2} \cong \theta_{y_1} \cong \theta_{y_2} \tag{3.2}$$

Subscripts 1 and 2 refer to the boundary points A_1 and A_2, respectively. ΔX_y and ΔY_y in Figure 3.1, x and y distances between the two virtual fringes measured from the point A_1, can be expressed as in equations (3.3) and (3.4).

$$\Delta X_y = - \Delta D_y \sin \theta_y - \Delta D_y \cos \theta_y \cot \phi_{y_2} \tag{3.3}$$

$$\Delta Y_y = \Delta D_y \cos \theta_y + \Delta D_y \sin \theta_y \tan \phi_{y_2} \tag{3.4}$$

On the other hand, ΔX_{yp} and ΔY_{yp}, x and y distances between the virtual fringes measured from the point A_2, were obtained as

$$\Delta X_{yp} = - \Delta D_y \sin \theta_y - \Delta D_y \cos \theta_y \cot \phi_{y_1} \tag{3.5}$$

$$\Delta Y_{yp} = \Delta D_y \cos \theta_y + \Delta D_y \sin \theta_y \tan \phi_{y_1} \tag{3.6}$$

On the assumption that the virtual fringes are nearly parallel, equation (3.7) is obtained:

$$\phi_y \equiv \frac{\phi_{y_1} + \phi_{y_2}}{2} \cong \phi_{y_1} \cong \phi_{y_2} \tag{3.7}$$

and

$$\Delta X_y \approx \Delta X_{yp} \tag{3.8}$$

$$\Delta Y_y \approx \Delta Y_{yp} \tag{3.9}$$

Localized strain components are calculated by the following equations:

$$\frac{\partial V}{\partial y} \approx \frac{N_{y_2} - N_{y_1}}{f\ \Delta Y_y} \tag{3.10}$$

$$\frac{\partial V}{\partial x} \approx \frac{N_{y_1} - N_{y_2}}{f\ \Delta X_y} \tag{3.11}$$

where f is the frequency of the virtual reference grating, and N_{y_1} and N_{y_2} are the fringe orders. Substituted by equations (3.1) - (3.9), equations (3.10) and (3.11) become

$$\frac{\partial V}{\partial y} \approx \frac{\Delta N_y}{\Delta \theta_y} \frac{1}{Rf} \frac{1}{\cos \theta_y + \sin \theta_y \tan \phi_y} \tag{3.12}$$

$$\frac{\partial V}{\partial x} \approx - \frac{\Delta N_y}{\Delta \theta_y} \frac{1}{Rf} \frac{1}{\sin \theta_y + \cos \theta_y \cot \phi_y} \tag{3.13}$$

However, since the virtual fringes are neither nearly parallel nor quite close to one another in some regions, equations (3.12) and (3.13) are not yet suitable for practical purposes in those regions. Only when $\Delta\theta_y$ is very small, the approximations in equations above are valid. In order to validate the assumptions introduced above, ϕ_y and N_y can be interpolated with respect to θ_y. An example is the plate near the centerline of the specimen (Figure 2.7) where the fringes are not closely spaced along the boundary; additional fractional fringes can be sketched systematically between existing fringes such that the

increment ΔN_y is sufficiently small, e.g. $\Delta N_y = 1/5$ fringe order. ΔN_y and ϕ_y can be assessed from these interpolated functions, respectively. Similarly, the strain components from U-displacement fringe patterns can be obtained by the following equations;

$$\frac{\partial U}{\partial x} = - \frac{\Delta N_x}{\Delta \theta_x} \frac{1}{Rf} \frac{1}{\sin \theta_x + \cos \theta_x \cot \phi_x} \tag{3.14}$$

$$\frac{\partial U}{\partial y} = \frac{\Delta N_x}{\Delta \theta_x} \frac{1}{Rf} \frac{1}{\cos \theta_x + \sin \theta_x \tan \phi_x} \tag{3.15}$$

By the equations (3.12) - (3.15) the strains in x-y coordinate systems are determined. These strains are then transformed into r - θ coordinate systems to obtain ε_r, ε_θ, and $\gamma_{r\theta}$. Using the constitutive equations for plane-stress configurations, the stresses σ_r, σ_θ, and $\tau_{r\theta}$ are calculated at the pin plate boundary.

CHAPTER IV

RESULTS AND DISCUSSION - STRESS ANALYSIS

4.1 Introduction

Stress fields involved with a clearance-fit pin joint are highly nonlinear and complicated in general. This complexity is caused by the combination of the effects of friction and the nonlinear variation of contact geometry between the pin and the plate. The changing sense of friction during the loading and unloading phases of the loading cycle adds to the complexity of the problem. This chapter deals with the influences of friction and the changing configuration of contact geometry. First, the strain fields obtained from the displacement patterns are used to produce the stress fields along the pin/plate boundary by Hooke's law. Strains were determined by the algorithm of section 3.3 along three different outside concentric circles and the results were extrapolated to the true contact boundary to assess the strains. See Appendix A for basic data of all load levels. Stresses in x-y coordinate system are transformed into the cylindrical coordinates. Variation of radial stress distribution at the contact region with the load will be examined during the loading and unloading phases of a cycle of loading. Effects of friction on the shear stress distribution will also be investigated, and the shear stress during each of the two phases in the loading cycle will be compared. Contact region will be determined by the boundary condition that the radial stress and the shear stress are zero where the pin and the plate are not in

contact. The hoop stress distribution will show another feature of the stress fields at the pin joint of plates with the changing sense of friction. Factors of stress concentration will be measured using the maximum tensile stress. Also the variation of the location of the maximum stress with loading will be investigated.

4.2 Preliminary Analysis of Displacement Patterns

Fringe patterns in Figure 4.1 - 4.2 show the characteristics of U and V-displacement fields at the load level of 1240 lb. These patterns were taken during the first half of the loading cycle, i.e., load-increasing phase. The numbers shown in the figures are the fringe orders. U and V displacements are calculated by the equations (2.1) and (2.2).

One of the unique features of contact problems is that the compressive normal stress and the frictional shear stress at the contact region are not independent of each other. Due to geometrical configurations between the pin and the plate, the deformation of the plate is larger than that of the pin near the boundary. As a result friction arises from the relative displacements at the contact region. During the phase of increasing load the frictional forces may act on the interface in the opposite sense to the loading direction. Subsequently, during the second half of the loading cycle, i.e., load-decreasing phase, the sense of the friction may be reversed affecting displacement fields significantly. In Figure 4.3 two fringe patterns for V-displacement obtained almost at the same load level for load-increasing and load-decreasing phases are compared with each other.

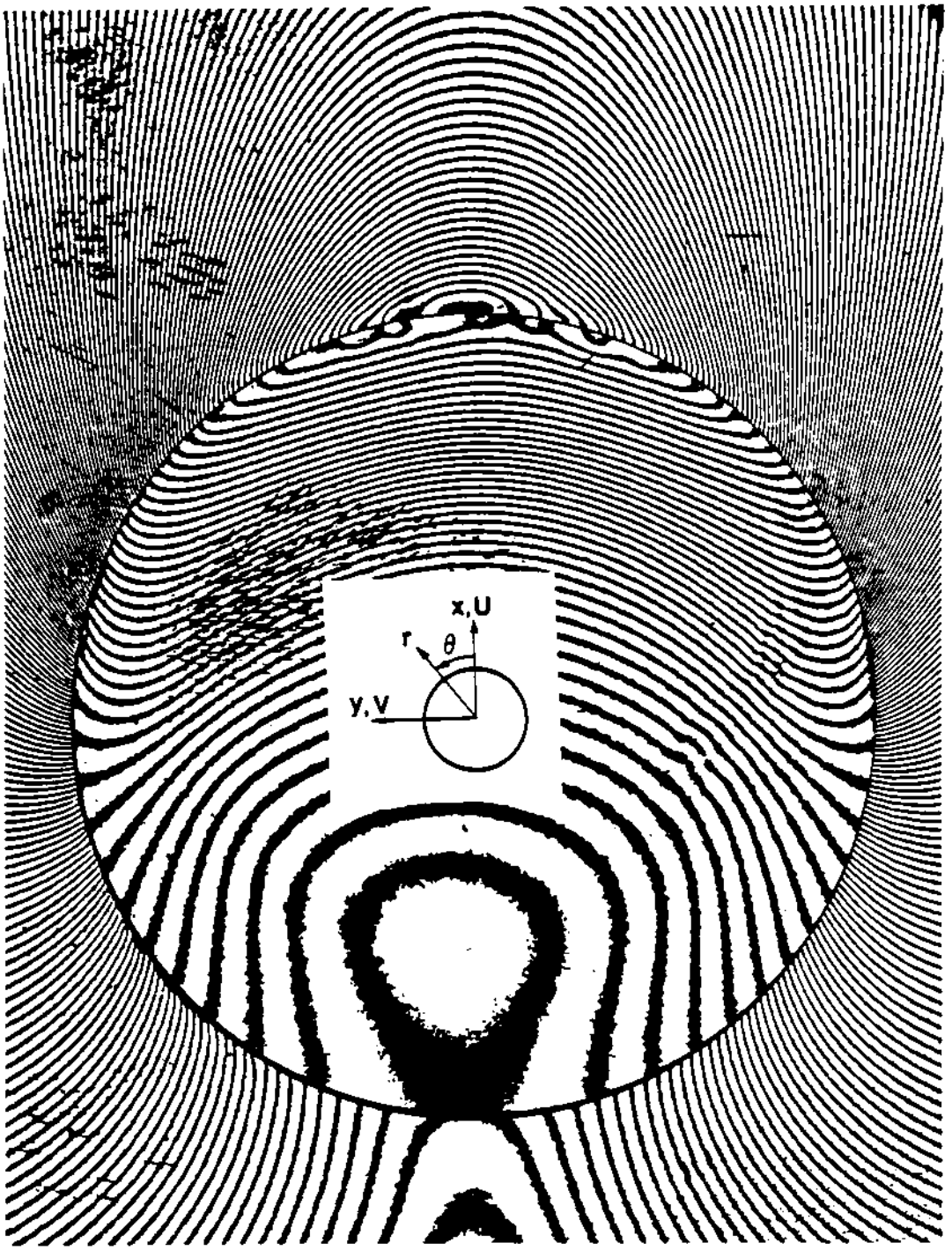

Figure 4.1 U-displacement fringe pattern at the load level of 1240 lb during the load-increasing phase.

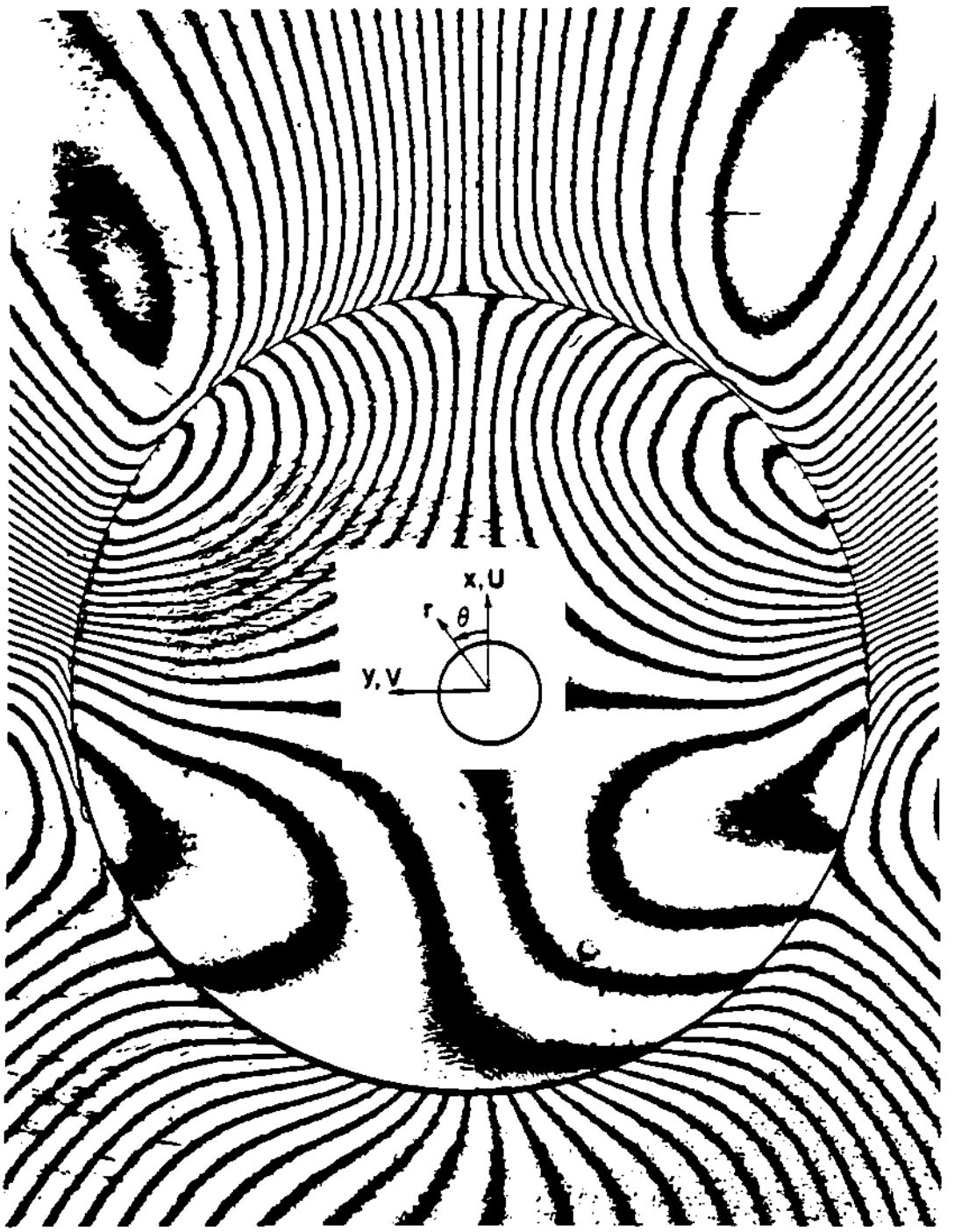

Figure 4.2 V-displacement fringe pattern at the load level of 1240 lb during the load-increasing phase.

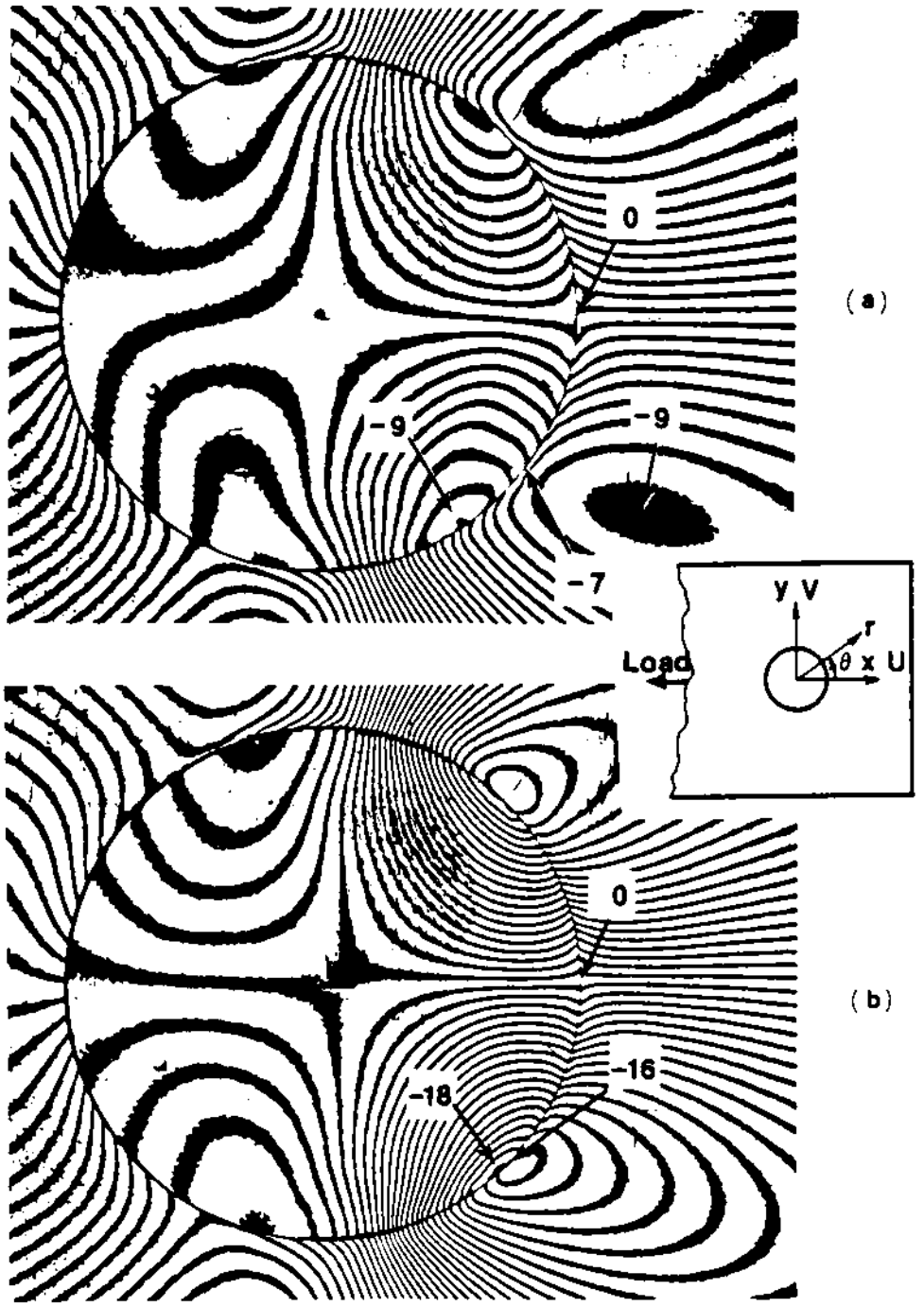

Figure 4.3 Two fringe patterns of V-displacements obtained at almost the same load level: (a) 1040 lb for the load-increasing phase and (b) 1070 lb for the load-decreasing phase. Note that the point of first contact is at fringe order zero.

It can be seen that the maximum fringe orders are distinctly different between the two phases of the loading cycle.

4.3 Radial Stress and Shear Stress

Figure 4.4 shows the distribution of radial stress σ_r at the pin/plate interface for a few load levels during the load-increasing phase. σ_r has the maximum value near the axis of symmetry. The shape of the curve changes slightly with the increase of the load in the manner such that the stress/load ratio is decreased near the axis of symmetry. This can be explained in conjunction with the frictional shear stress developed at the contact region, as shown in Figure 4.5. The load on the plate is supported by the normal stress σ_r and the shear stress $\tau_{r\theta}$ at the contact boundary between the pin and the plate. With the expansion of the frictional shear stress region to a larger angle the load bearing effect of the shear stress increases, and the normal stress is mitigated at lower angle of contact in order that the force equilibrium condition shall be satisfied. This argument is supported by the stress distributions during the load-decreasing phase of the loading cycle. As shown in Figure 4.6, it is observed that the magnitude of the radial stress σ_r has increased relative to that of the load-increasing phase. This increase is attributed to the changed distribution and sense of the frictional shear stress $\tau_{r\theta}$, as shown in Figure 4.7. As the load is decreased from the maximum value, the reversed sense in the relative tangential displacement at the contact region gives rise to the reversal of the sense of friction. However, as demonstrated in Figure 4.7, the reversion does not occur in a global sense over the entire contact

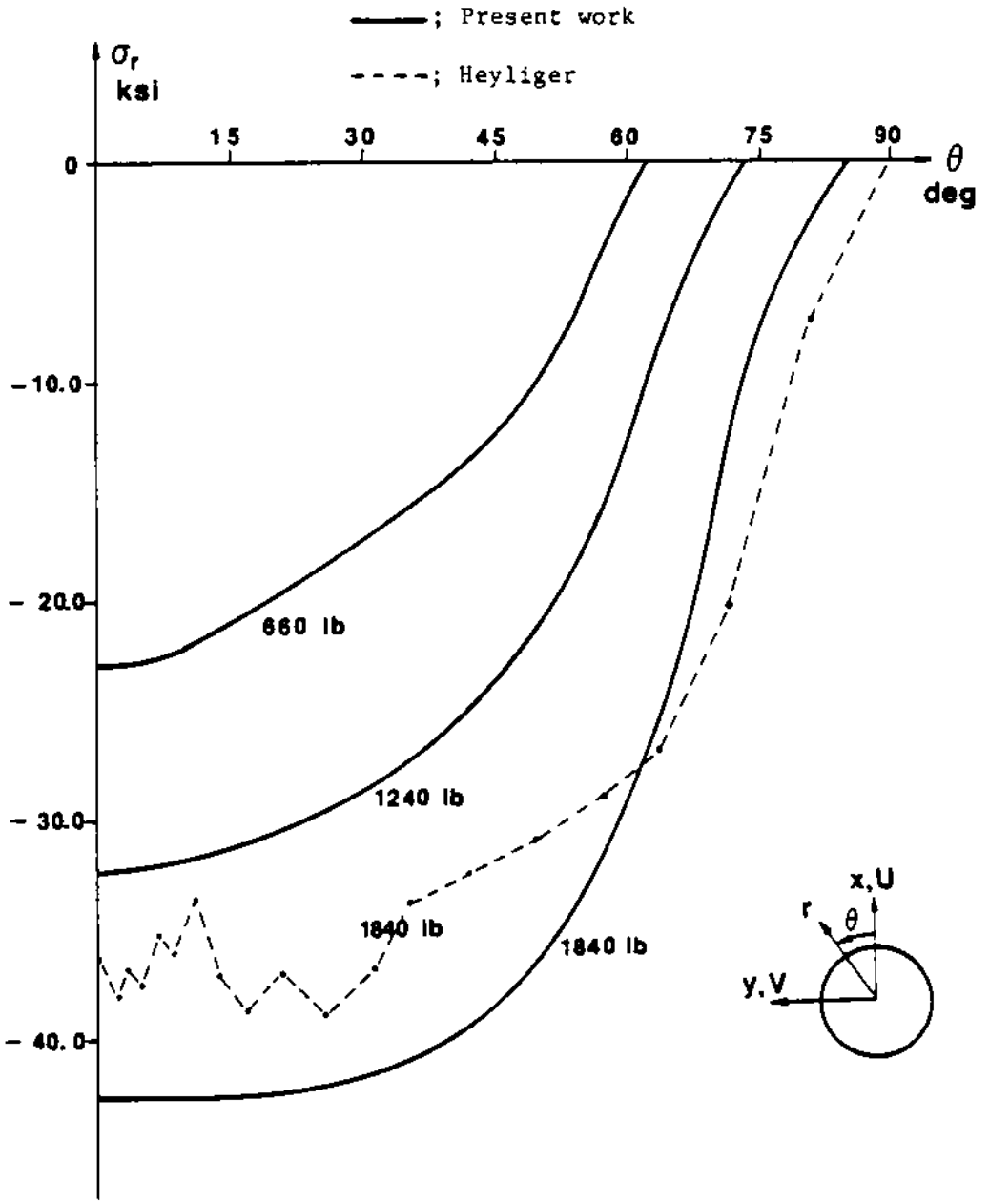

Figure 4.4 Distributions of radial stress σ_r at three load levels during the load increasing phase: 660 lb, 1240 lb, and 1840 lb.

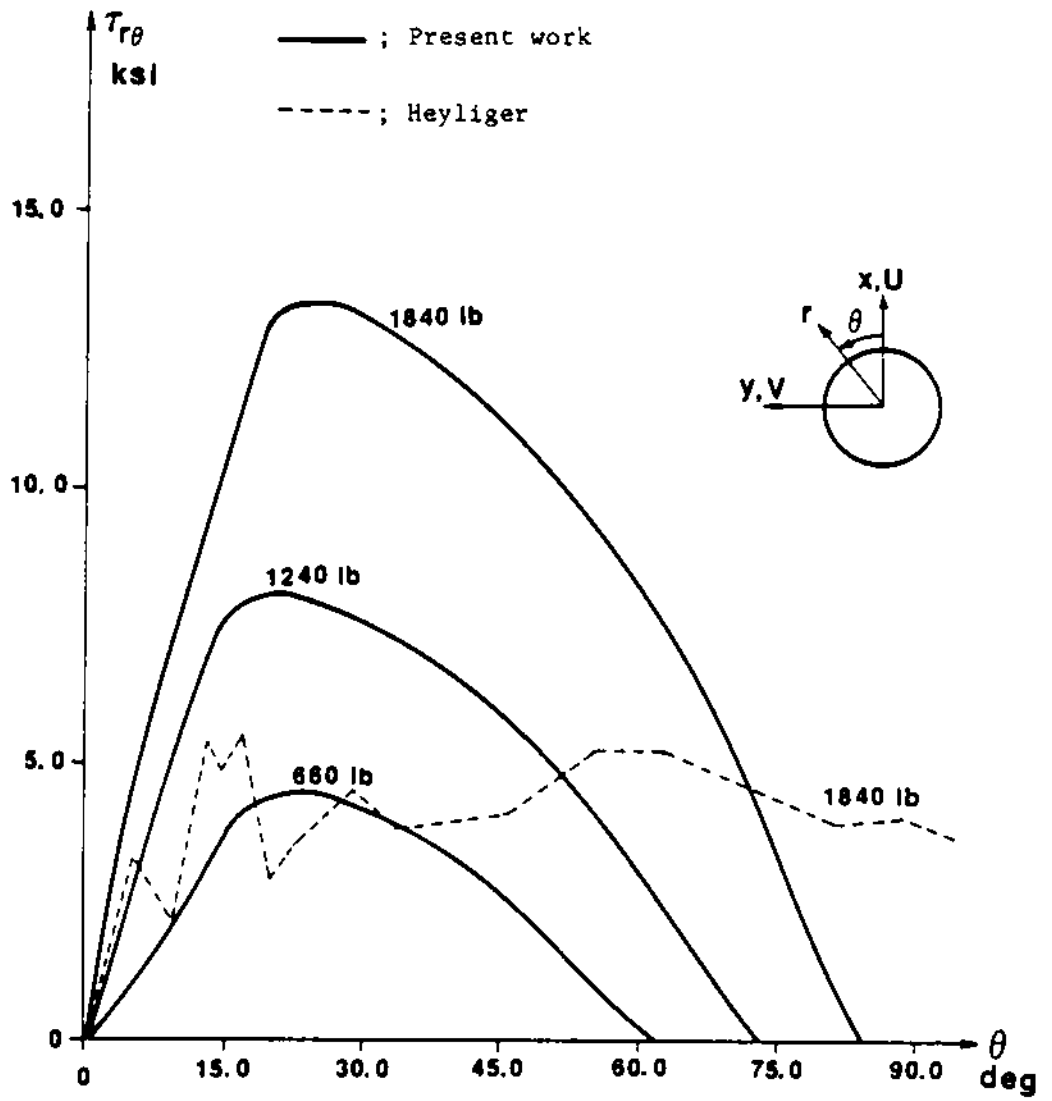

Figure 4.5 Frictional shear stress at the contact region developed with the load increments.

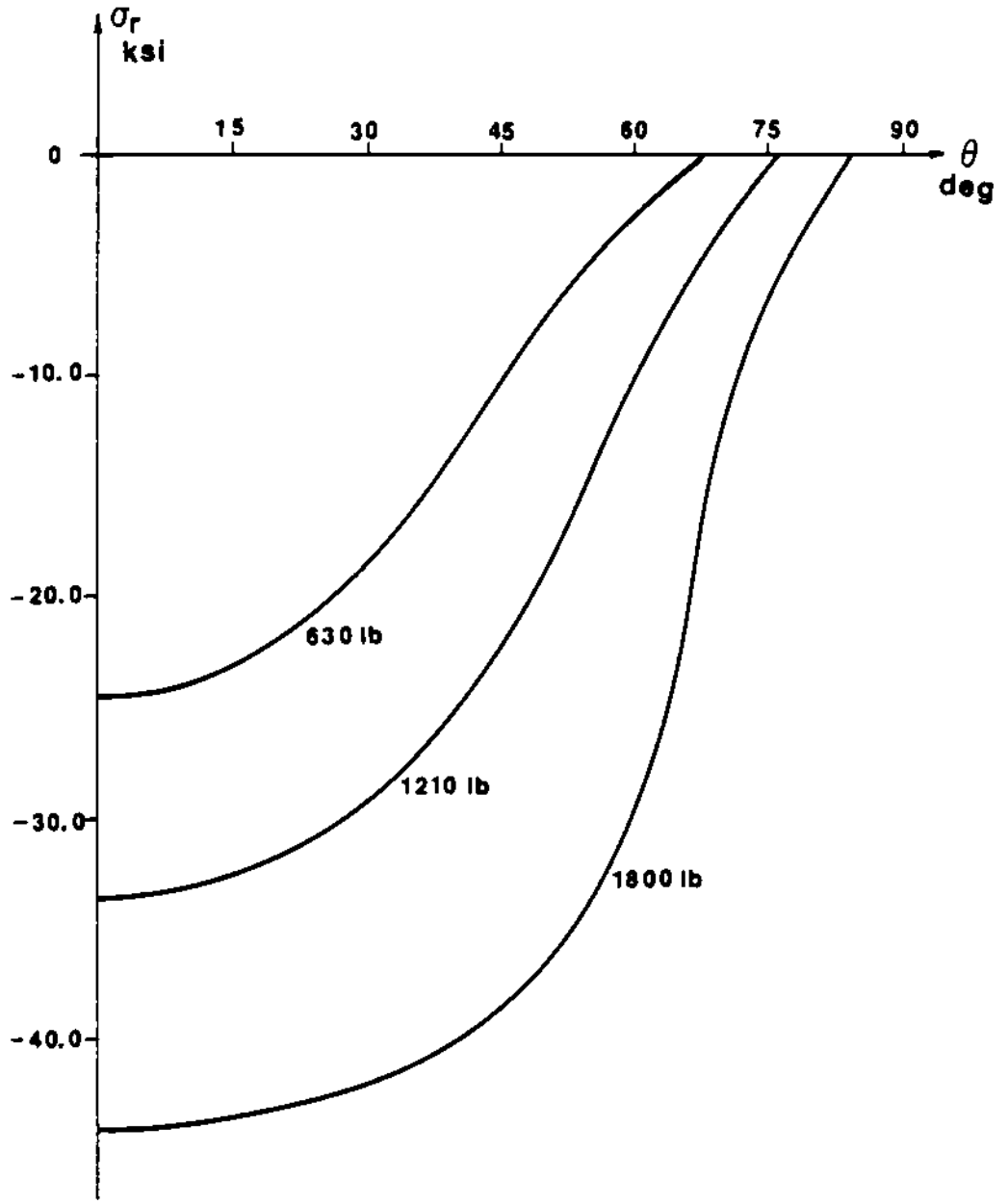

Figure 4.6 Distributions of radial stress σ_r at three load levels during load-decreasing phase: 630 lb, 1210 lb, and 1800 lb.

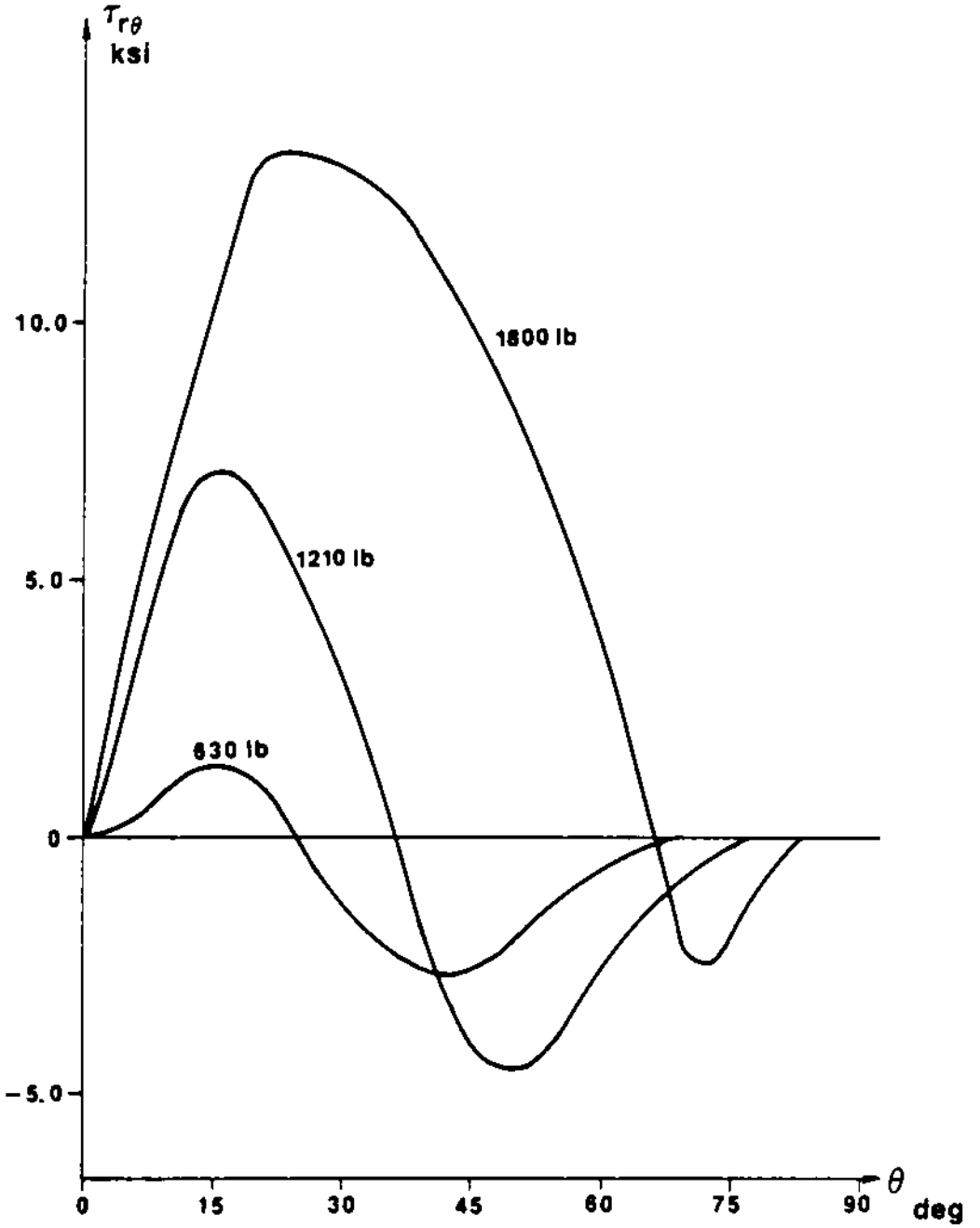

Figure 4.7 Frictional shear stress at the contact region: the sign is being reversed progressively with decrements of load.

region. The change of slip in the opposite direction occurs initially at the end of the contact region, and the region of negative shear stress is expanded into the region of the lower contact angle. The radial stress increases to compensate for the loss of support by tangential shear at the contact region satisfying the force equilibrium condition. This argument is convinced by Figure 4.8, in which the curves provide a good comparison of the stress distributions between the two phases of loading cycle. The radial and the shear stresses are plotted against the angle for both the loading and unloading phases at nearly the same load levels. With the changed sign of $\tau_{r\theta}$ during the load-decreasing phase it is observed that the σ_r curve is lifted upward to satisfy the force equilibrium conditions.

4.4 Contact Region

One of the most challenging problems in the study of the frictional phenomena of pin joints is to measure the contact region between the pin and the plate. The information on the contact region varying with load levels is also very important for the analytical study. This will provide, in Chapter V, a guideline to determine the slip amplitude.

Once the radial stress distribution is obtained, the limit of contact region can be defined where the normal stress becomes zero since the free surface should be stress free in normal direction. In Figure 4.9 the contact region is shown by the contact angle versus the load for the whole cycle of loading. A noticeable difference in the size of the contact region is observed between the loading and

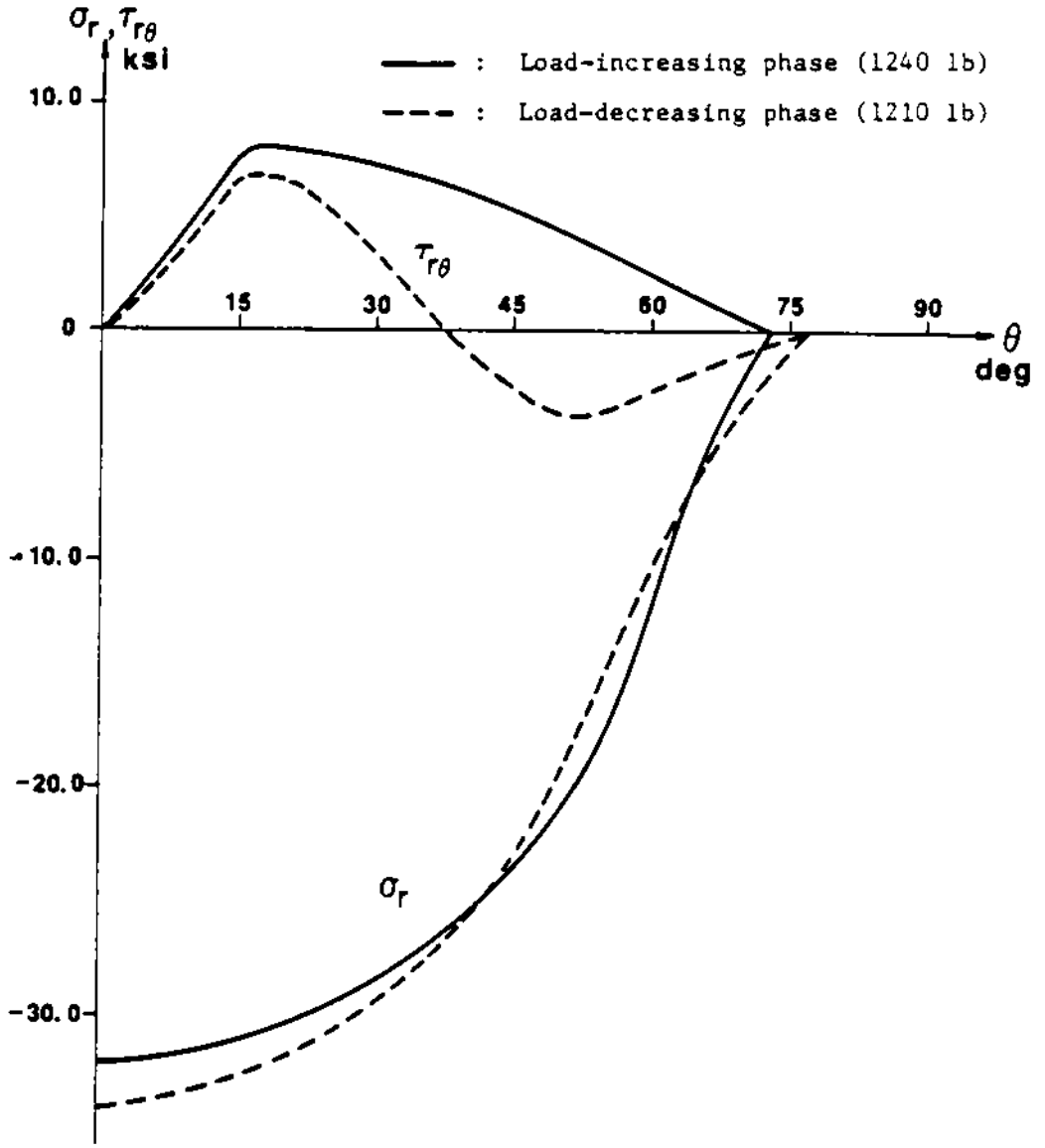

Figure 4.8 Comparisons of radial and shear stress distributions between the two phases of the loading cycle.

unloading phases. The friction at the contact region, acting as the constraint against the relative motion between the two bodies of the specimen, causes the deformation-lag between the two halves of the loading cycle. As the curve in Figure 4.9 shows, the contact region in the unloading half of the load cycle is larger than that of the load-increasing phase. Maximum difference of the contact region was observed near the load level of 500 lb at the angle around 60°.

4.5 Hoop Stress

Figure 4.10 shows the hoop stress σ_θ along the circumference of the hole at the load level of 1240 lb. The curve of solid line indicates the distribution of σ_θ during the load increasing phase and the dashed line represents the load-decreasing phase.

When the load is increasing σ_θ has the negative value for the contact angle less than 28 degrees. This is caused by the large value of compressive radial stress and the frictional constraints from the pin. The maximum slope of σ_θ curve is obtained just outside of the contact region where there is no frictional constraint from the pin. It must be noted that the hoop stress within the contact region is influenced by the slip between the pin and the plate. By the slip, the frictional constraints are released to allow the hoop stress to increase.

The hoop stress shows a different behavior when the load is decreased from the maximum value, 1980 lb. First, it is noticed that the slope of the curve is decreased as a whole. As a result the maximum hoop stress is reduced significantly. This phenomenon is

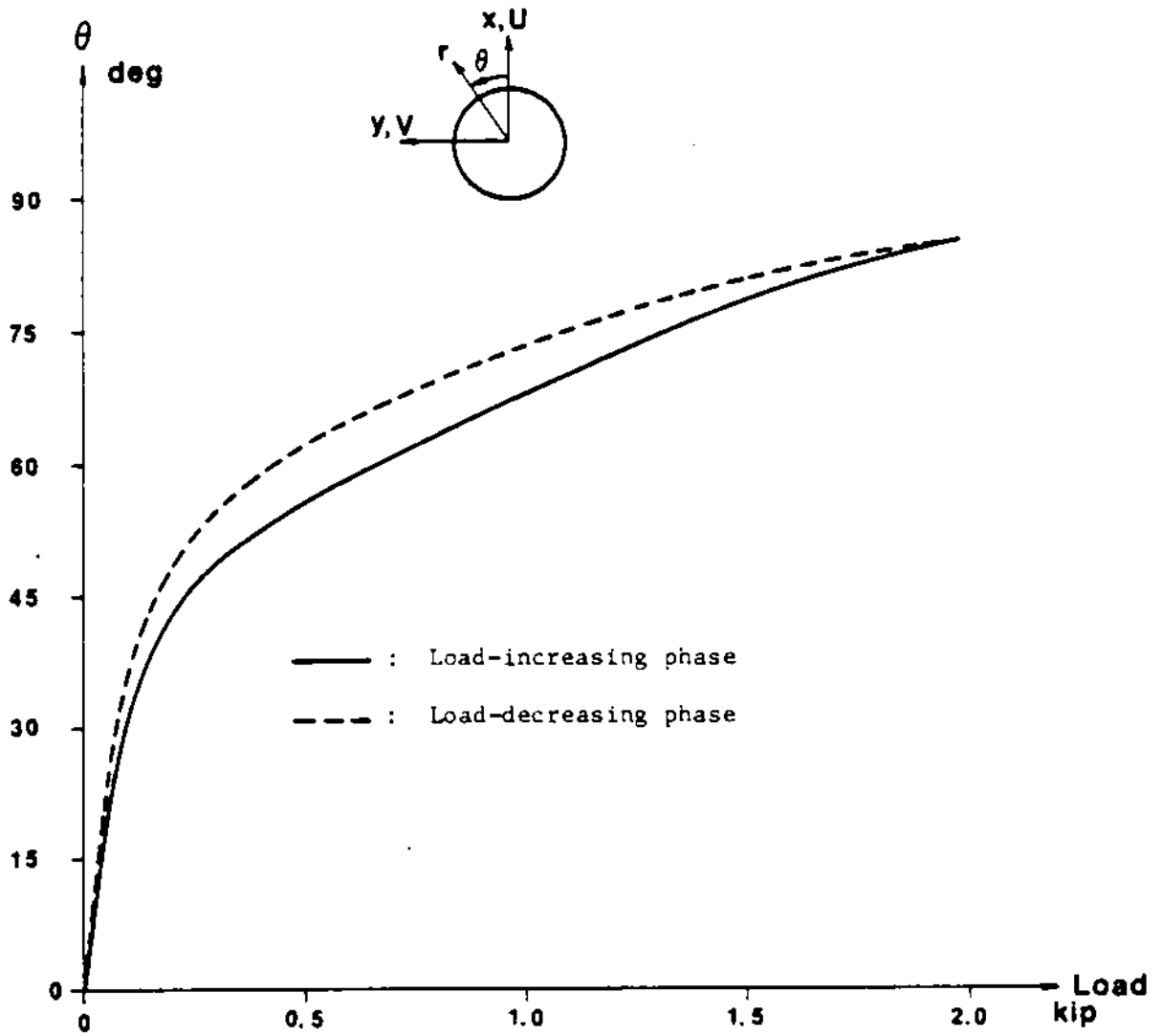

Figure 4.9 Contact region extends from 0 to θ, where θ is shown for the whole cycle of loading.

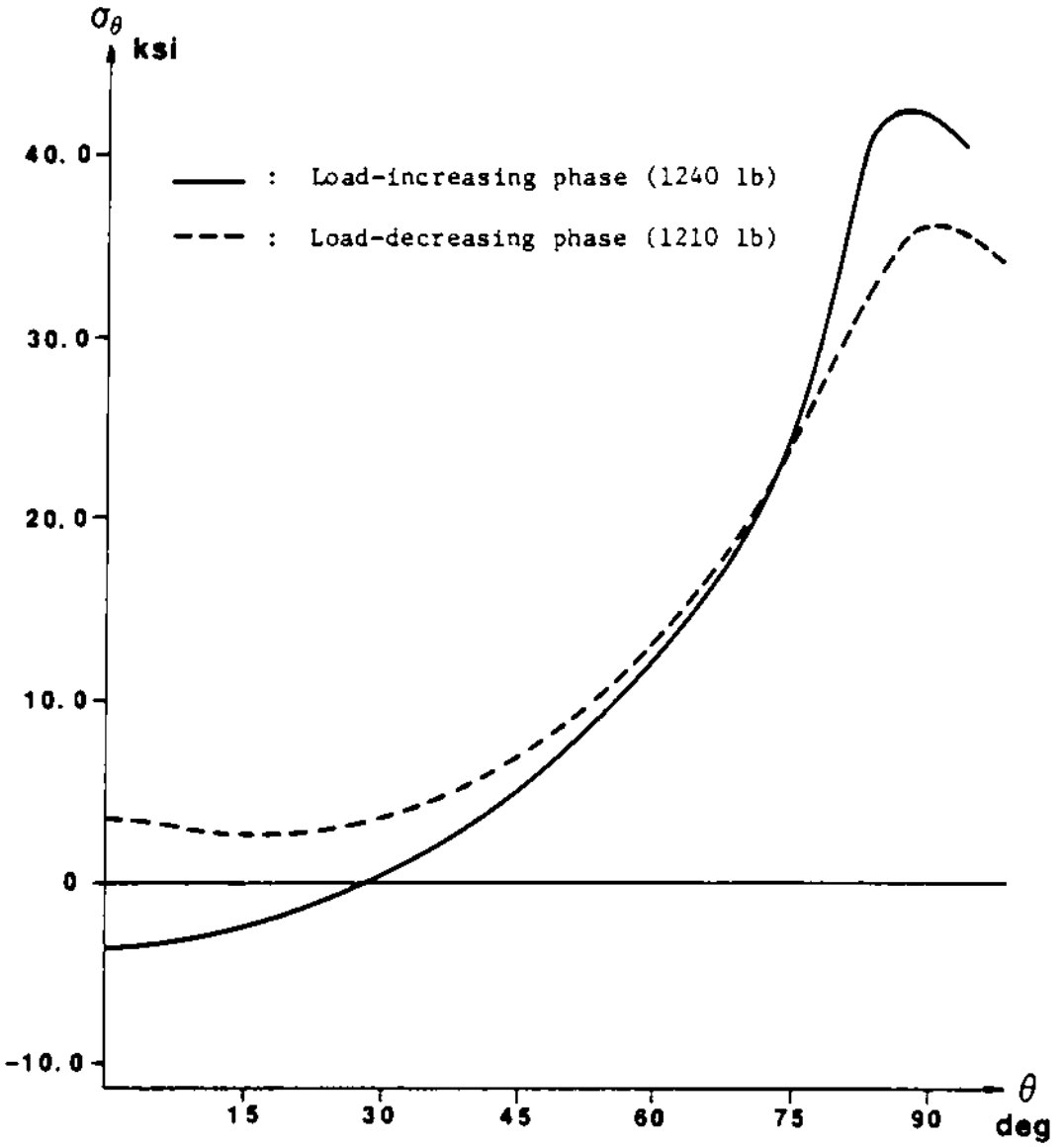

Figure 4.10 The hoop-stress distributions along the circumference of the hole for the two phases of loading cycle.

caused by the reversed sense of the frictional shear stress.

At the lower angle of contact a positive value of σ_θ is observed. The accumulated slip at the maximum load is considered to generate the tensile stress σ_θ at the decreased load level due to the predominant stick phenomena observed during the load decreasing phase and also due to the decreased radial compression.

4.6 Stress Concentration Factor

In most practical cases, the maximum tensile stress is the most crucial variable to determine the strength of the plate with a hole. While the stress concentration factor is constant for the plate with a hole without the pin, the nonlinearities induced by the changing contact configuration and the variation of frictional effects cause difficulties for the stress analysis of the pin joints of plates.

Even though there is no remarkable shifting of the location of the stress-concentration point with the load levels, it is observed that the magnitude of the stress concentration factor is a function of loading. In Figure 4.11 the stress concentration factor is plotted with respect to load levels for the entire loading cycle. The strong differences of stress concentration factors between the two phases of loading cycle is caused by the changed direction of frictional contribution to the deformation field.

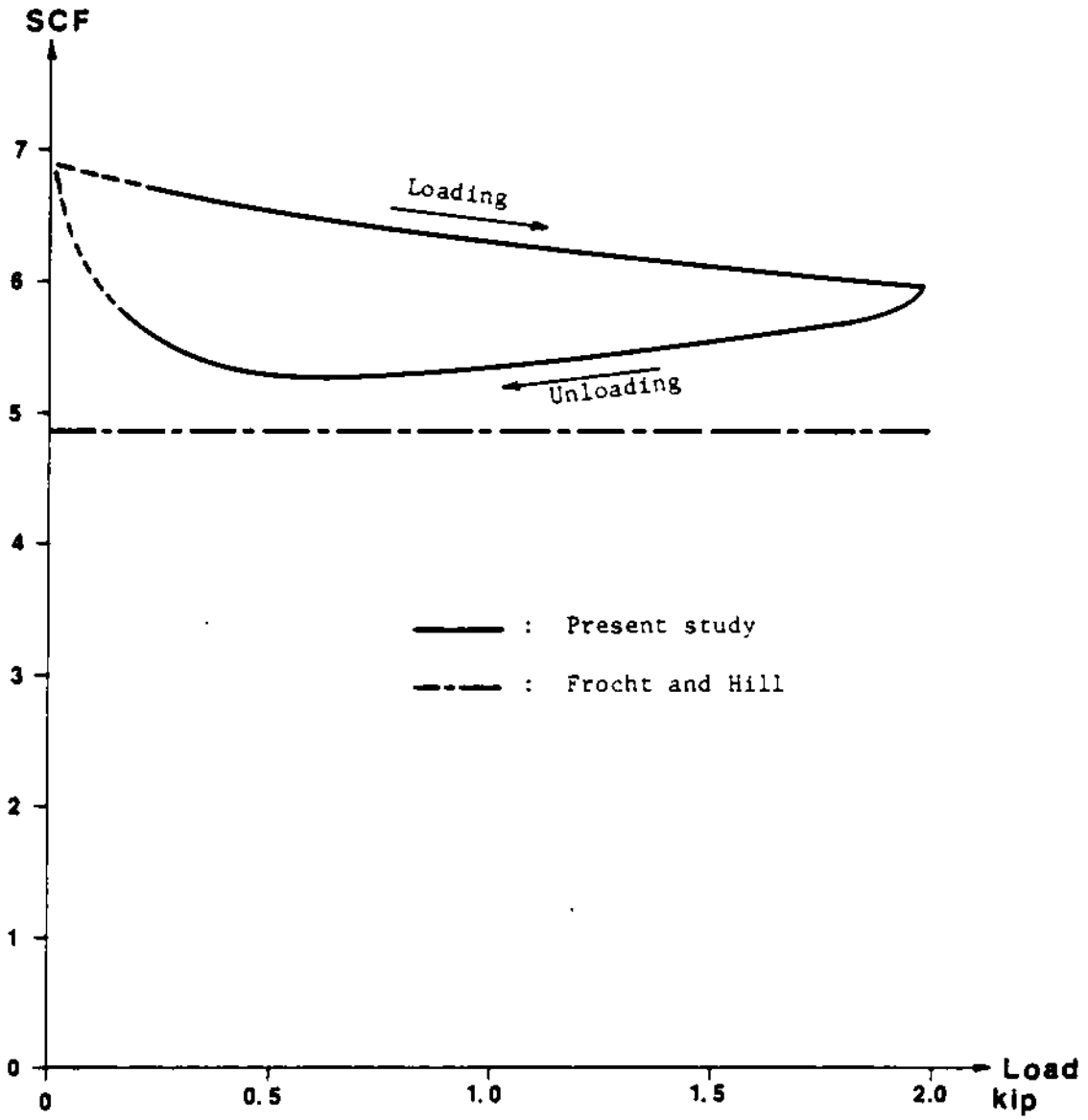

Figure 4.11 The variation of stress concentration factors plotted for the whole cycle of loading.

4.7 Discussion

There were not found any comparable data on the stress distribution in the literature obtained from experimental analyses with the same conditions as in the present study. Analytical studies of Klang [52] include friction, clearance fit, elastic pin, and both increasing and decreasing phases of load. His study provides good results for comparison with the present study, though he used an infinite plate model. Only the results which show a remarkable disagreement are considered here.

In Figure 4.12 shear stresses are shown for the unloading phase. The assumption in the analytical study as seen in the work of Klang is that the sign of the shear stress is fully reversed immediately after the unloading starts. However, as shown by the curves of experimental results, the sign of the shear stress is progressively reversed with unloading until it is reversed all over the contact region which is reduced to a small region at a low load level.

In Figure 4.13 hoop stresses are shown for both loading and unloading phases. During the load increasing phase the maximum hoop stress appeared where the angle is 86 degrees. However, after the onset of unloading, the point of the maximum hoop stress was shifted to the point of 90 degrees. Moreover, the shape of the curve changes with load levels even in the same phase of loading cycle, which is not considered in the analytical works.

The stress concentration factor is not constant with load levels. In the results of experimental study of Frocht and Hill [37], as shown in Figure 4.11, the variation of the concentration factor was not

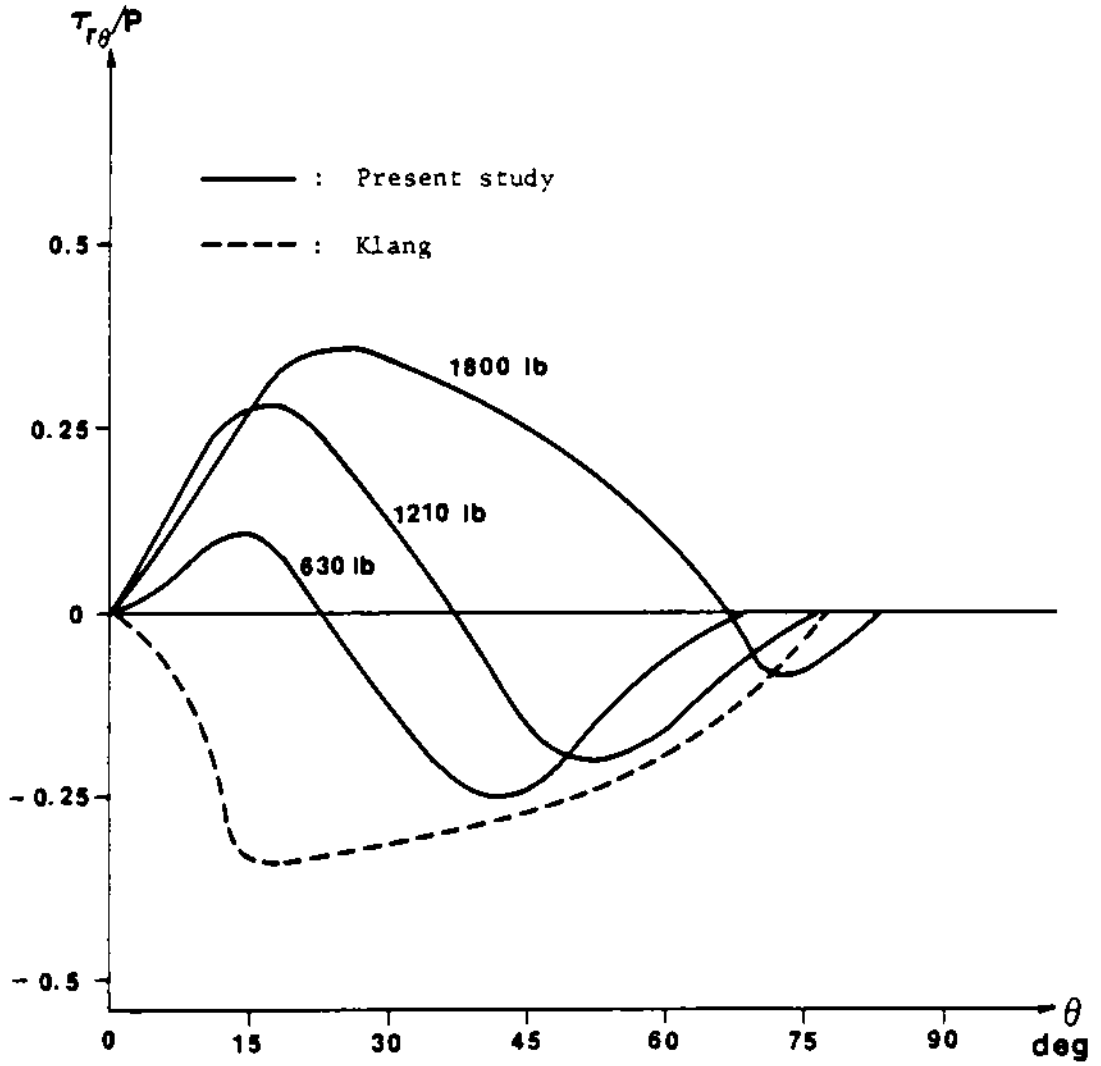

Figure 4.12 Comparison of the shear stress distributions between the results of the present study and the analytical work for the load-decreasing phase.

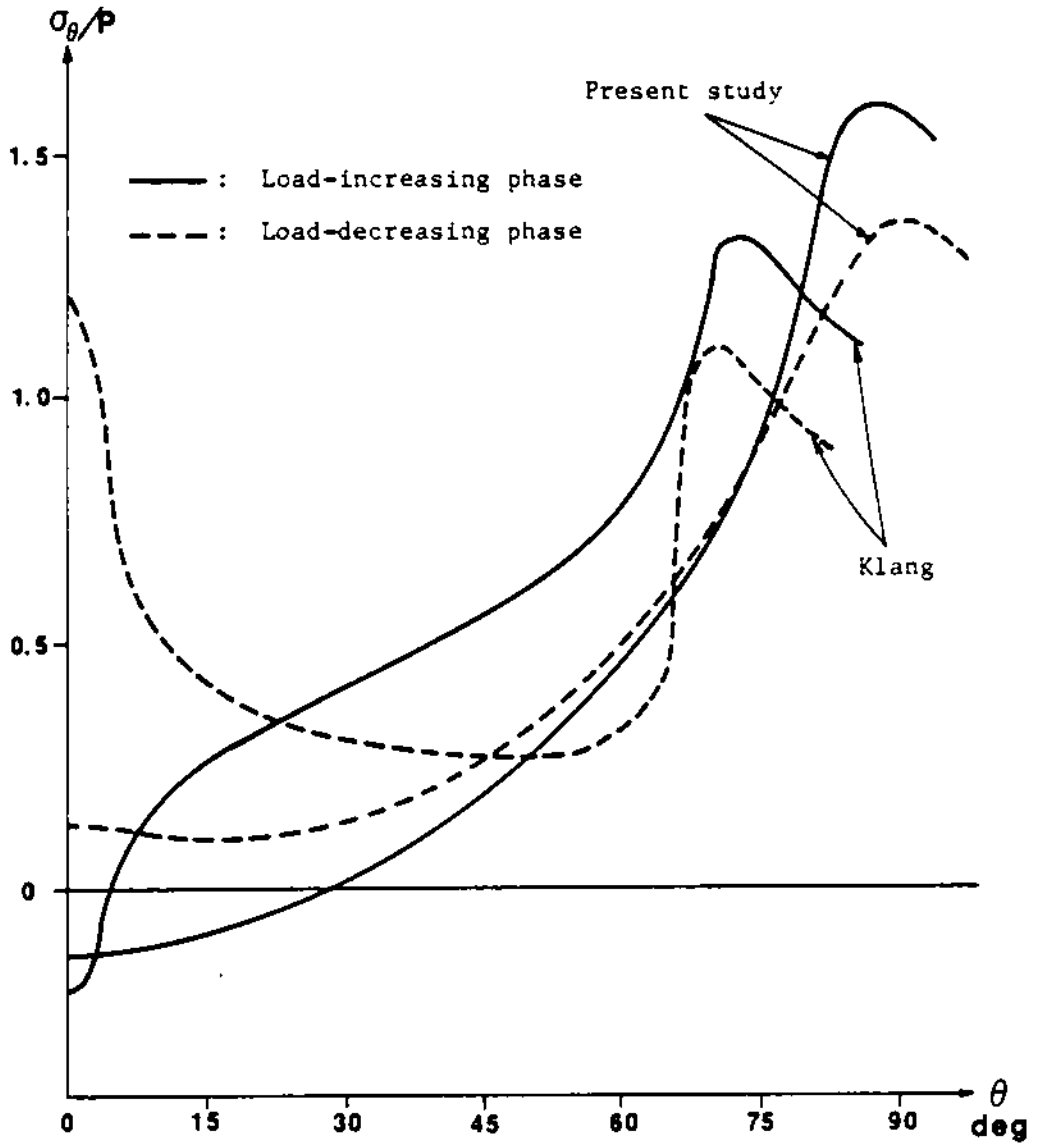

Figure 4.13 Comparison of the hoop stress distributions between the results of the present study and the result of the analytical study.

mentioned. However, the concentration factor varies with the load and shows a totally different behavior when the specimen is being unloaded. These are the combined effects of changing contact region and the sense of frictional shear stress being reversed progressively. The magnitude of the concentration factor was found to be larger in the present study than that of Frocht and Hill.

To confirm the flexural rigidity of the pin, which was a matter of concern due to the cantilever type loading configuration, the axial components of stresses along the hole boundary were integrated for comparison with the load. They showed a reasonable agreement over the whole load range, as presented in Figure 4.14. Considering the band of uncertainty which is intrinsic in the reduction of experimental data, this disagreement is regarded to be admissible.

Heyliger [58] used the displacement data along the periphery of the hole as the boundary conditions for his finite element scheme. The data was collected from the same experiment of the present work. The results of Heyliger's work are compared to those of the present work as shown in Figures 4.4 - 4.5. The discrepancies between the results of Heyliger and the present work are remarkable, which might have been caused by the method of analysis. The compressive radial stresses are comparable with each other as plotted in Figure 4.4, but the shear stress distribution of Heyliger does not show the zero value outside the contact region.

Initial deformations of the specimen grating at the boundary were considered to be caused by scraping in the process of specimen grating replication. To avoid this anomaly, strains were determined by the

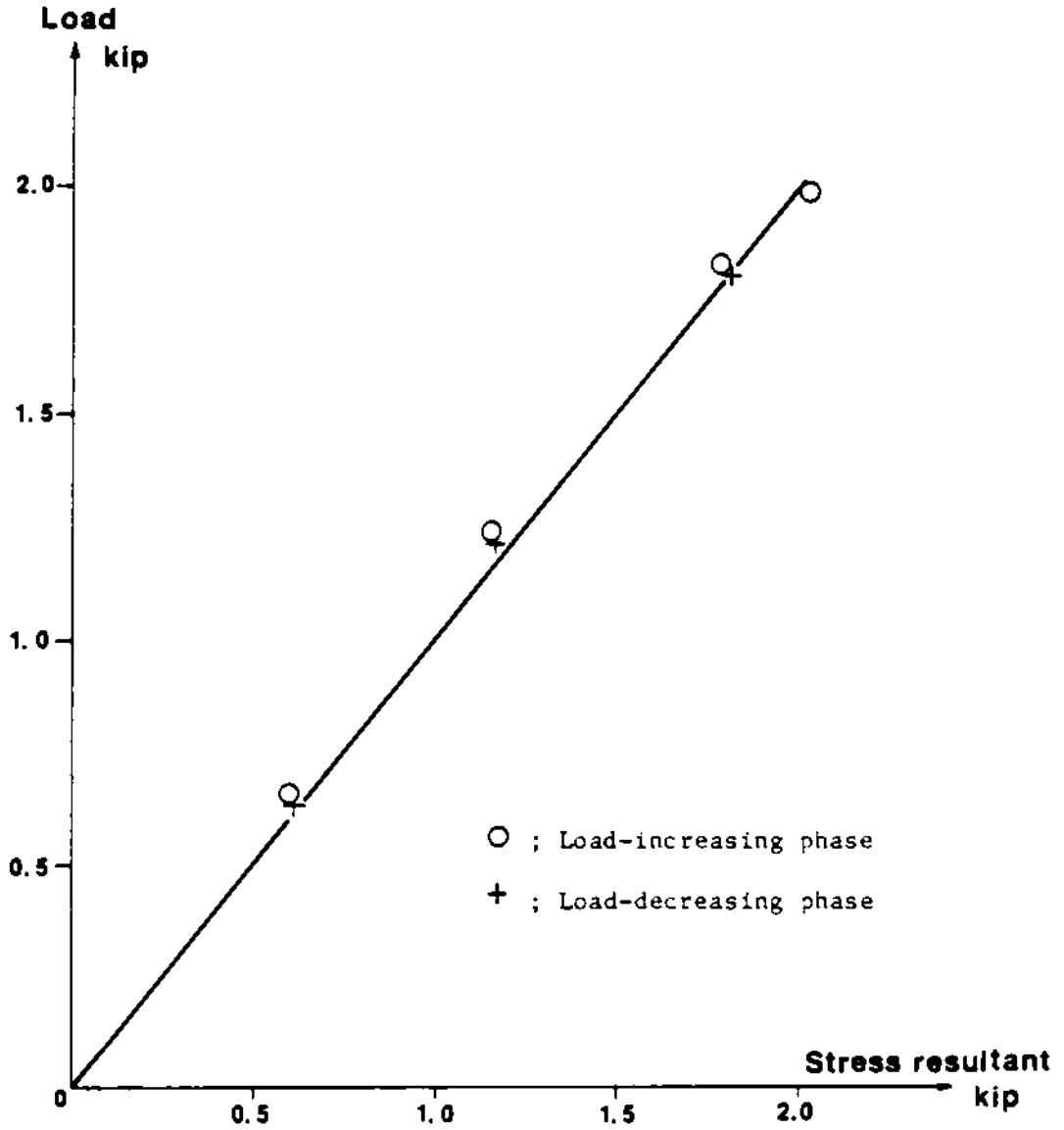

Figure 4.14 Load assessment by the integration of contact stresses. The flexural rigidity of the pin is confirmed within a reasonable error boundary.

algorithm of section 3.3 along three different outside concentric circles with the radius increment of 1.2 mm, and the results were extrapolated to the true contact boundary on the assumption of quadratic variation in radial direction.

The shear/normal stress ratios are plotted against the angle for the loading and the unloading phases at nearly the same load levels in Figure 4.15. Variations of stress ratios are interrelated to slip-stick phenomena which will be discussed in Chapter V. During the load-increasing phase nearly all the contact region is the slip region, and the ratio cannot have the maximum value larger than the kinetic coefficient of friction. As plotted by the dashed line in Figure 4.15, the magnitude of the negative ratio has the maximum value at 60 degrees which is the transition point between the slip and the stick regions. Thus, the kinetic coefficient of friction is 0.23, and the static coefficient of friction is 0.33.

This represents the contact condition of this experiment. The hole in the plate was bored with a single-pointed tool to a very fine machine finish and the pin was turned in a lathe to a fine finish. After replication of the gratings on the (noncontact) surface, the contact surfaces were prepared by scraping with a soft scraper and cleaned by solvents.

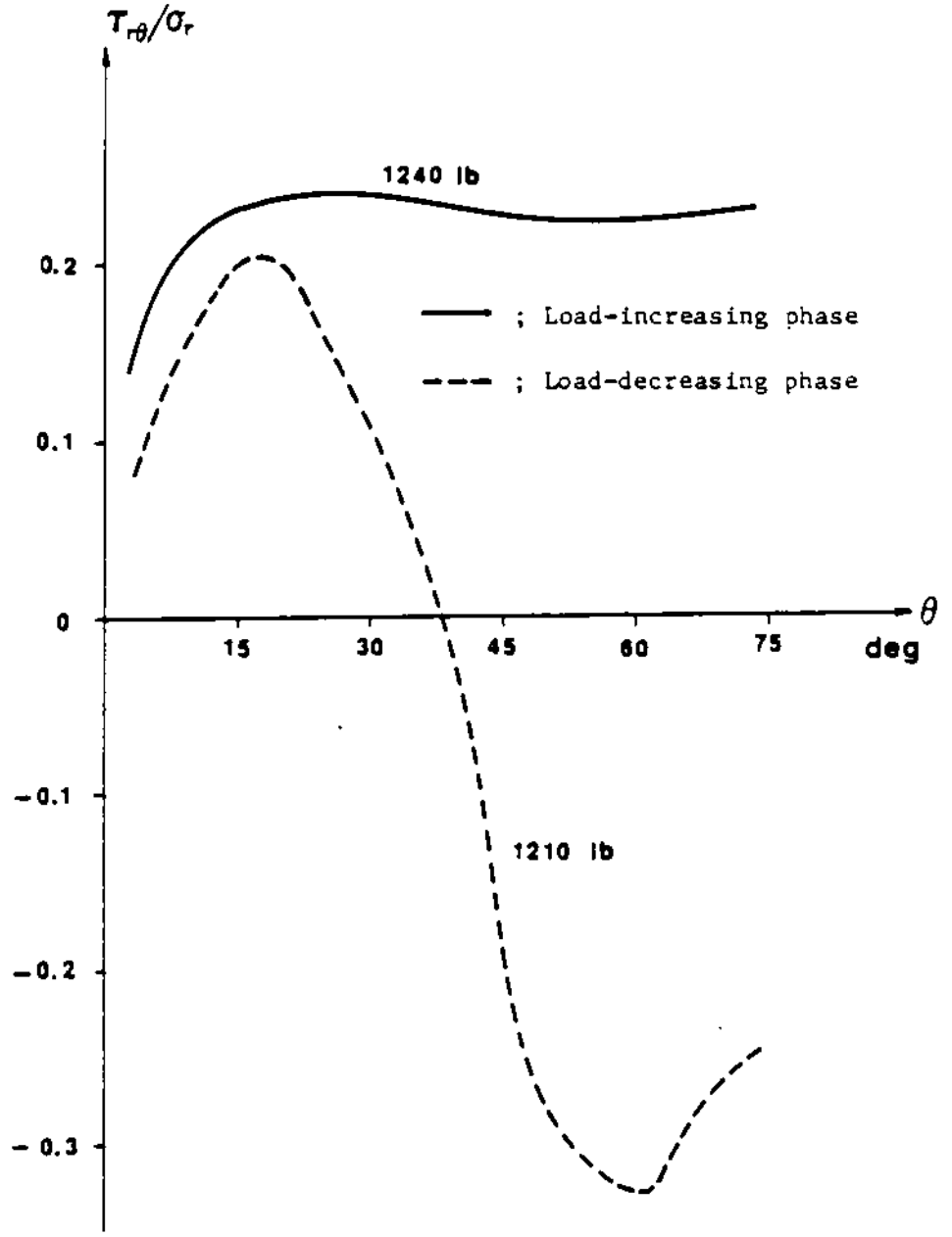

Figure 4.15 The shear/normal stress ratios for the two phases of loading cycle.

CHAPTER V

SLIP MEASUREMENTS

5.1 Introduction

One of the most serious effects of friction is fretting. Fretting is defined as a process of wear and fatigue occurring between the two surfaces having tangential relative motion of small amplitude. A systematic study of the fretting process requires that each of the variables in a fretting experiment be carefully measured. The relative motion of the two fretting surfaces is difficult to measure accurately because the amount of relative motion is small. Furthermore, the slip is not uniform over the contact region due to the elastic deformation of two bodies in contact. In order to obtain a value of slip in a fretting experiment, various methods have been employed, optical as well as mechanical [24,34]. However, none of these offers the high sensitivity or spatial resolution needed for measuring the distribution of slip. Besides, the mechanical system to measure the slip amplitude employs a few mechanical members. The deformation of the members and the relative displacements at the connections are of the same order of magnitude as the slip amplitude to be measured. There has been some controversy in the literature on wear rate and fretting fatigue, and it has been pointed out that this may be due to difficulties in accurately measuring slip amplitude. Especially, slip measurement along a curved interface, e.g., the contact region between the pin and the plate, is very difficult to measure with conventional methods.

Fretting fatigue between the pin and the plate, or pin-lug system, has long been a challenging problem to many investigators, and it has come to be generally agreed that the slip amplitude and the contact stress are the important factors to define the fretting phenomena. Nonetheless, there has been no serious attempt to measure the slip and slip amplitude at the contact region due to lack of appropriate techniques.

In this chapter, using the method of slip measurements presented in Appendix B, the slip-stick phenomena will be discussed. Then the slip amplitude will be determined by the graphical method. Slip amplitudes will be correlated with contact stresses and load levels.

5.2 Slip-Stick Phenomena

The high resolution and sensitivity of moiré interferometry employed in the present study allows the measurement of slip and non-uniform distribution of its amplitude over the contact region with sensitivity of a fraction of micron. Using the method of Appendix B, slip-stick region is first defined as shown in Figure 5.1. Tangential displacements in both the pin and plate were determined along their mutual boundaries from the fringe patterns, and the relative displacements were calculated. The curves of the relative tangential displacement are shown for each load level during the load-increasing phase of the loading cycle. Using the result obtained in Figure 4.9, the contact region is incorporated into Figure 5.1. The relative tangential displacement which occurs after the two surfaces come into contact is the slip. Curve A indicates the limit of the contact region at each load

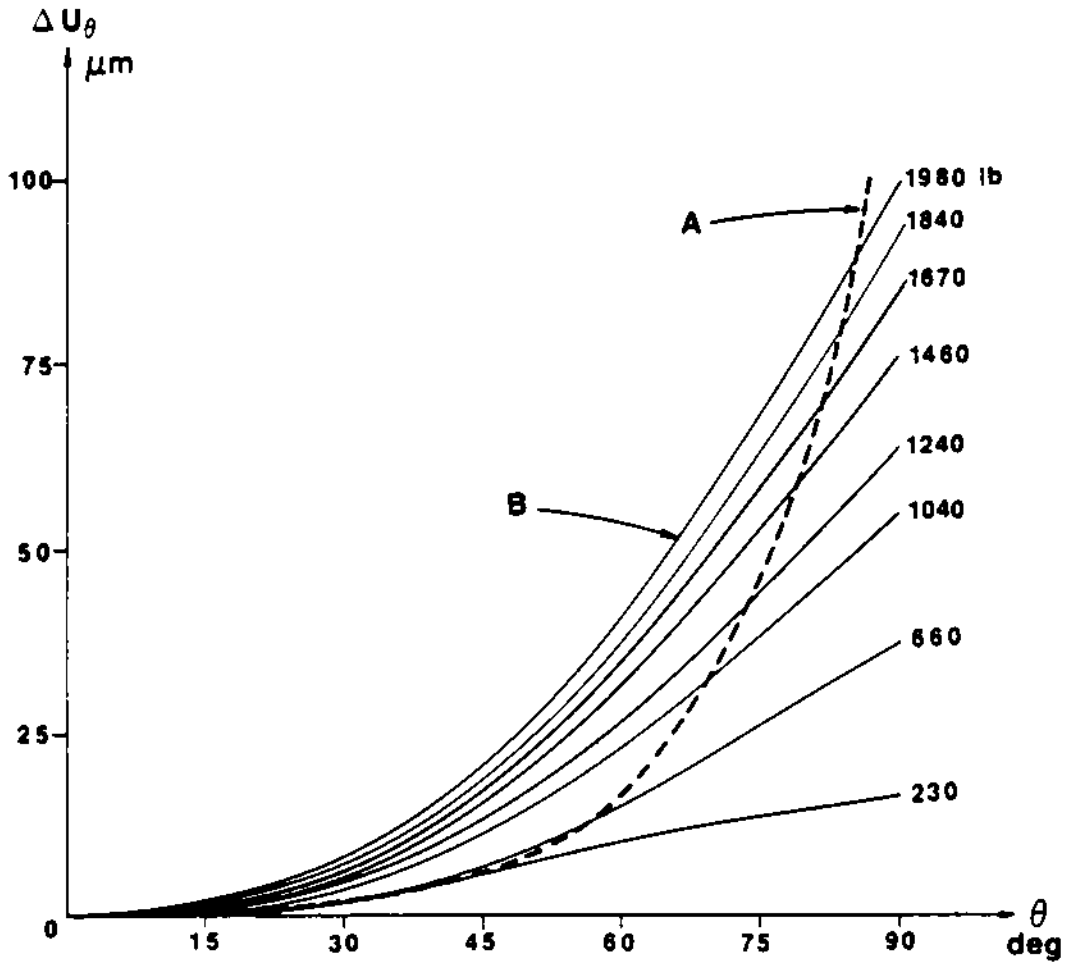

Figure 5.1 Slip-stick regions during the load-increasing phase are determined from these data.

level. The slip is measured from this curve upward. The sections where any two loading curves are overlapped represent the stick region between the two load levels. The stick regions are not observed except for the region near the initial contact point.

The slip amplitude can be obtained by measuring the height in the shaded band formed by the two curves (curve A and the ΔU curve at any load level) as explained in Appendix B. In Figure 5.2 the curves are the slip initiation curve and the curve for the final load level 1980 lb, respectively. Slip termination curve is defined by the maximum load applied to the specimen, while the slip initiation is fixed in the graph, determined by the points at the outer limit of the contact region at each load level.

Another family of curves showing slip-stick regions can be obtained from the load-decreasing phase as shown in Figure 5.3. It is observed that the two graphs in Figure 5.1 and 5.3 look quite different from each other. When the specimen is being unloaded, a large stick region is developed between the pin and the hole of the plate. In spite of the larger contact region during the load decreasing phase, the slip amplitude is smaller than in the load-increasing phase, which is attributed to the large stick region. Furthermore, the slip occurs at relatively low load levels, that is, with small contact stresses.

The distributions of slip amplitudes are plotted in Figure 5.4 for the whole cycle of loading and unloading.

The point of maximum slip amplitude also varied with the maximum load level for the specimen used in the present study. Figure 5.5 shows the location of the maximum slip amplitude which varies with the

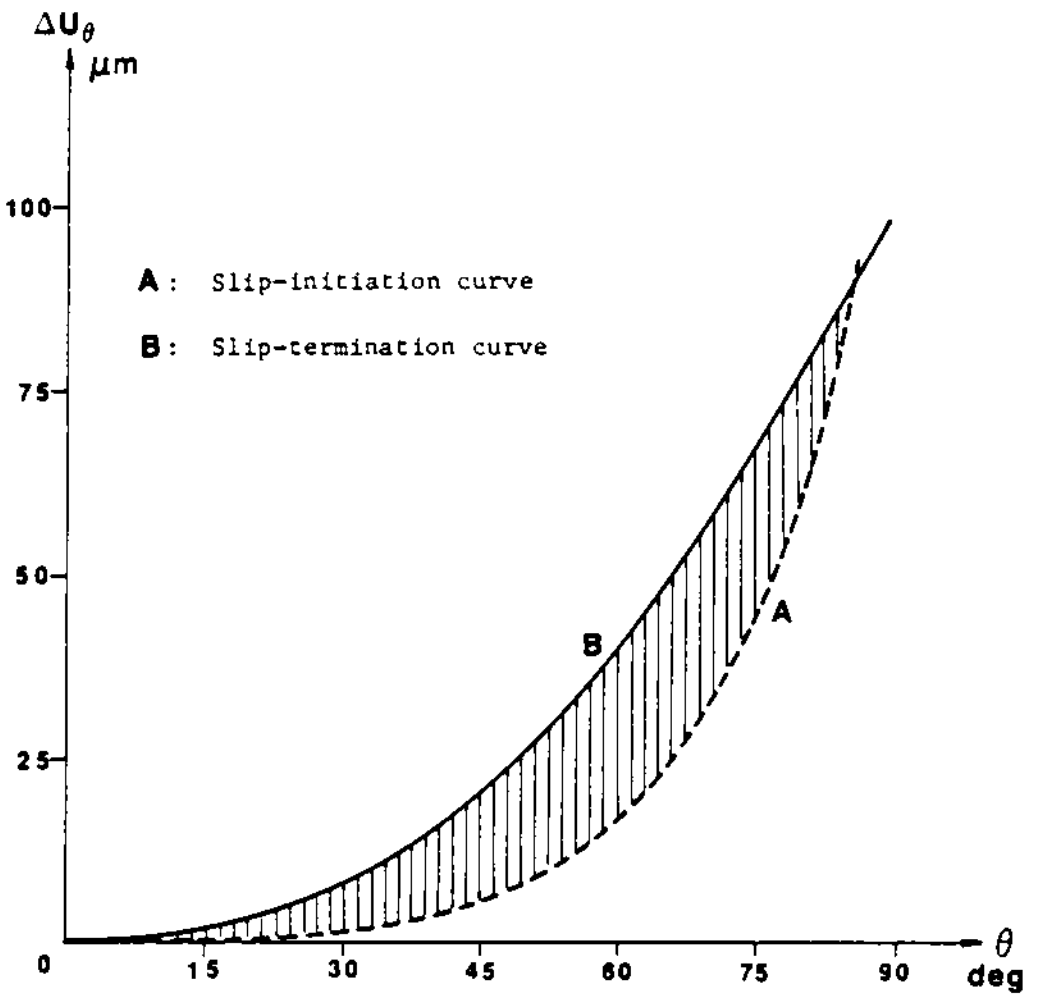

Figure 5.2 Slip amplitude can be determined by measuring the vertical width of the band defined by the two curves A and B.

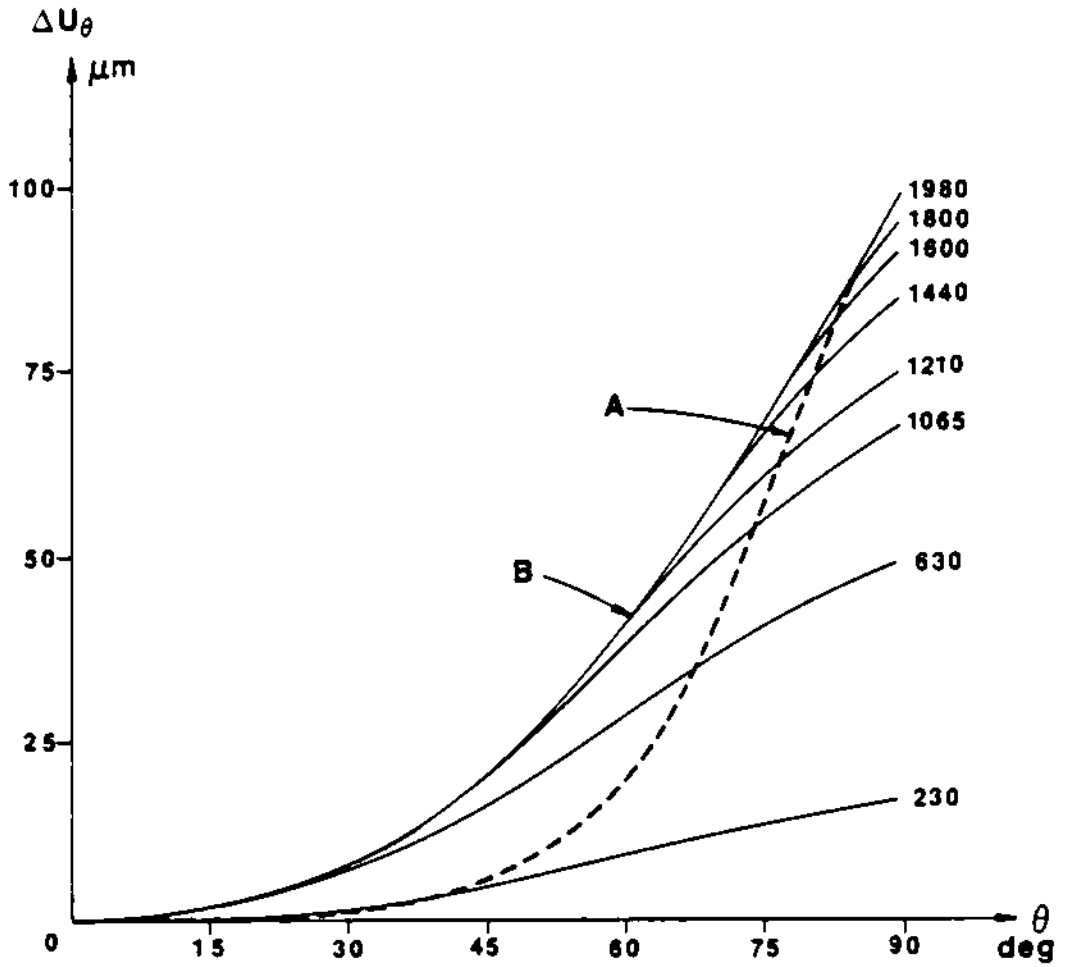

Figure 5.3 Slip-stick regions defined during the load-decreasing phase.

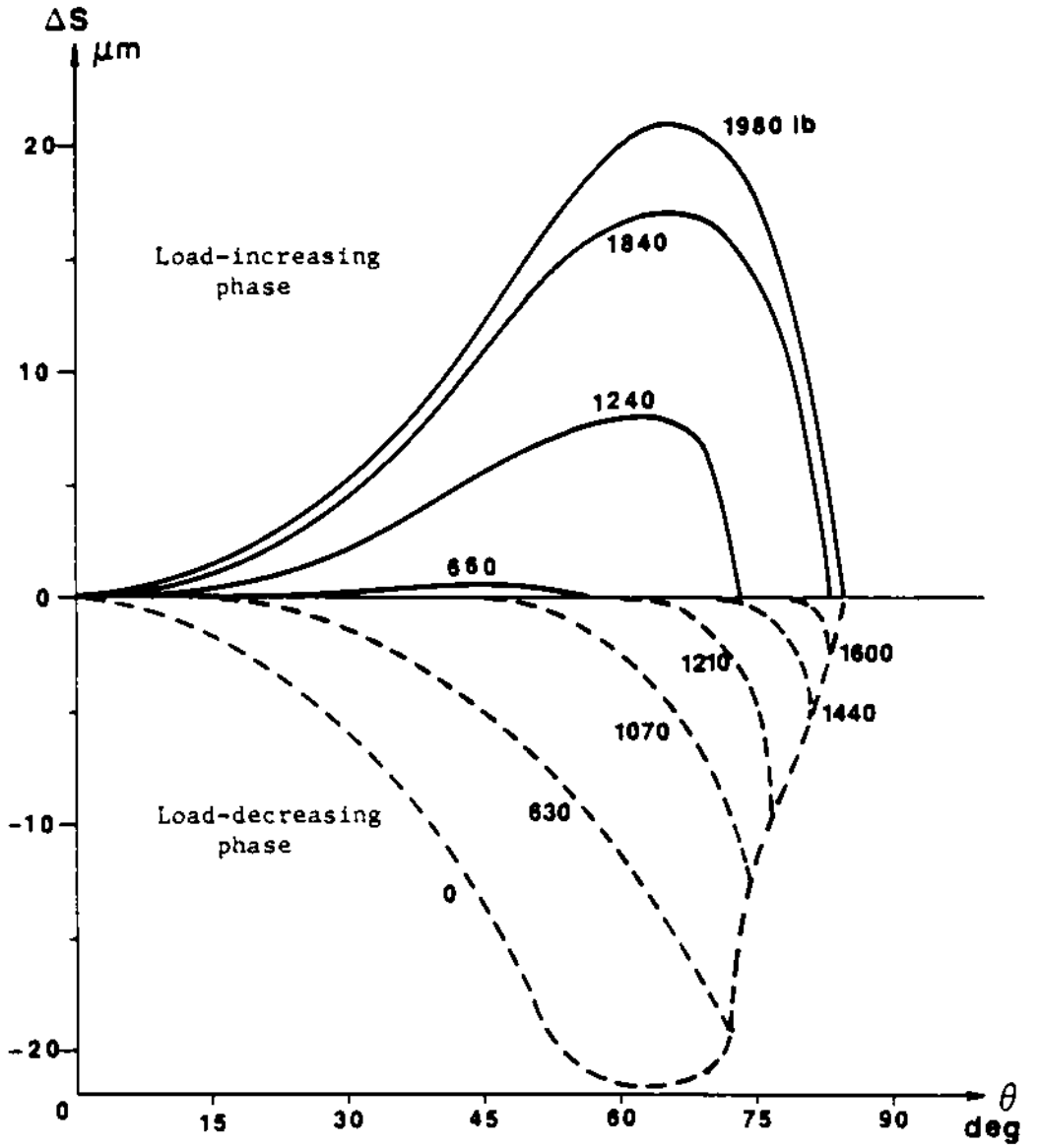

Figure 5.4 Variations of slip amplitudes plotted for the whole cycle of loading.

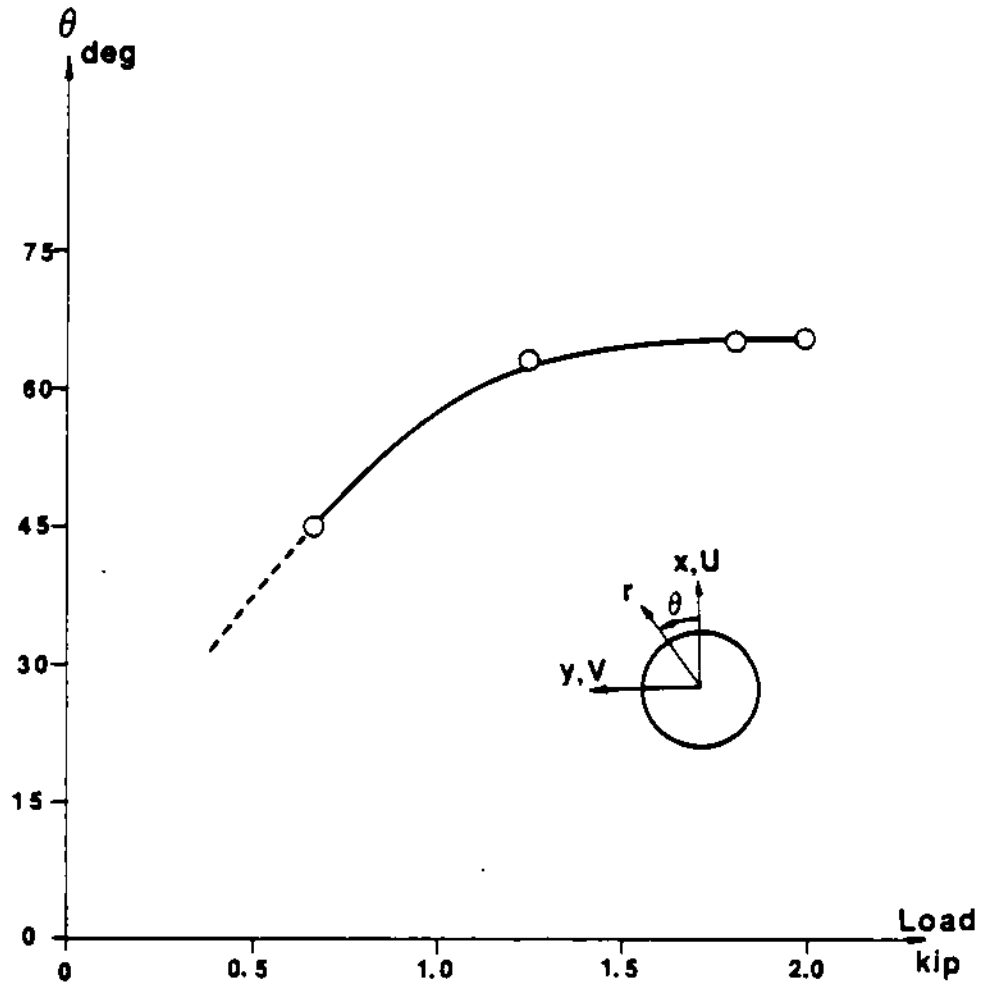

Figure 5.5 Location of the point of maximum slip-amplitude which varies with load levels.

load levels. The maximum slip amplitude was 22.5 μm at the angle of 63 degrees for the specimen in this study.

5.3 Discussion

Accurate measurements of cyclic slip during fretting experiments have been a significant problem in studies of fretting phenomena. The optical measurement technique used in this work not only allows the high sensitivity up to sub-wavelength levels, but also allows the spatial resolution to obtain the whole-field view of the slip-stick phenomena.

The measured distributions of slip and slip amplitude changing with the load indicate the importance of an accurate measurement of slip in a fretting experiment.

The stick was not observed during the load-increasing phase of the loading cycle, whereas the stick region was sustained during the load-decreasing phase over a large step of unloading. This observation is of great importance in building a model for the analysis of the fretting process. One of the features common to many proposed models of the fretting phenomena is the proposal that welding occurs between the two surfaces, and the subsequent breaking of such welds results in the removal or transfer of surface material. In the present study the slip did not vary monotonously with load during the load-decreasing phase due to the tenacious stick at the contact region. Thus the present result indicates that welding may occur mainly during the unloading phases.

A recent investigation into the relationship between the fatigue life and a fretting damage parameter k, defined as $\sigma_r \tau_{r\theta} \Delta s$, has been established by Boddington and Ruiz using the dovetail-joint model of turbine-blade root connections. Using the maximum stresses and slip magnitude, the variation of the parameter k is obtained with respect to the contact angle θ as shown in Figure 5.6. Parameter k has the maximum value at 52 degrees, which implies that the fretting damage is most likely to occur at 52 degrees with cyclic loading.

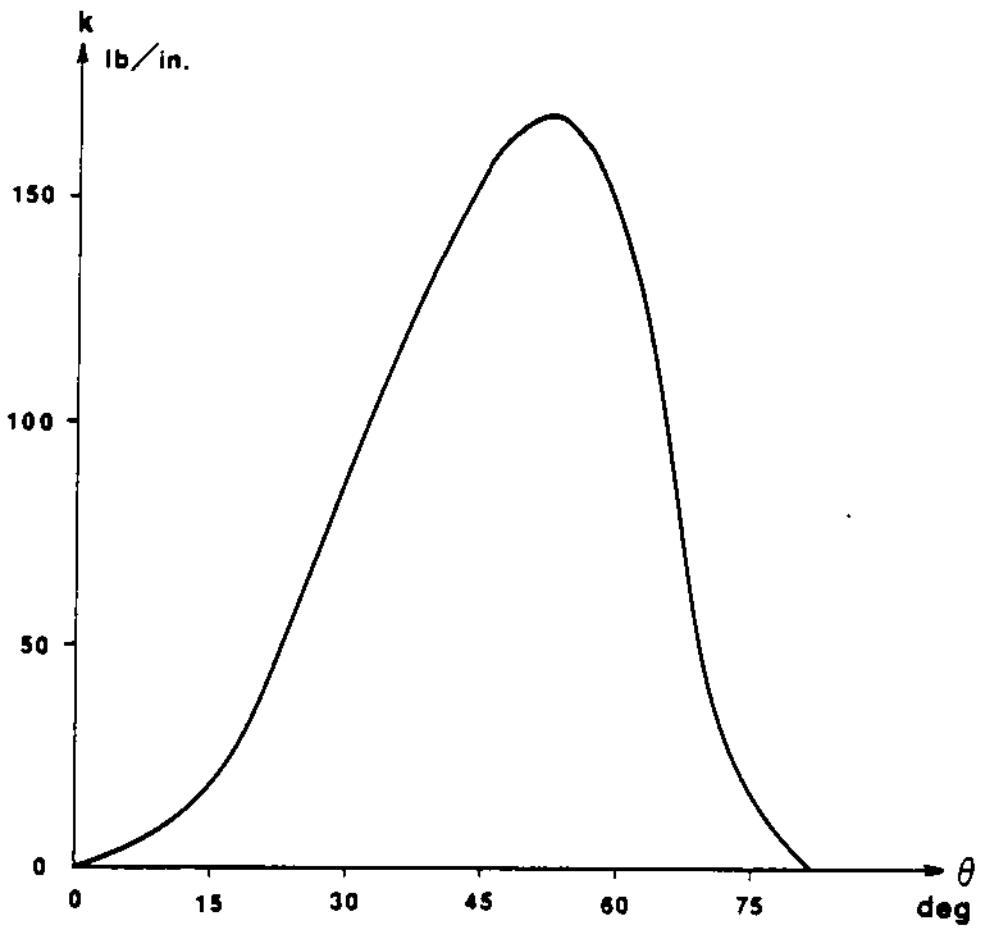

Figure 5.6 The fretting parameter k.

CHAPTER VI

SUMMATION AND CONCLUSIONS

6.1 Summation

An optical technique, moiré interferometry, was applied to study the frictional phenomena around the pin joints of plates. Stress fields along the interface between the pin and the plate, variation of contact region with load increments, and slip-stick phenomena were measured.

(1) Stress Fields

The radial stress increases with load during the load-increasing phase, but the rate of increase is not the same all over the contact region. Due to the frictional constraints the deformation at the lower contact-angle region is restricted, and the increasing rate of radial compression is small in this region. During the load-decreasing phase the changing direction of frictional force influences the radial stress field. At any load level, the radial stress is larger in the load-decreasing phase.

The change of shear stress (tangential to the contacting surface) is reversed during the load-decreasing phase. This is due to the reversed sense of relative tangential displacement at the contact region. However, the change of the magnitude of shear stresses occurs progressively with the decrease of load. This contrasts with the assumptions of other investigators who conclude that the direction of the friction force changes immediately with the onset of unloading.

Hoop stresses along the circumference of the hole is also influenced by friction. The hoop stress increases with the contact angle and load level during the load increasing phase. The hoop stress is observed to attain the maximum value at the angle 86° for the load-increasing phase. Then when the load is decreased from the maximum level, the tangential deformation of the hole returning back to the state of lower load level is restrained by the reversed shear stress. The value of the hoop stress at the non-contact region is decreased rapidly, while within the contact region, the decreasing rate of the hoop stress is very small, which is attributed to the stick phenomenon between the pin and the plate.

(2) Stress Concentration Factor

The point of maximum hoop stress was at the angle of 86° for the load-increasing phase. By many investigators the point of maximum hoop stress was predicted near the end of the contact region. However, the results of the present work differs from those predictions. It was observed in the present study that the maximum hoop stress is achieved at 86° without regard to the size of contact region, or load level.

During the load-decreasing phase the stick phenomenon within the contact region and the reversed shear stress direction caused the maximum hoop stress to be relieved significantly. In this case the maximum hoop stress is achieved at 90°.

Stress concentration factors were influenced by the geometrical configuration, i.e., changing contact regions, and by the shear stresses in the contact region.

(3) Contact Region

Maximum contact angle obtained at the load level of 1975 lb was 85 degrees. Contact regions of the load decreasing phase were larger than those of the load decreasing phase due to the frictional constraints against the relative deformations between the pin and the plate.

(4) Slip Amplitude

Slip occurs with different amplitudes between the two phases of the loading cycle. In spite of the larger contact angles during the load-decreasing phase the slip amplitude is smaller than during the load-increasing phase. It is explained by the stick phenomena which occurs at high load levels.

6.2 Conclusions

Moiré interferometry has been applied for measuring frictional phenomena around the pin-joints of plates. From the experimental analysis, the following conclusions are drawn.

(1) The measurements of the relative deformations between the pin and the plate can be easily achieved with a sub-wavelength resolution.

(2) The algorithms developed have been shown to be effective.

(3) Stress concentration factors are greatly different between the two phases of loading and unloading.

(4) The sign of frictional shear stress is reversed gradually from the outer limit of contact region as the unloading progresses.

(5) Radial compressive stresses are larger during the load-decreasing phase than during the load-increasing phase.

(6) Variation of contact region does not alter the location of the stress-concentration point.

(7) Stick phenomenon is prominent during the load-decreasing phase.

6.3 Recommendations

The principal aim of the present study was to provide experimental evidence of the influence of friction around the pin joint of plates. Although it was not intended to be an exhaustive survey of all branches of the subjects, the following recommendations will offer a more comprehensive understanding of the frictional phenomena around the pin joints of plates:

(1) Use of a large plate with negligible end effects for the comparison with the theoretical results.

(2) Use of lubricants for absolute measurements of frictional effects.

(3) Preparation of the contact surfaces free of contaminations.

(4) Fatigue tests to compare the results of stress analysis with the post-failure results.

(5) Different materials of specimens.

REFERENCES

1. Forsyth, P.J.E., "Occurrence of Fretting Fatigue Failure in Practice," Fretting Fatigue, Ch.4, ed. Waterhouse, R.B., Applied Science Publishers LTD, (1981).

2. Waterhouse, R.B., "Theories of Fretting Process," Fretting Fatigue, Ch.9, ed. Waterhouse, R.B., Applied Science Publishers LTD, (1981).

3. Waterhouse, R.B., "Physics and Metallurgy of Fretting," AGARD-CP-161, pp 8.1-8, Jan (1975).

4. Poon, C. and Hoeppner, D.W., "The Effect of Environment on the Mechanism of Fretting Fatigue," Wear, 52, pp.175-191, (1979).

5. Waterhouse, R.B., "Avoidance of Fretting Fatigue Failures," Fretting Fatigue, Ch.10, ed. Waterhouse, R.B., Applied Science Publishers LTD, (1981).

6. Harris, W.J., "The Influence of Fretting on Fatigue," AGARD-CP-161, pp. 7.1-12, Jan (1975).

7. Bowden, F.P. and Tabor, D., "Friction," Heinemann Educational Books, Ltd., (1974).

8. Johnson, R.L. and Bill, R.C., "Fretting in Aircraft Turbine Engines," AGARD-CP-161, pp. 5.1-17, Jan. (1975).

9. Lee, J.R., "Fretting in Helicopters," AGARD-CP-161, pp. 3.1-10, Jan. (1975).

10. Hoeppner, D.W., "Fretting of Aircraft Control Surfaces," AGARD-CP-161, pp. 1.1-7, Jan. (1975).

11. Buch, A., "Fatigue and Fretting of Pin-Lug Joints With and Without Interference Fit," Wear, 43, pp.9-16, (1977).

12. Volker von Tein and Seibert, P.E., "Fretting of Structures for Modern V.G. Fighters," AGARD-CP-161, pp. 2.1-12, Jan. (1975).

13. Grundy, J.D., "Comments on 'The Effect of Fretting on Fatigue'," Wear, 55, pp.385-386, (1979).

14. Wharton, M.H. and Waterhouse, R.B., "Environmental Effects in the Fretting Fatigue of Ti-6Al-4V," Wear, 62, pp. 287-297, (1980).

15. Gansheimer, J. and Friedrich, G., "Testing Machines to Study Fretting Wear," Wear, 17, pp. 407-419, (1971).

16. Kovalevskii, V.V., "The Mechanism of Fretting Fatigue in Metals," Wear, 67, pp. 271-285, (1981).

17. Newcomb, T.P. and Spurr, R.T., "The Interaction between Friction Materials and Lubricants," Wear, 24, pp. 69-76, (1973).

18. Hoeppner, D.W. and Gates, F.L., "Fretting Fatigue Consideration in Engineering Design," Wear, 70, pp. 155-164, (1981).

19. Hoeppner, D.W., "Comments on 'Initiation and Propagation of Fretting Fatigue Cracks'," Wear, 43, pp. 267-270, (1977).

20. Endo, K. and Goto, K., "Effects of Environment on Fretting Fatigue," Wear, 48, pp. 347-367, (1978).

21. Reeves, R.K. and Hoeppner, D.W., "Scanning Electron Microscope Analysis of Fretting Fatigue Damage," Wear, 48, pp. 87-92, (1978).

22. Wharton, M.H., Waterhouse, R.B., Hirakawa, K., and Nishioka, K., "The Effect of Different Contact Materials on the Fretting Fatigue Strength of an Aluminum Alloy," Wear, 26, pp. 253-260, (1973).

23. Sandifer, J.P., "Evaluation of Methods for Reducing Fretting Fatigue Damage in 2024-T3 Aluminum Lap Joints," Wear, 26, pp. 405-412, (1973).

24. Ohmae, N. and Tsukizoe, T., "The Effect of Slip Amplitude on Fretting," Wear, 27, pp. 281-294, (1974).

25. Hoeppner, D.W. and Goss, G.L., "Metallographic Analysis of Fretting Fatigue Damage in Ti-6Al-4V MA and 7075-T6 Aluminum," Wear, 27, pp. 175-187, (1974).

26. Goss, G.L. and Hoeppner, D.W., "Normal Load Effects in Fretting Fatigue of Titanium and Aluminum Alloys," Wear, 27, pp. 153-159, (1974).

27. Hoeppner, D.W. and Goss, G.L., "A Fretting Fatigue Damage Threshold Concept," Wear, 27, pp. 61-70, (1974).

28. Waterhouse, R.B., "Comments on 'The Effect of Environment on the Mechanism of Fretting Fatigue'," Wear, 58, pp. 391-392, (1980).

29. Reeves, R.K. and Hoeppner, D.W., "The Effect of Fretting on Fatigue," Wear, 40, pp. 395-397, (1976).

30. Chivers, T.C. and Gordelier, S.C., "Fretting Fatigue Palliatives: Some Comparative Experiments," Wear, 96, pp. 153-175, (1984).

31. Waterhouse, R.B., "Fretting Wear," Wear, 100, pp. 107-118, (1984).

32. Alic, J.A. and Hawley, A.L., "On the Early Growth of Fretting Fatigue Cracks," Wear, 56, pp. 377-389, (1979).

33. Alic, J.A., Hawley, A.L., and Urey, J.M., "Formation of Fretting Fatigue Cracks in 7075-T7351 Aluminum Alloy," Wear, 56, pp. 351-361, (1979).

34. Sproles, E.S. and Duquette, D.J., "Results of High Resolution Slip Measurements in a Fretting Experiment," Wear, 52, pp. 95-104, (1979).

35. O'Connor, J.J., "The Role of Elastic Stress Analysis in the Interpretation of Fretting Fatigue Failures," Fretting Fatigue, Ch.2, ed. Waterhouse, R.B., Applied Science Publishers LTD, (1981).

36. Edwards, P.R., "The Application of Fracture Mechanics to Predicting Fretting Fatigue," Fretting Fatigue, Ch.3, ed. Waterhouse, R.B., Applied Science Publishers LTD, (1981).

37. Frocht, M.M. and Hill, H.N., "Stress-Concentration Factors Around a Central Circular Hole in a Plate Loaded Through Pin in the Hole," J. Appl. Mech., Trans. ASME, 62, pp. A5-A9, (1940).

38. Nisida, M. and Saito, H., "Stress Distributions in a Semi-infinite Plate Due to a Pin Determined by Interferometric Method," Exp. Mech., pp. 275-279, (1966).

39. Oplinger, D.W., Parker, B.S., and Katz, A., "Moire Measurement of Strains and Deformations in Pin-Loaded Composite Plates," Proc., SESA Spring Meeting, (1979).

40. Lambert, T.H. and Braily, R.J., "The Influence of Coefficient of Friction on the Elastic Stress Concentration Factor for a Pin-Jointed Connection," Aeronaut. Q., 13, pp. 17-29, (1962).

41. Jessop, H.T., Snell, C., and Holister, G.S., "Photoelastic Investigation on Plates with Single Interference Fit Pin with Load Applied (a) to Pin only and (b) to Pin and Plate Simultaneously," Aeronaut. Q., 9, pp. 147-163, (1958).

42. Hussain, M.A. and Pu, S.L., "Slip Phenomenon of a Circular Inclusion," J. Appl. Mech., Trans. ASME, 38, pp. 627-633, (1971).

43. Pih, H. and Knight, C.E., "Photoelastic Analysis of Anisotropic Fiber Reinforced Composites," J. Comp. Matls., 3, pp. 94- , (1969).

44. Ghosh, S.P., Dattaguru, B., and Rao, A.K., "Photoelastic Studies on Progress of Separation in Interference Fits," Exp. Mech., pp 8-15, (1982).

45. Chang, F.K., Scott, R.A., and Springer, G.S., "Strength of Mechanically Fastened Composite Joints," J. Comp. Matls., 16, pp. 470-494, (1982).

46. Prabhakaran, R., "Photoelastic Investigation of Bolted Joints in Composites," Composites, 13(3), pp. 253-256, (1982).

47. Wilkinson, T.L. and Rowlands, R.E., "Analysis of Mechanical Joints in Wood," Exp. Mech., 21(11), pp. 408-414, (1981).

48. Wong, C.M.S. and Matthews, F.L., "A Finite Element Analysis of Single and Two-Hole Bolted Joints in Fiber Reinforced Plastic," J. Comp. Matls., 15, pp. 481-491, (1981).

49. Bremond, C. and Durelli, A.J., "Experimental Analysis of Displacements and Shears at Surfaces of Contact," Exp. Mech., 21(3), pp. 105-110, (1981).

50. Cox, H.L. and Brown, A.F.C., "Stresses Round Pins in Holes," Aeronaut. Q., pp. 357-372, (1964).

51. De Jong, Th., "Stresses around Pin-Loaded Holes in Elastically Orthotropic or Isotropic Plates," J. Comp. Matls., 11, pp. 313-331, (1977).

52. Klang, E.C., "The Stress Distribution in Pin Loaded Orthotropic Plates," PhD Dissertation, VPI & SU, (1983).

53. Post, D., et al., "Relative Displacement Measurements for Two-Body Problems," Proc. SESA Spring Conference, (1985).

54. Post, D., "Optical Interference for Deformation Measurements - Classical Holographic and Moiré Interferometry," Mech. of Nondest. Testing, ed. Stinchcomb, W.W., Plenum Press, NY, pp. 1-53, (1980).

55. Post, D., "Moiré Interferometry at VPI & SU," Exp. Mech., , 23(2), pp. 203-210, (1983).

56. Ruiz, C., Post, D. and Czarnek, R., "Moiré Interferometric Study of Dovetail Joints," J. Appl. Mech., 107, pp. 109-114, (1985).

57. Durelli, A.J. and Parks, V.J., "Moiré Fringes as Parametric Curves," Exp. Mech., 7(3), pp. 97-104 (March 1967).

58. Heyliger, P.R., "Frictional Phenomena in Planar Elastic Contact Stress Problems," Ph.D. Dissertation, VPI & SU, (1986).

APPENDIX A

BASIC DATA

Fringe patterns are the basic data for the analysis. At lower load levels the fringe patterns are not symmetric. The dissymmetry of the patterns is caused by the relative magnitude of the perturbed alignment of the specimen compared to the magnitude of loads. It is decreased with the increase of loads as shown in Figure A.1 - A.2, and at higher load levels the influence of these fluctuations becomes negligible.

Figure A.1 Fringe patterns at each load level during the load-increasing phase: (1) U-20 lb

(2) V - 20 lb

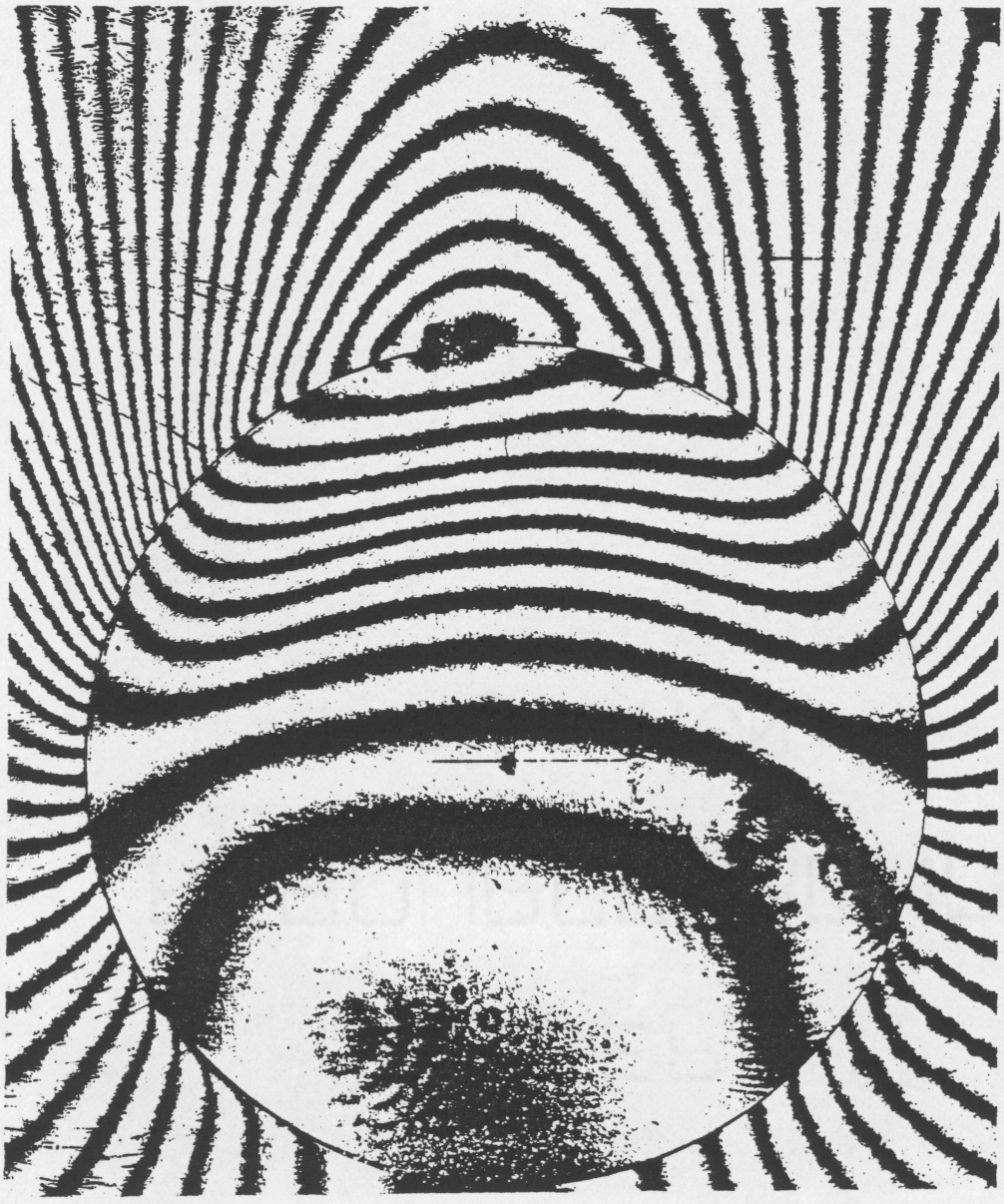

(3) U - 230 lb

(4) V - 230 lb

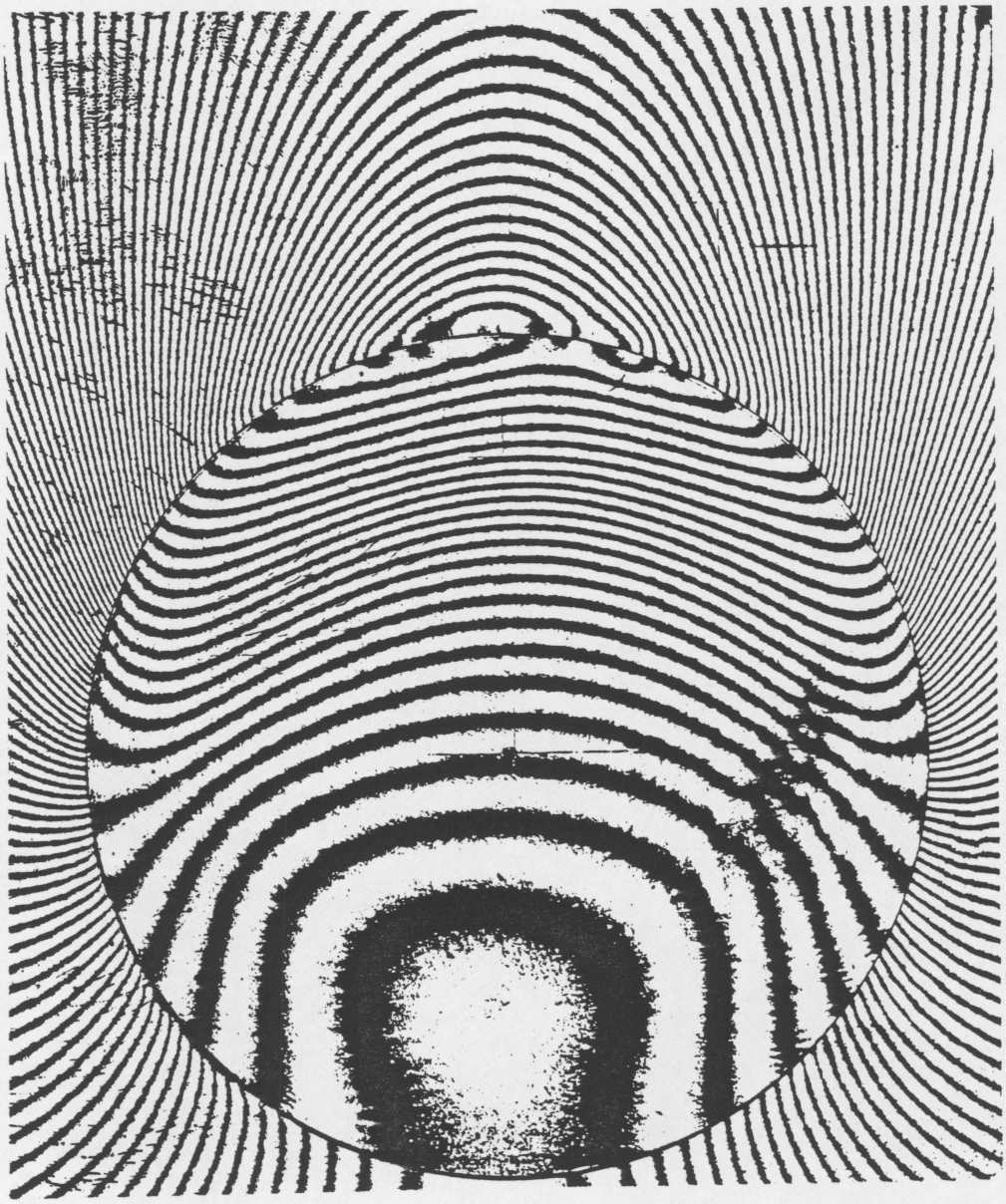

(5) U - 660 lb

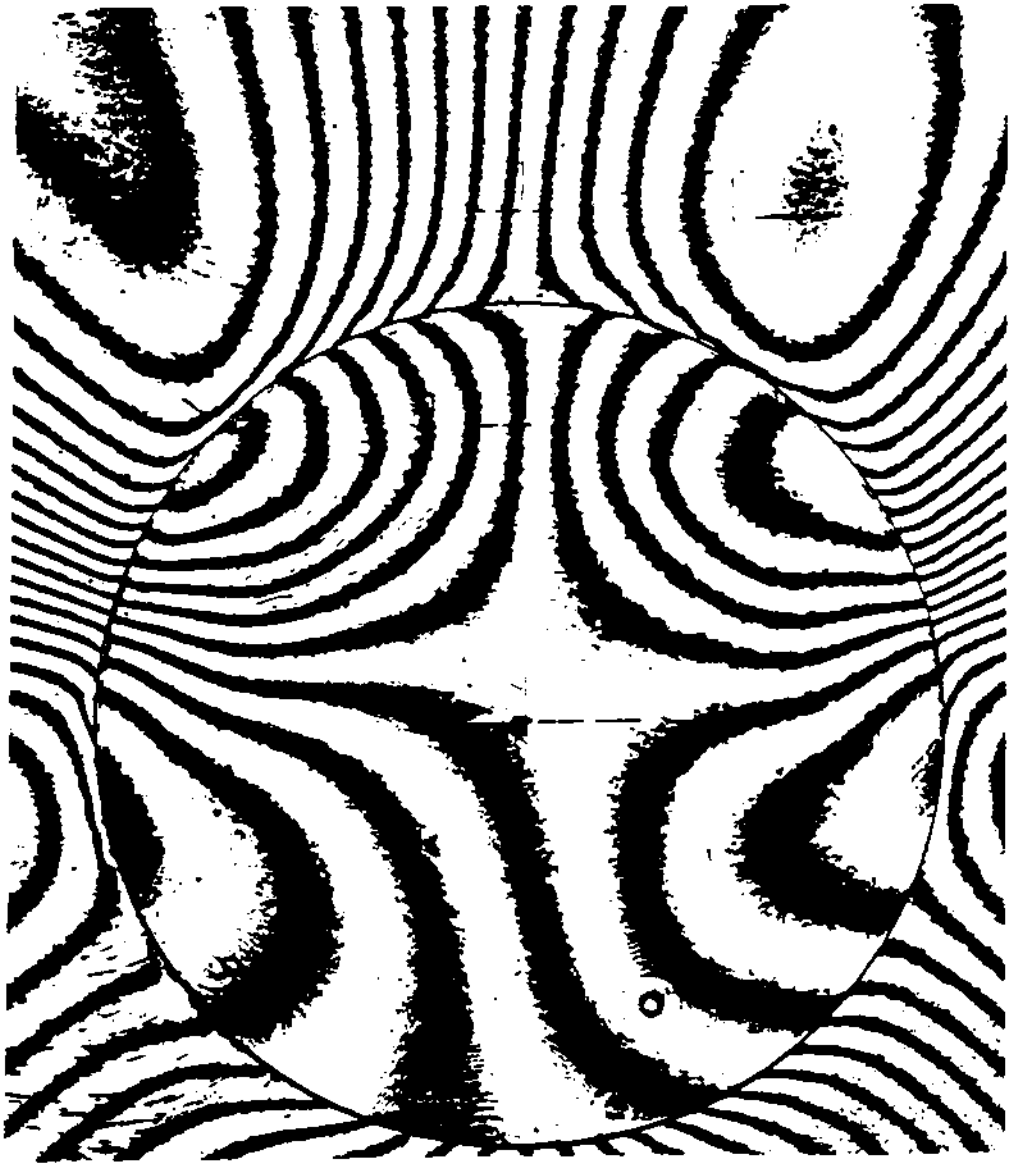

(6) V - 660 lb

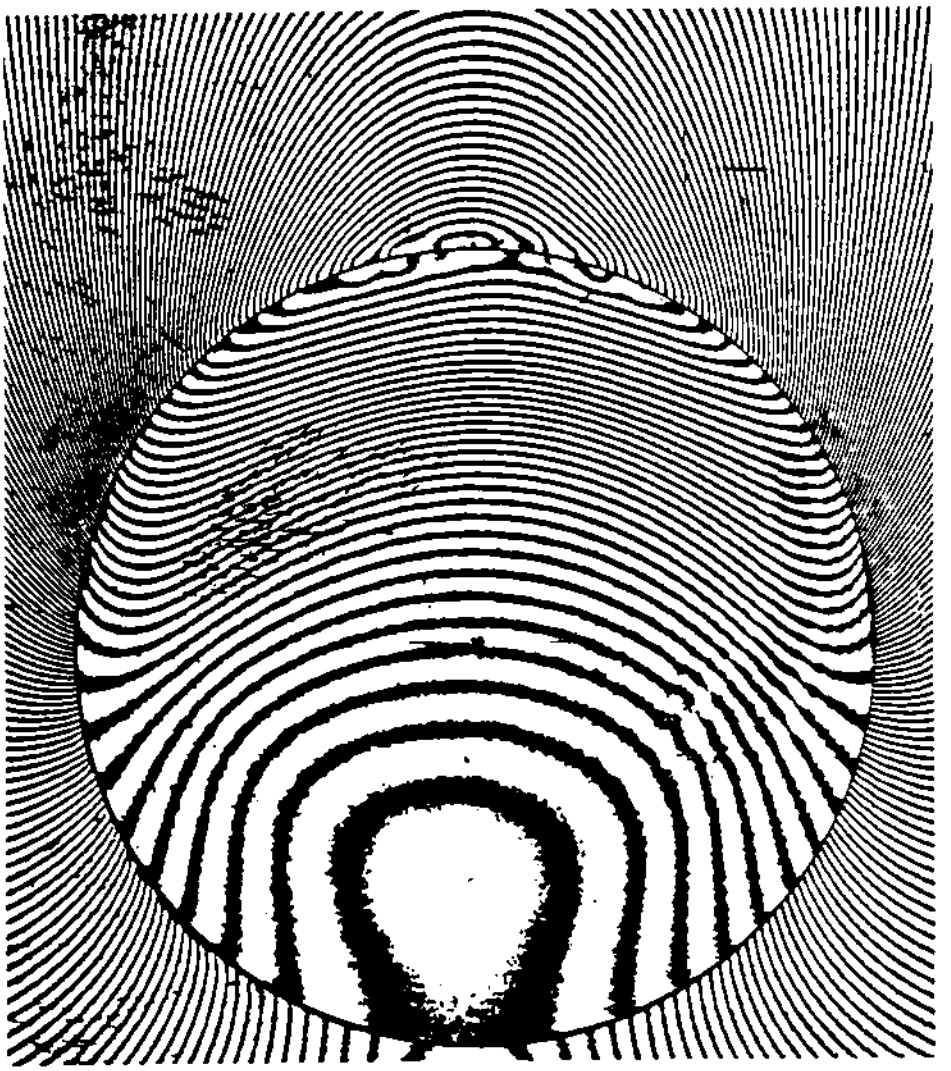

(7) U - 1040 lb

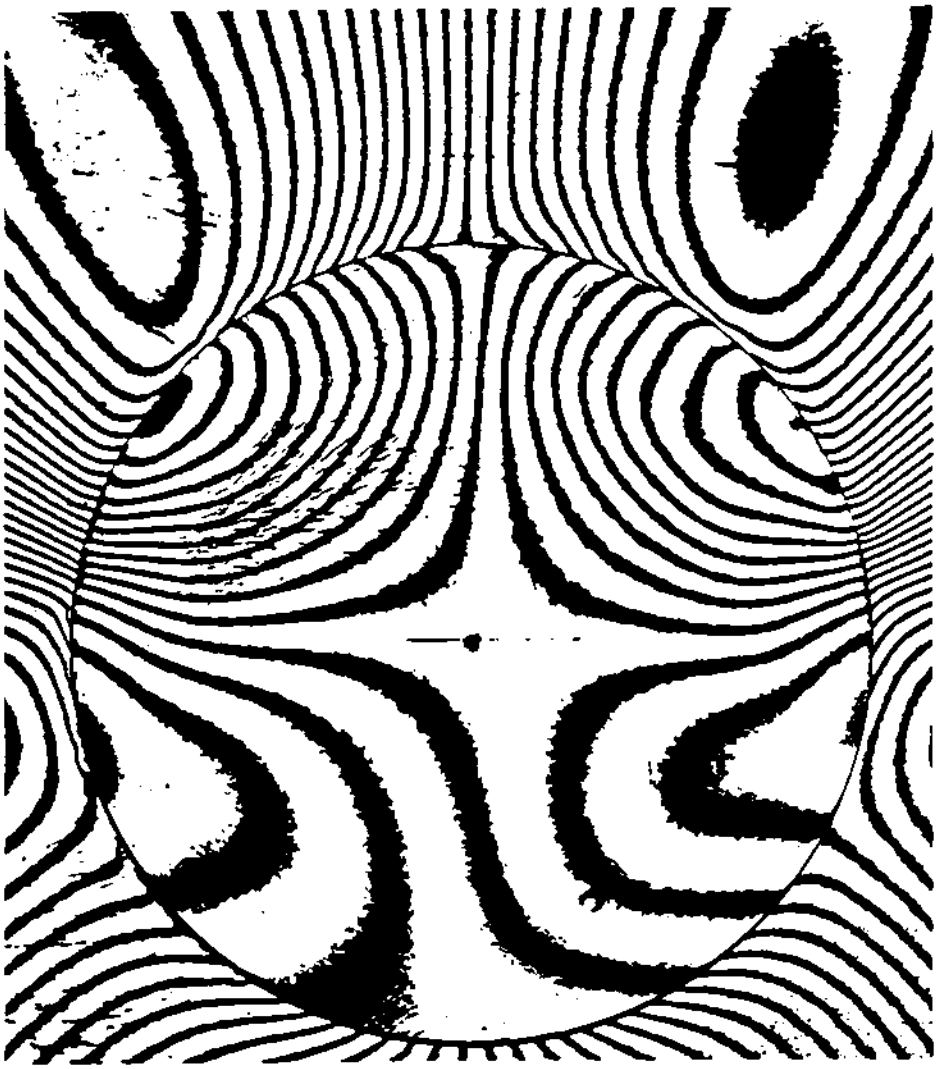

(3) V - 1040 lb

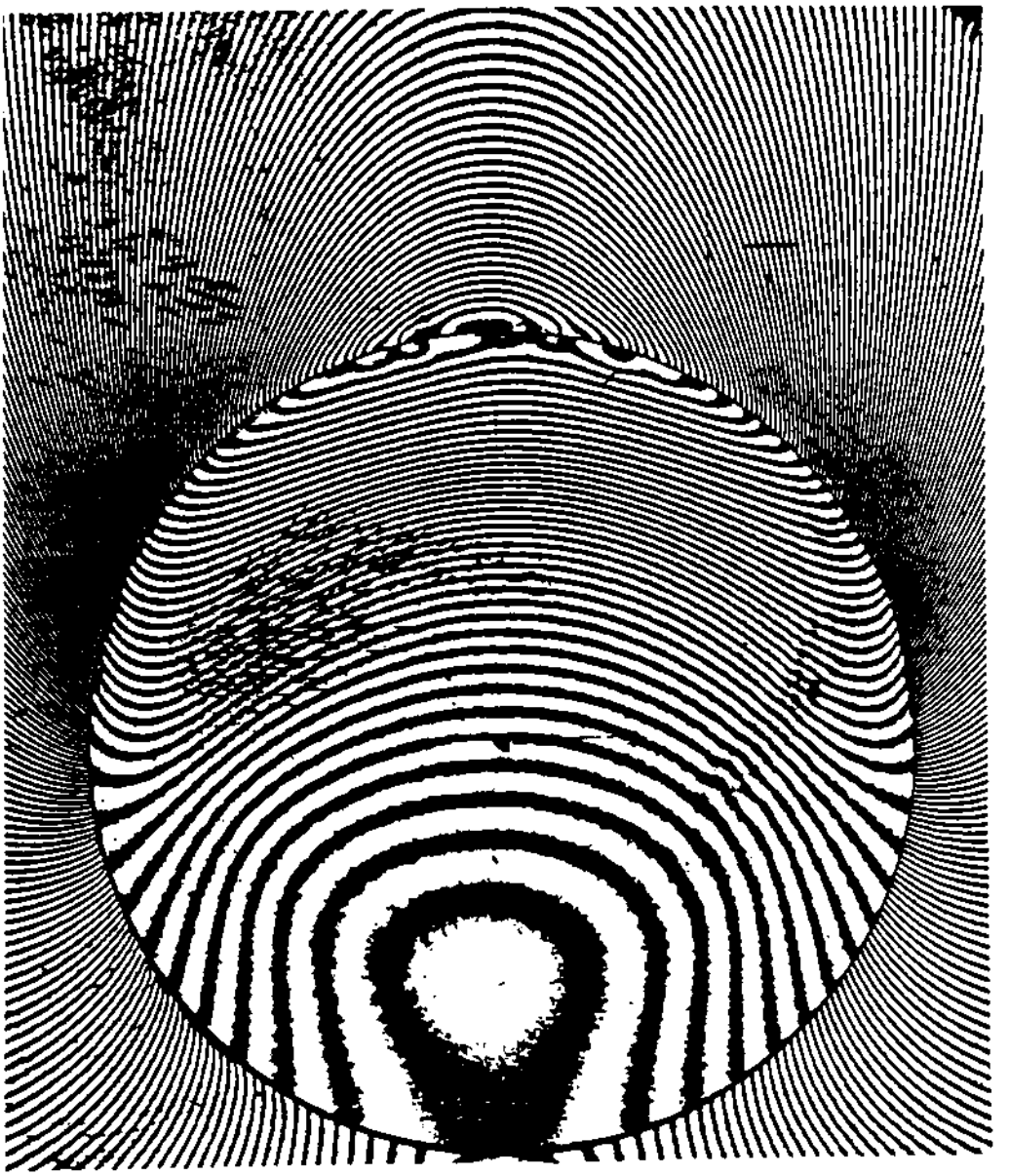

(9) U - 1240 lb

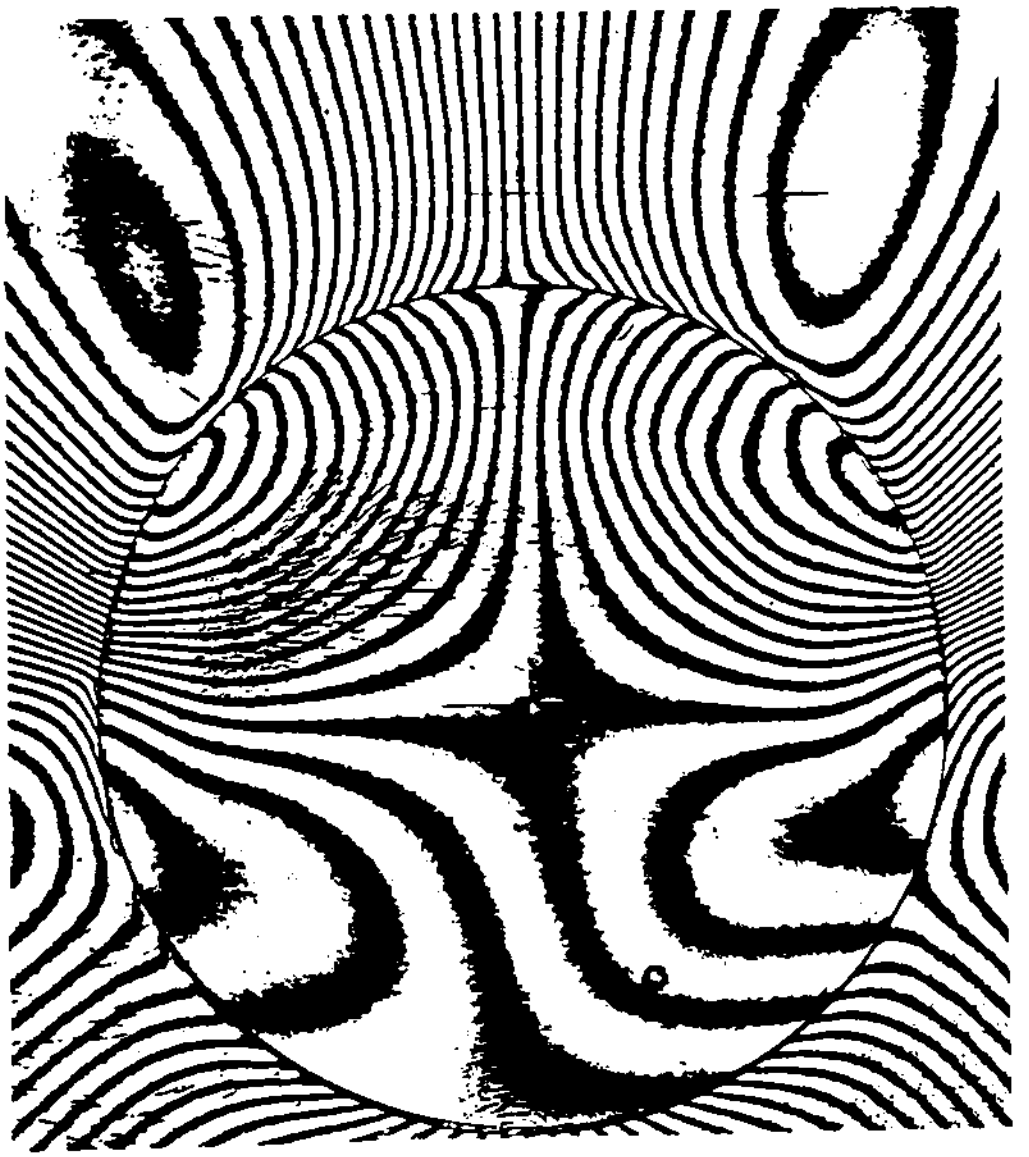

(10) V - 1240 lb

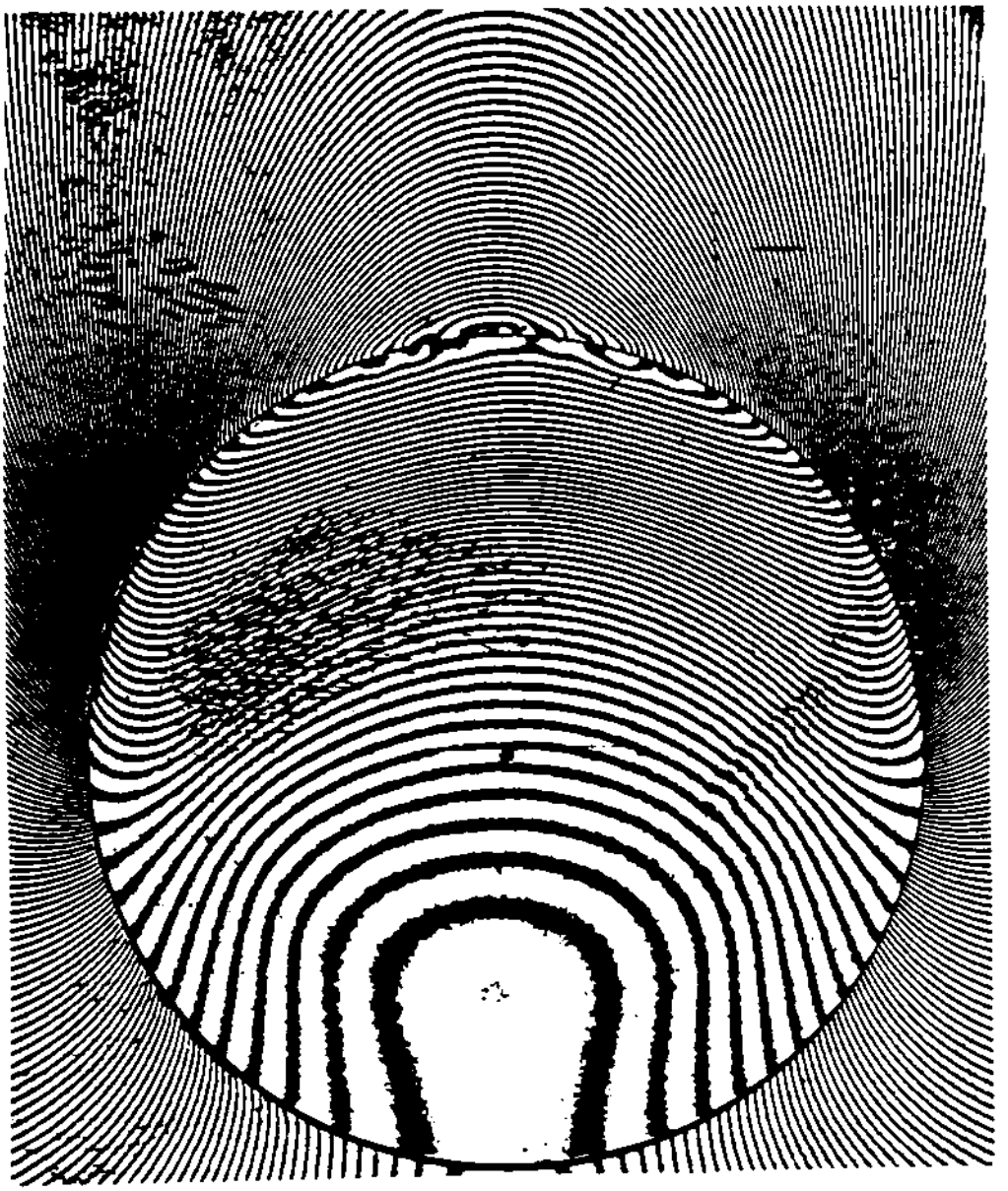

(11) U - 1460 lb

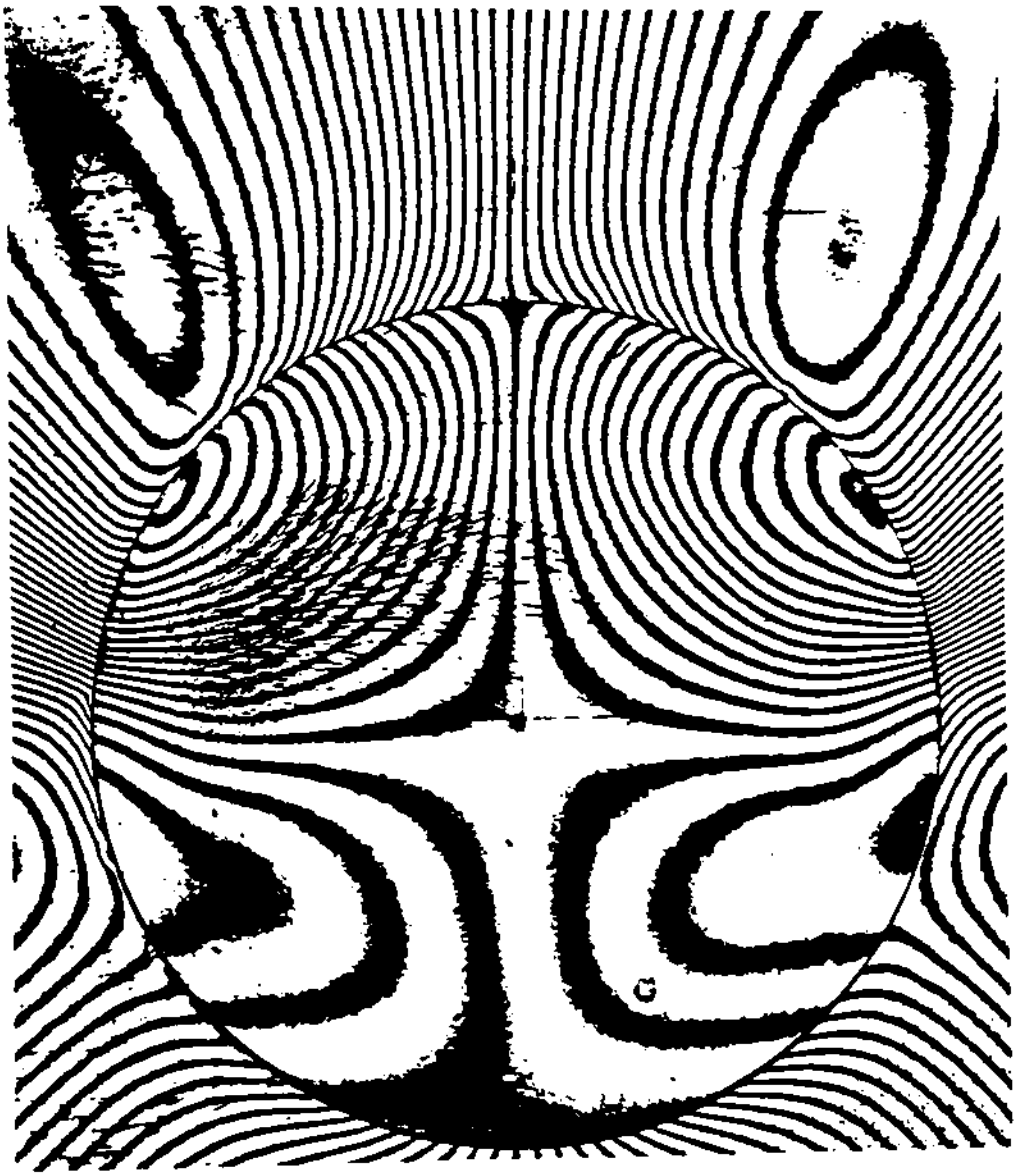

(12) V - 1460 lb

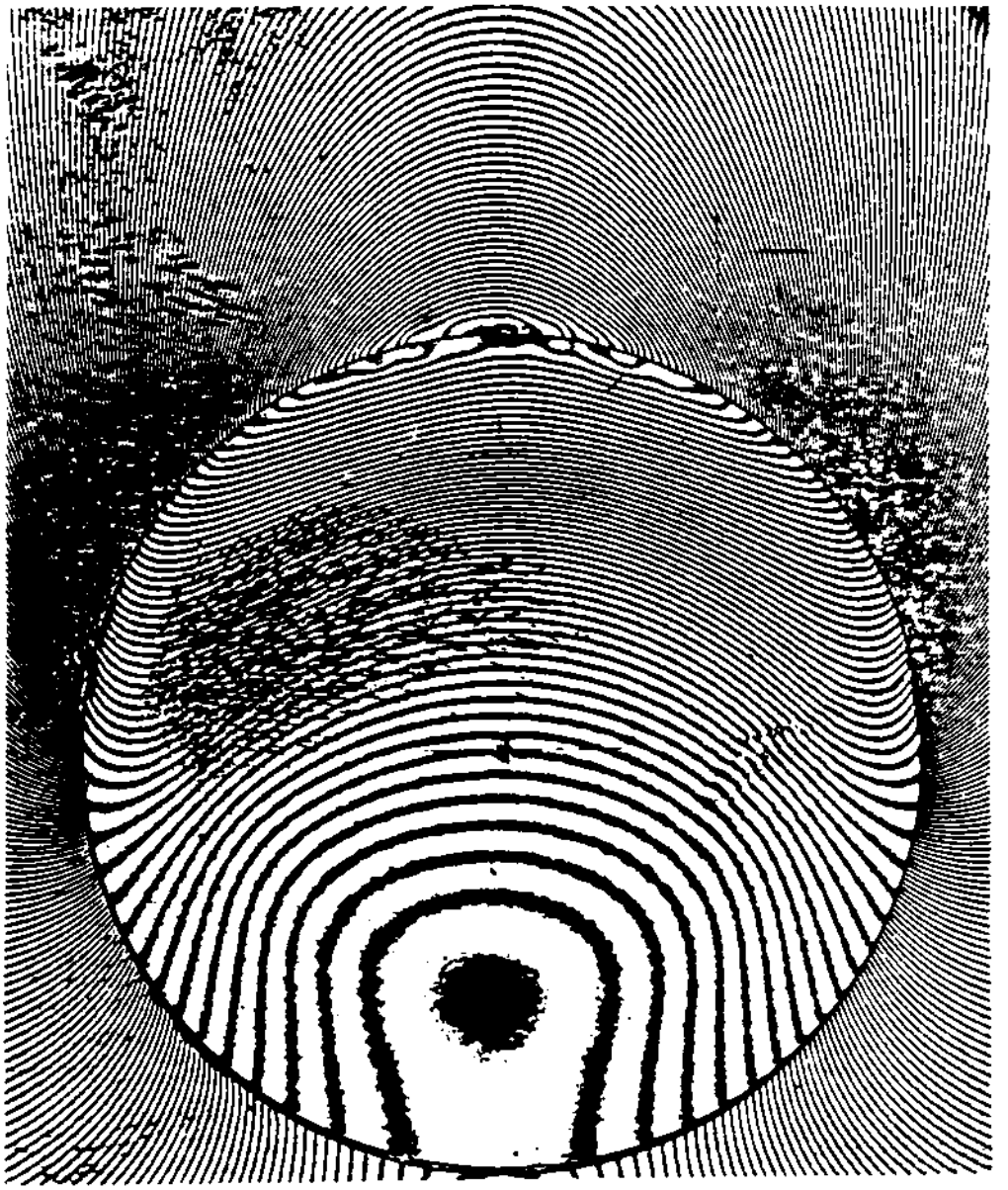

(13) U - 1670 lb

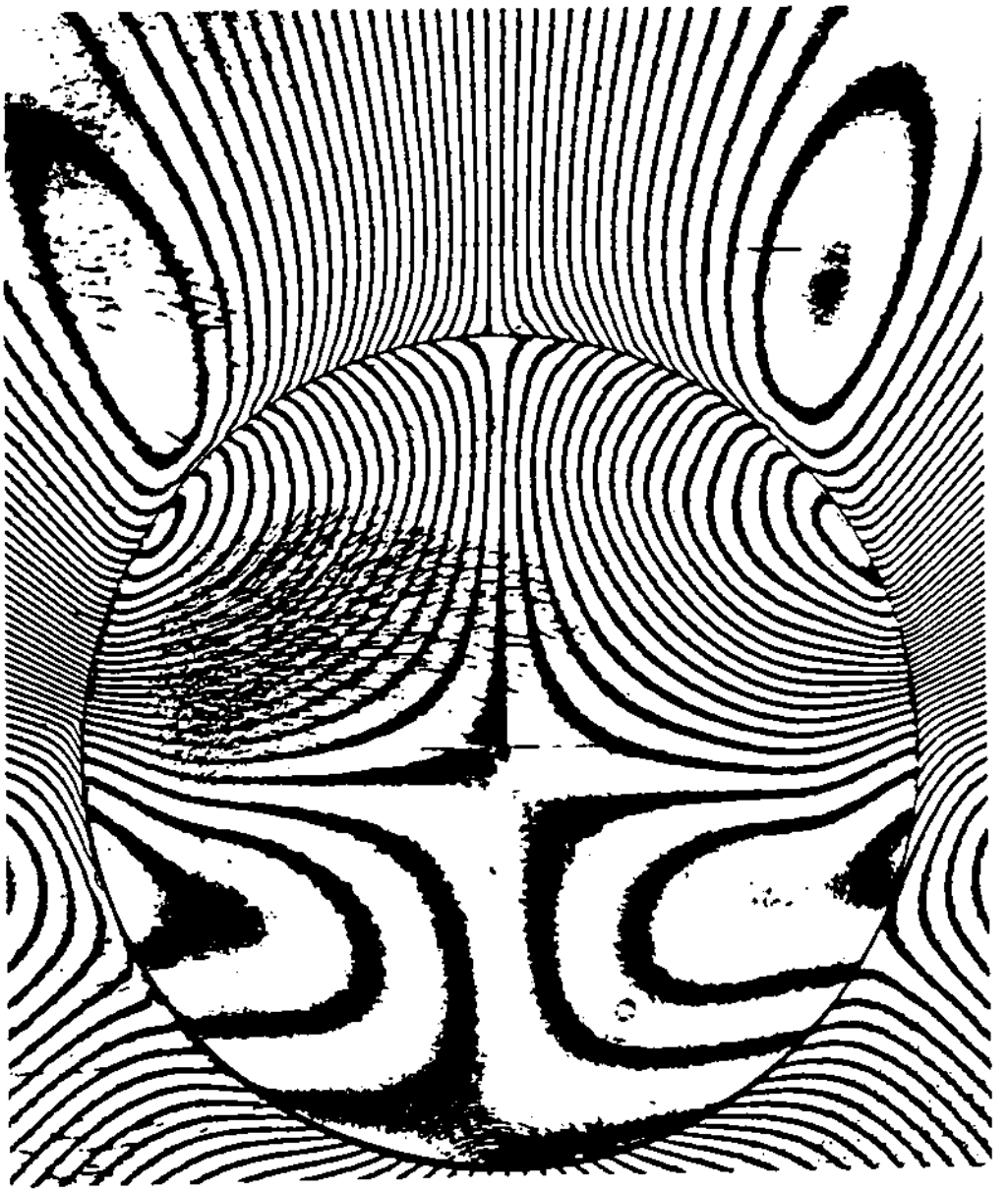

(14) V - 1670 lb

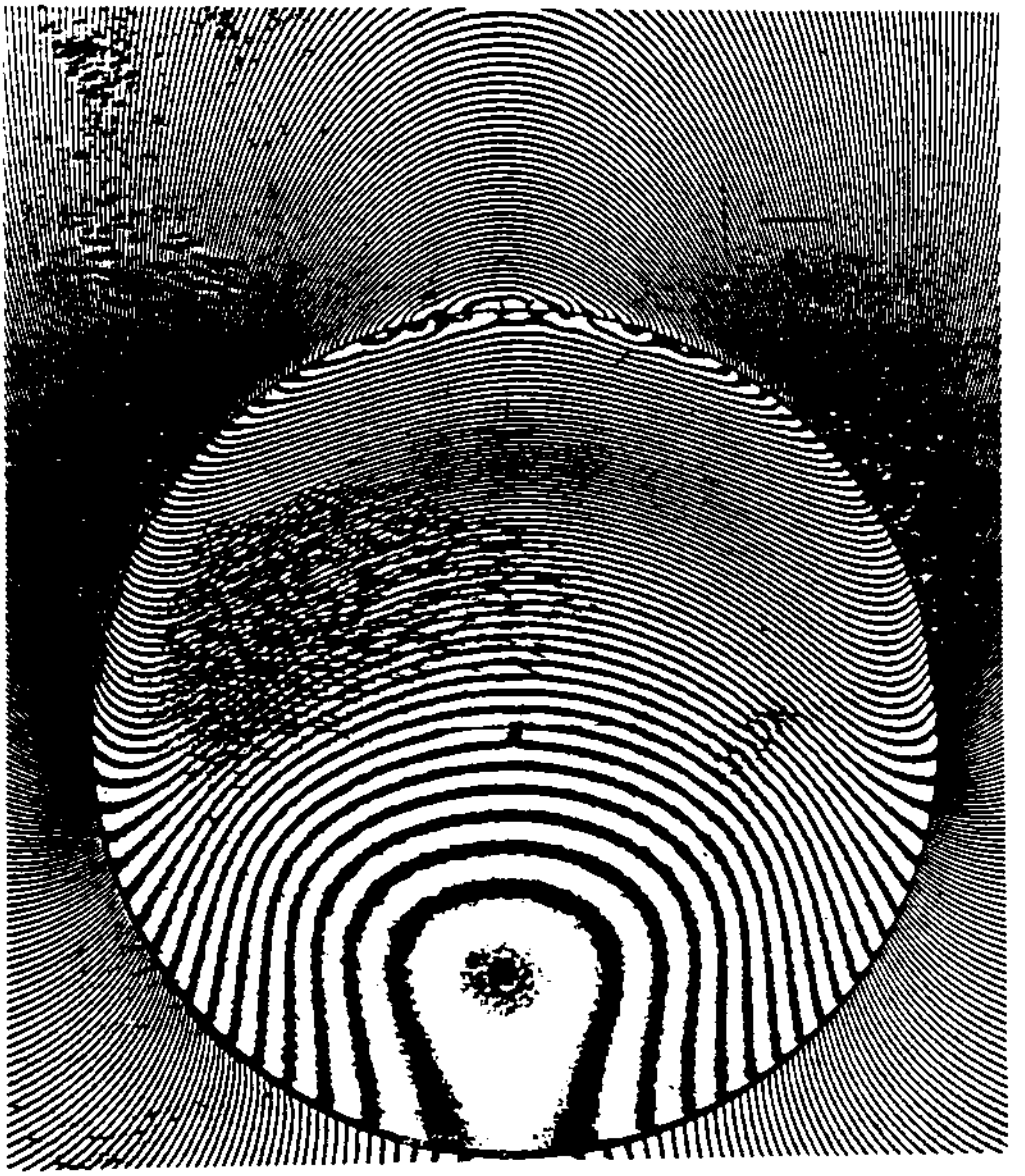

(15) U - 1840 lb

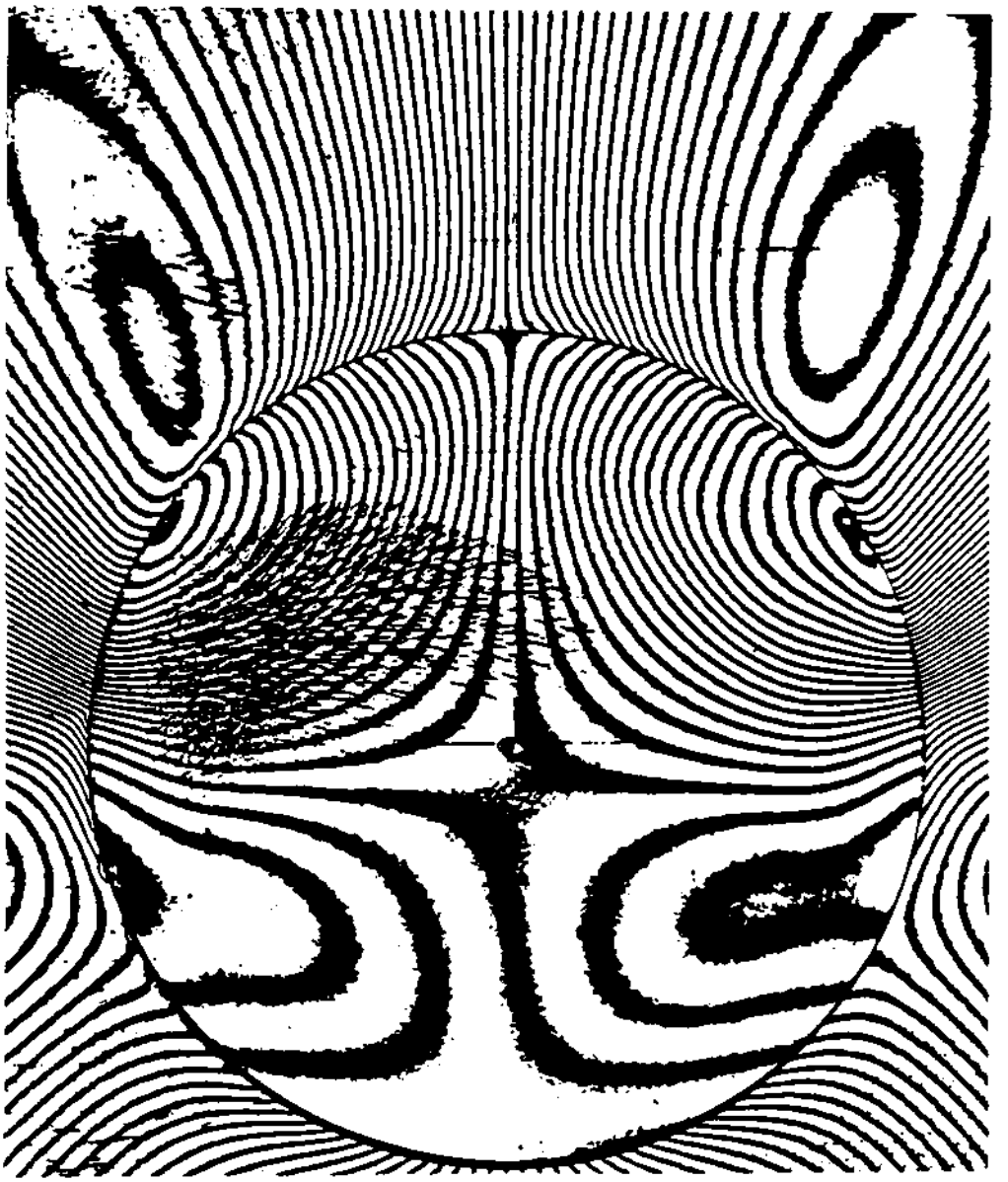

(16) V - 1840 lb

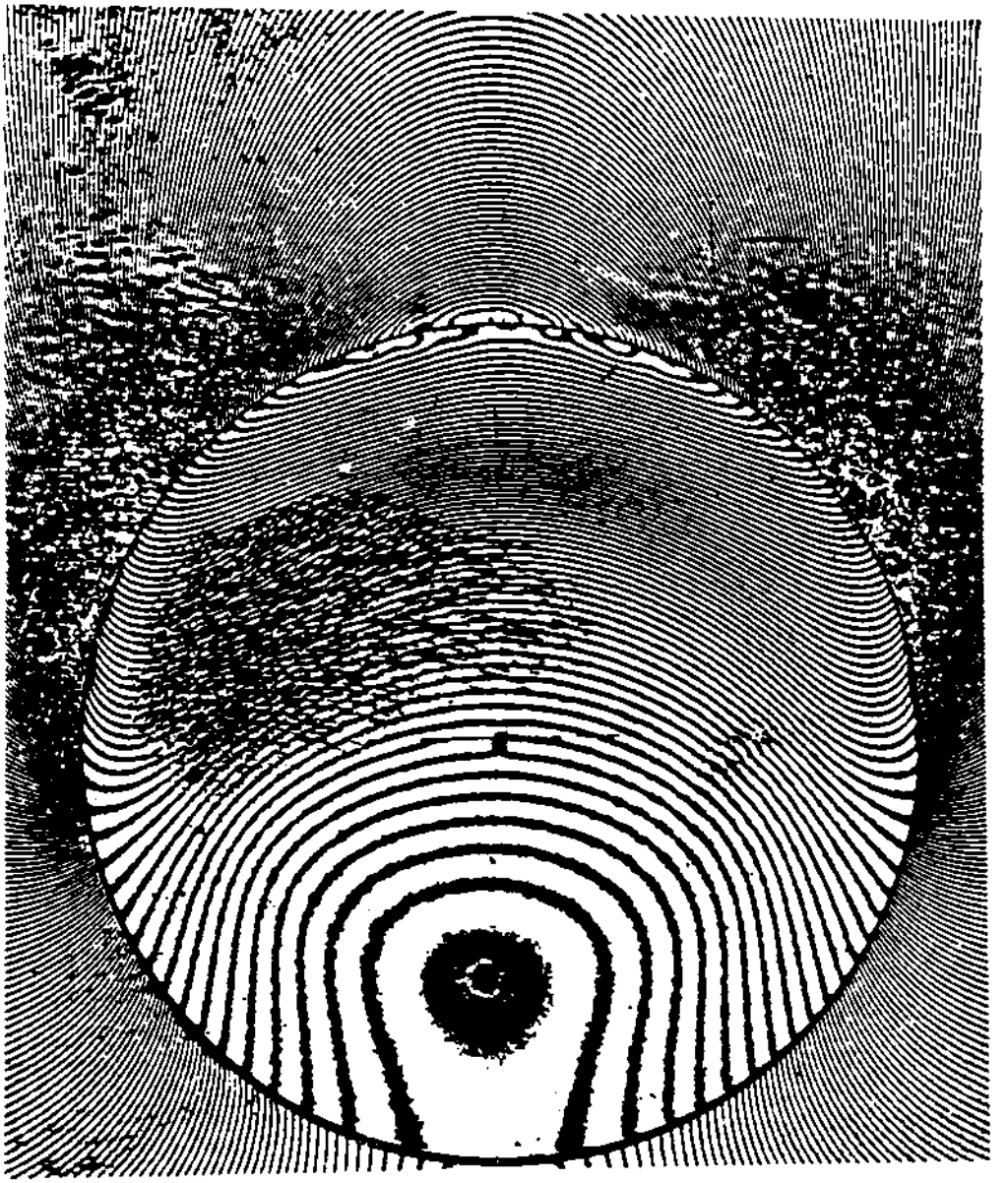

(17) U - 1980 1b

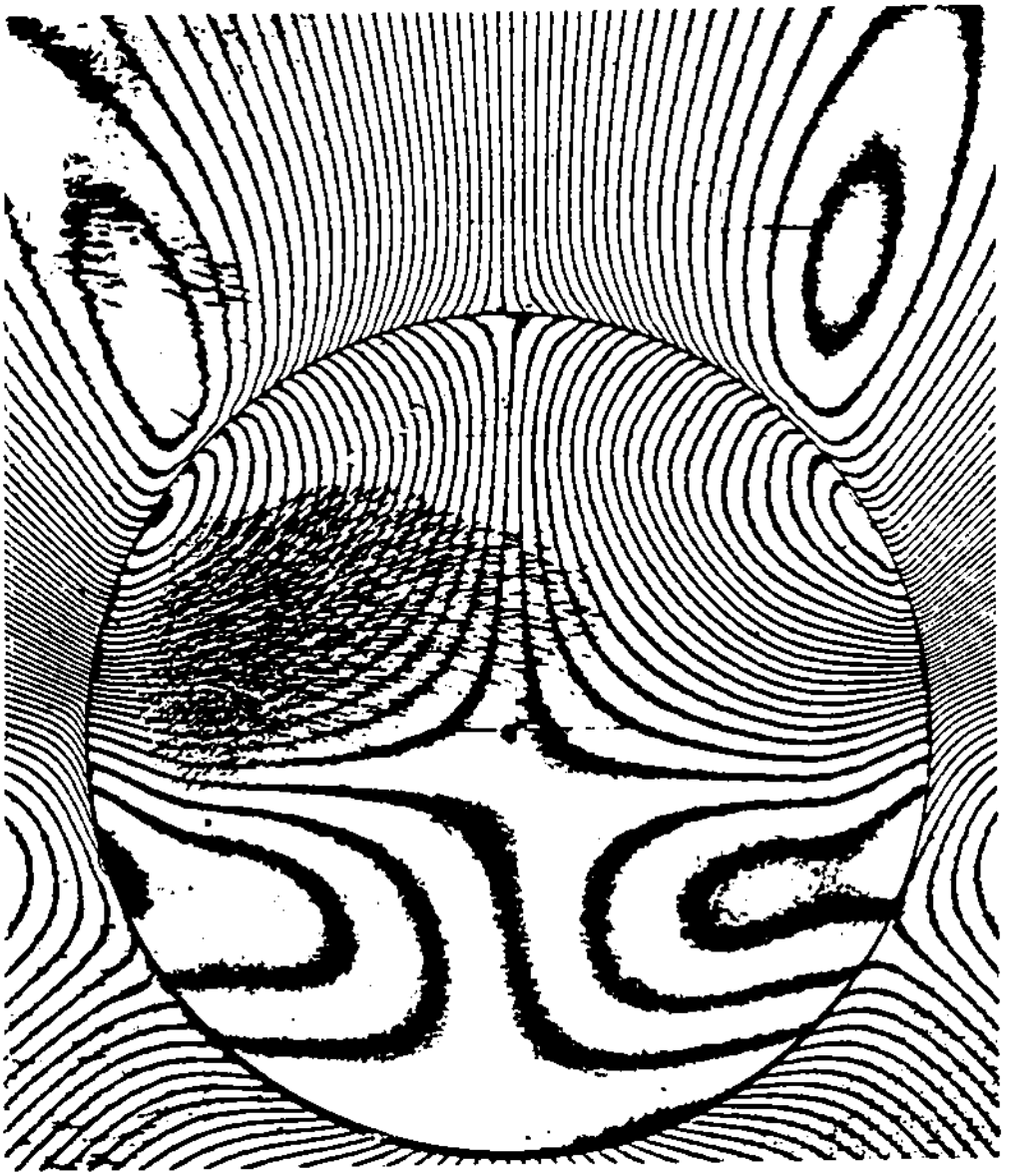

(18) V - 1980 1b

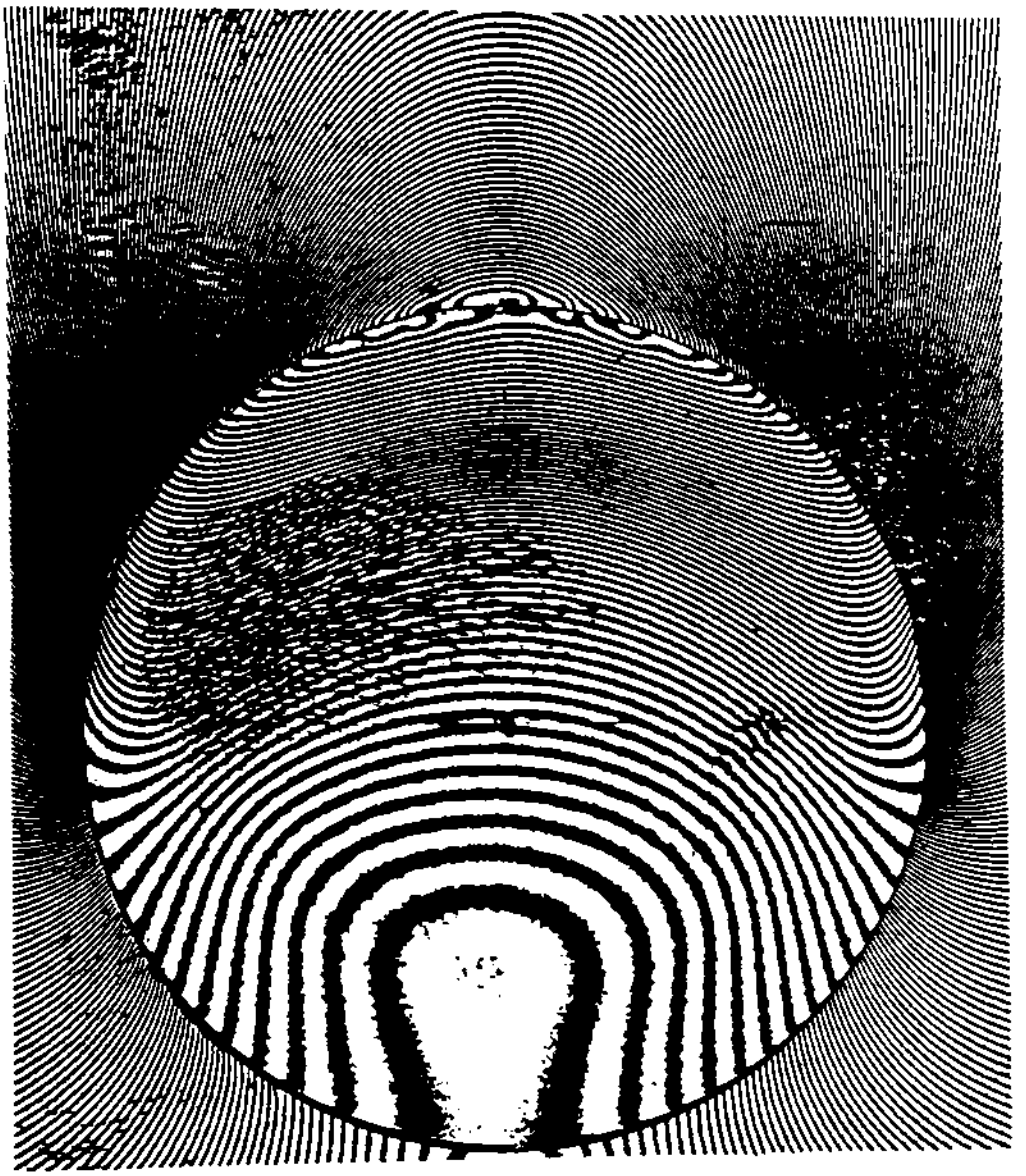

Figure A.2 Fringe patterns at each load level during the load-decreasing phase: (1) U - 1800 lb

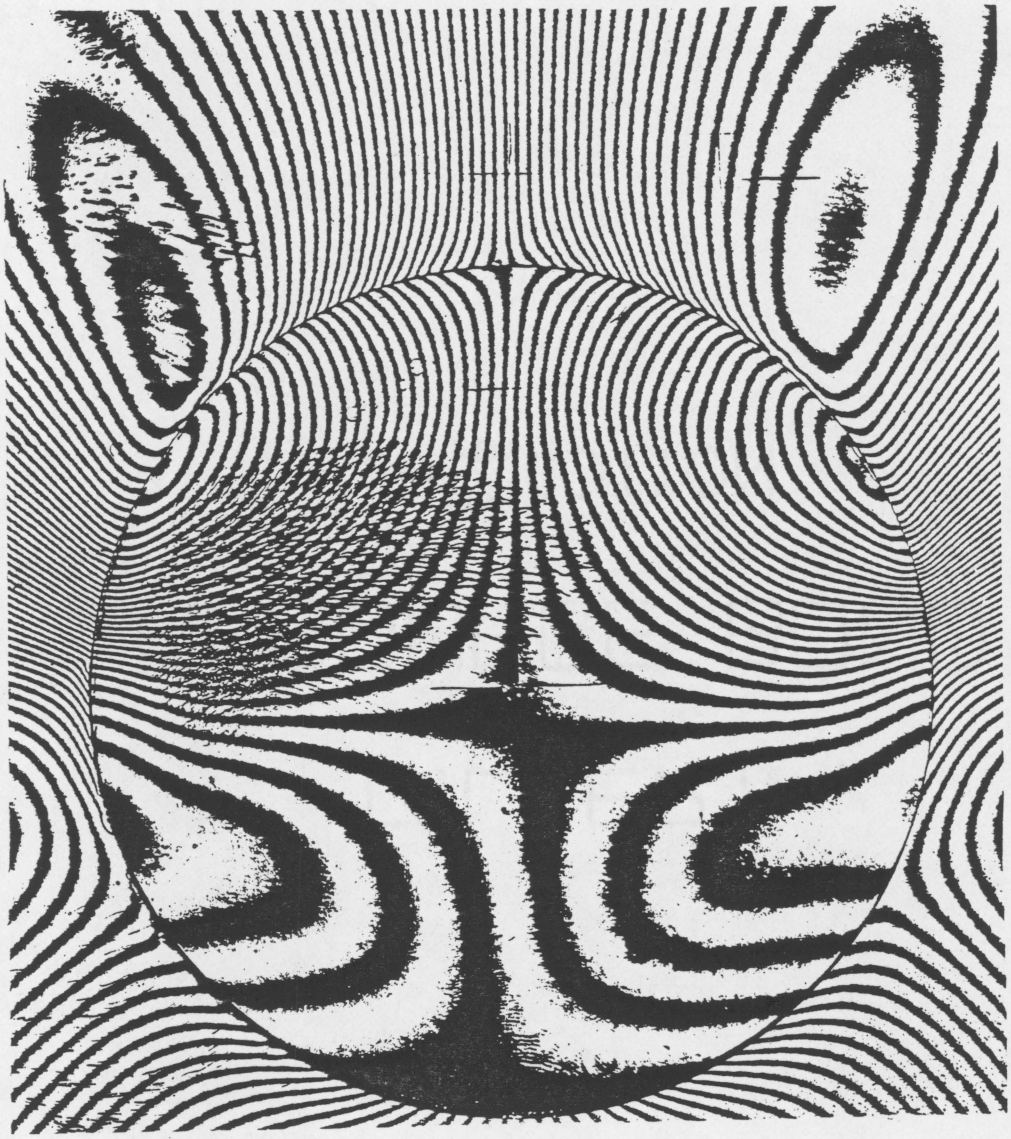

(2) V - 1800 lb

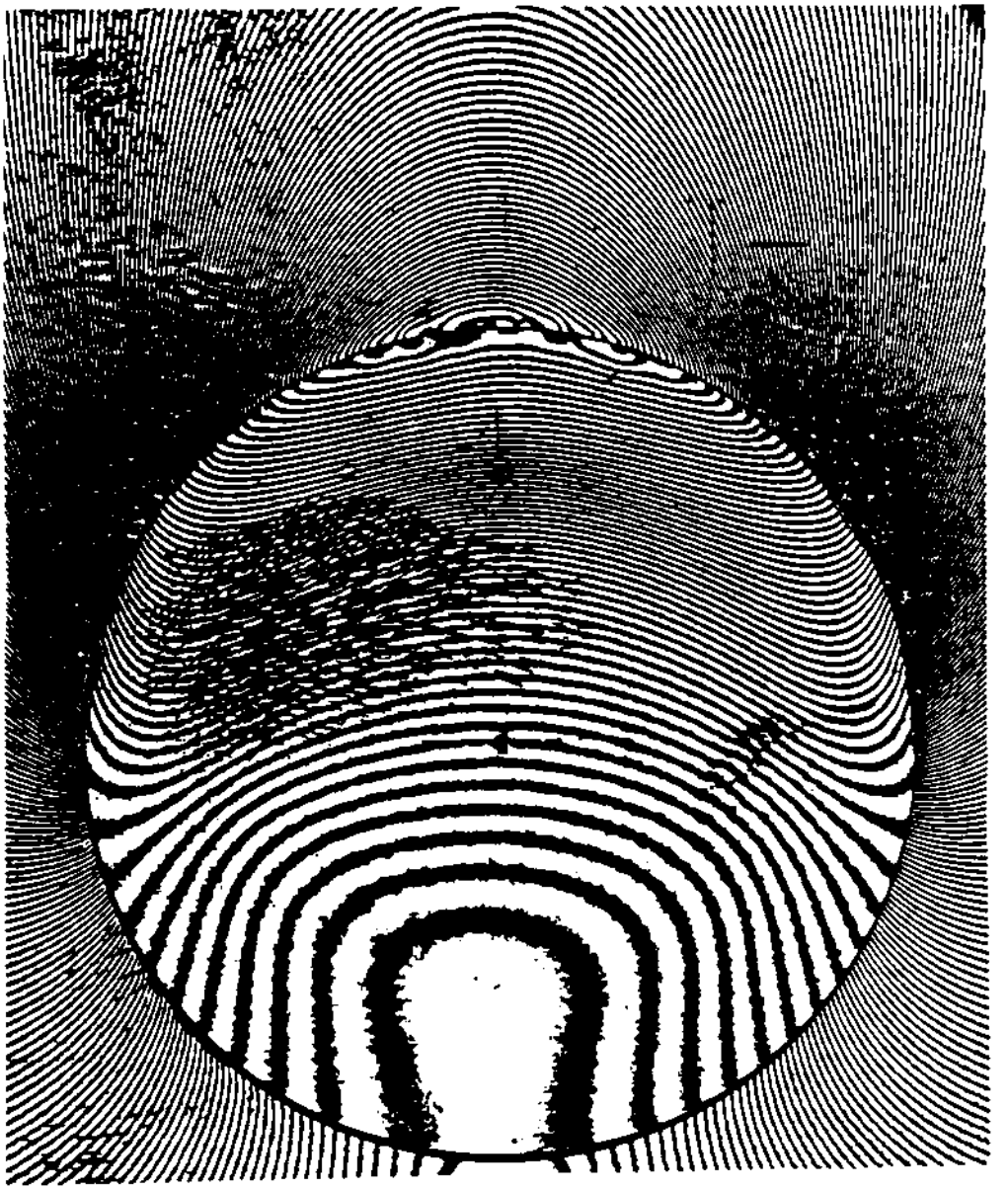

(3) U - 1600 lb

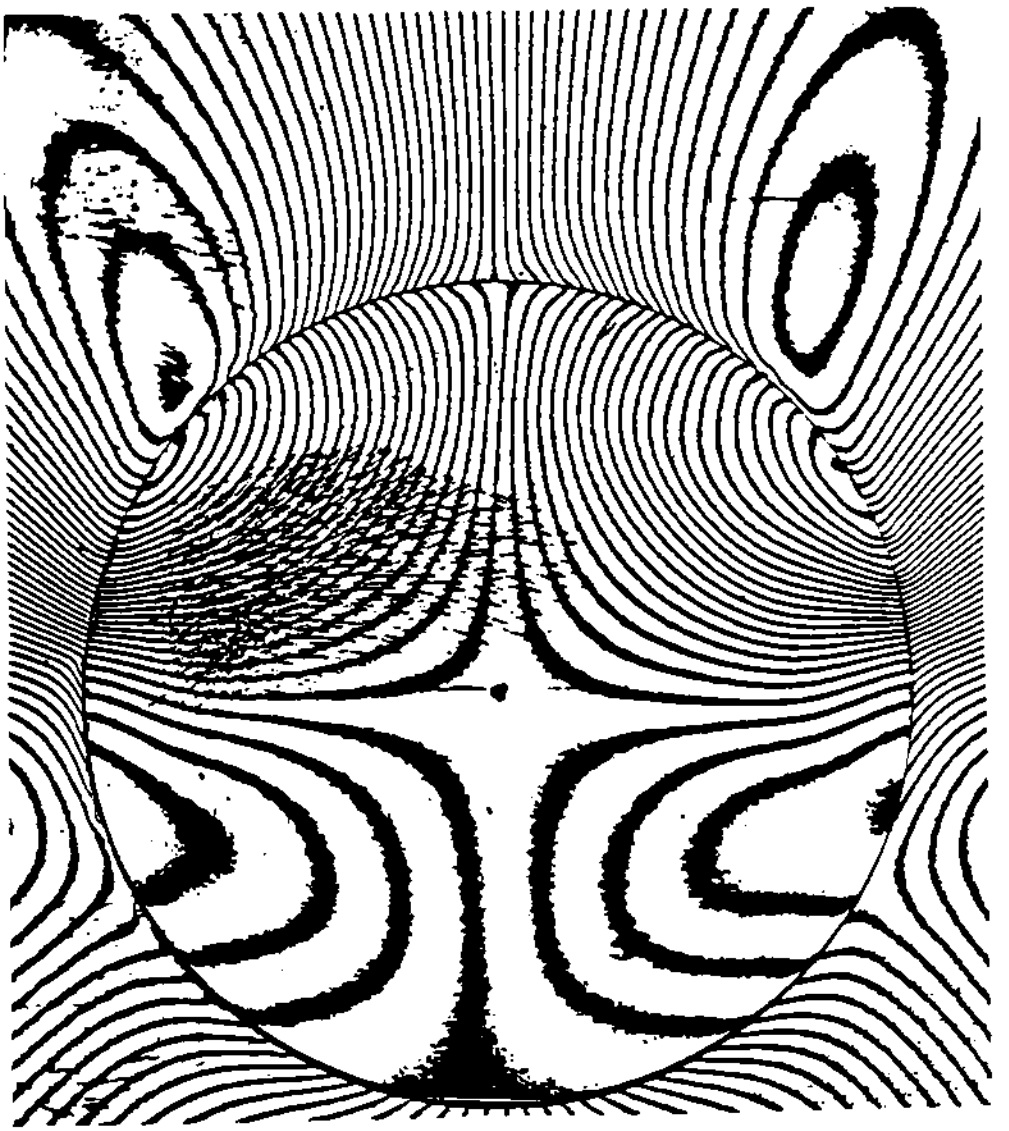

(4) V - 1600 lb

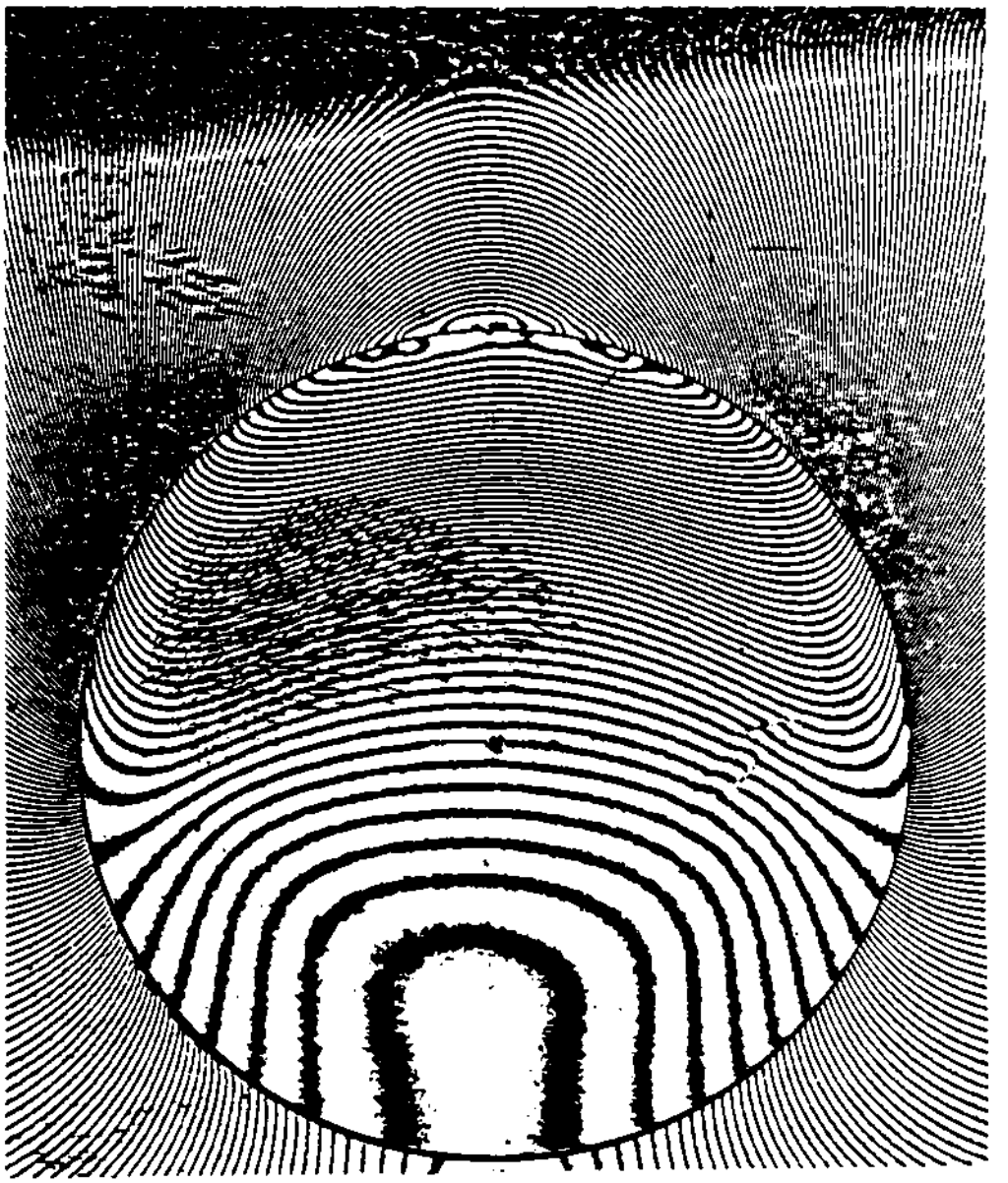

(5) U - 1440 lb

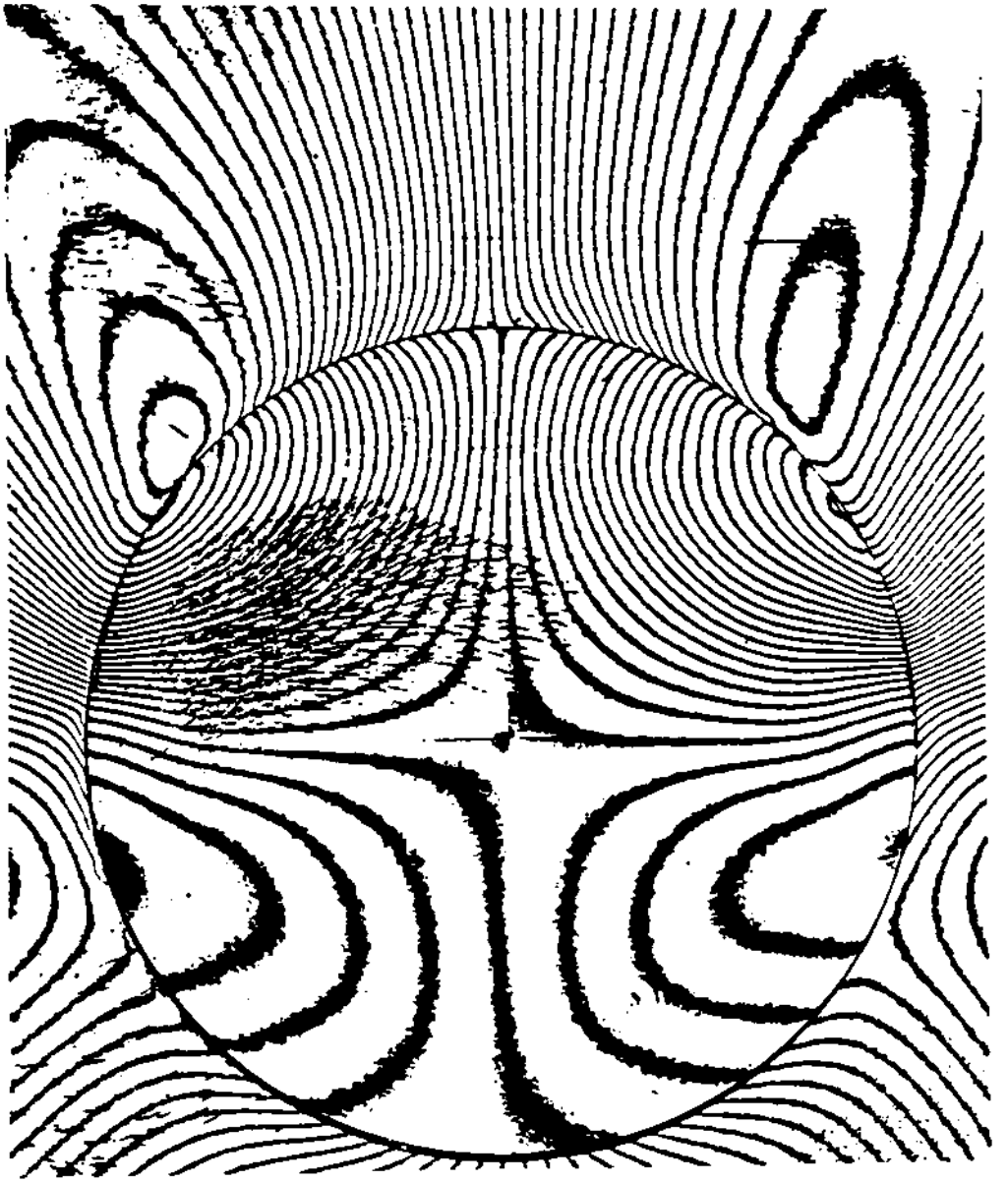

(6) V - 1440 lb

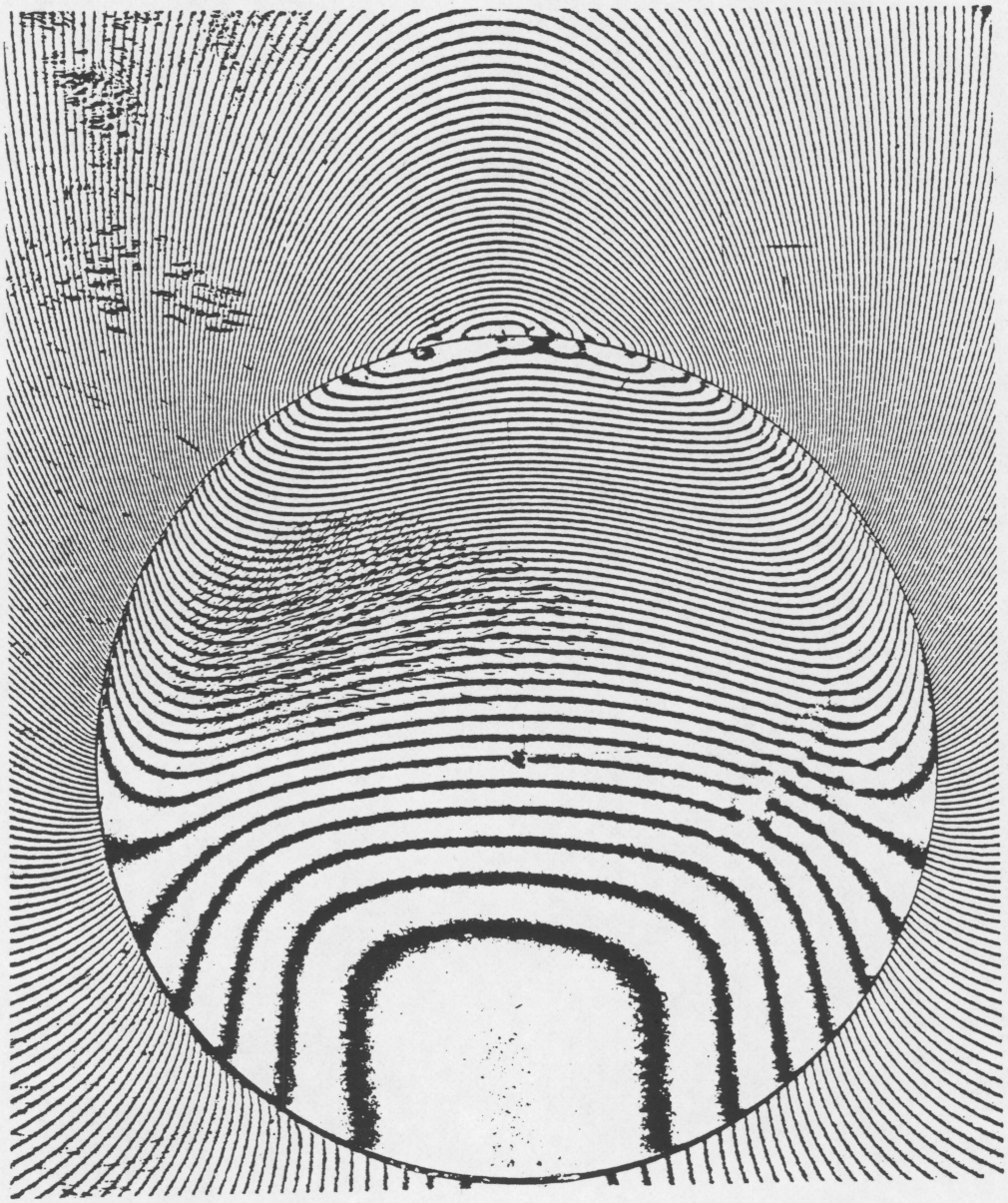

(7) U - 1210 lb

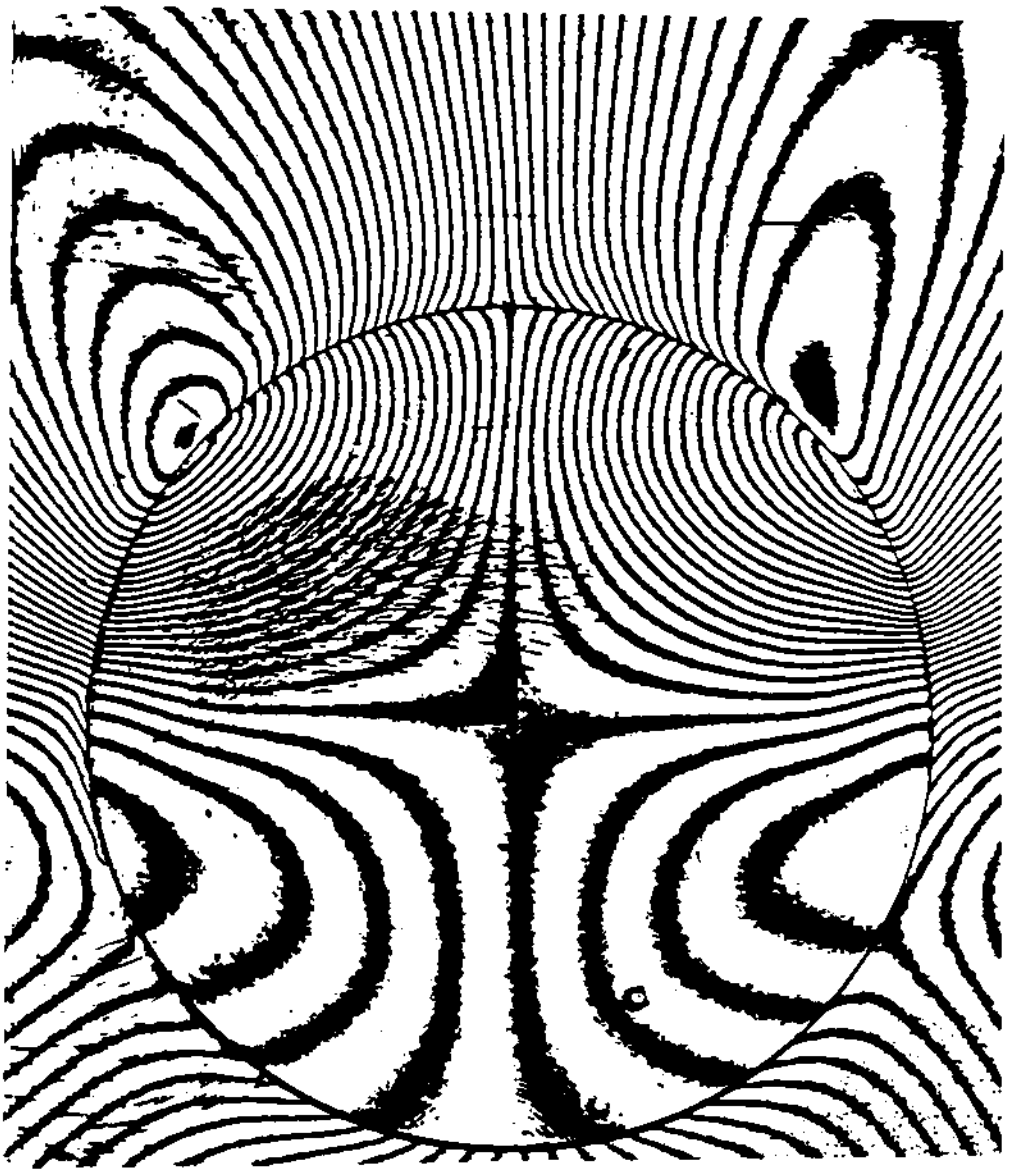

(8) V - 1210 lb

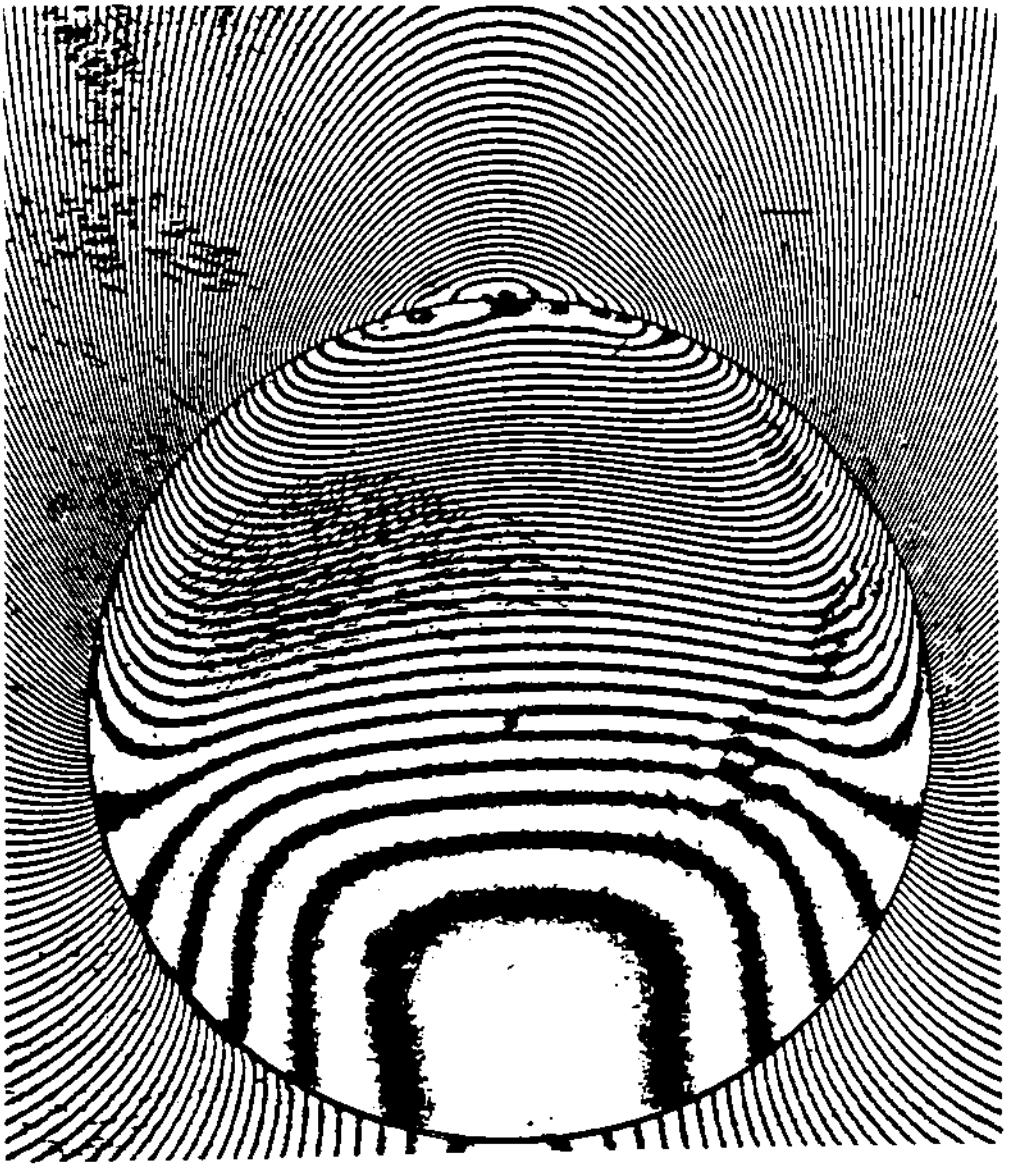

(9) U - 1070 lb

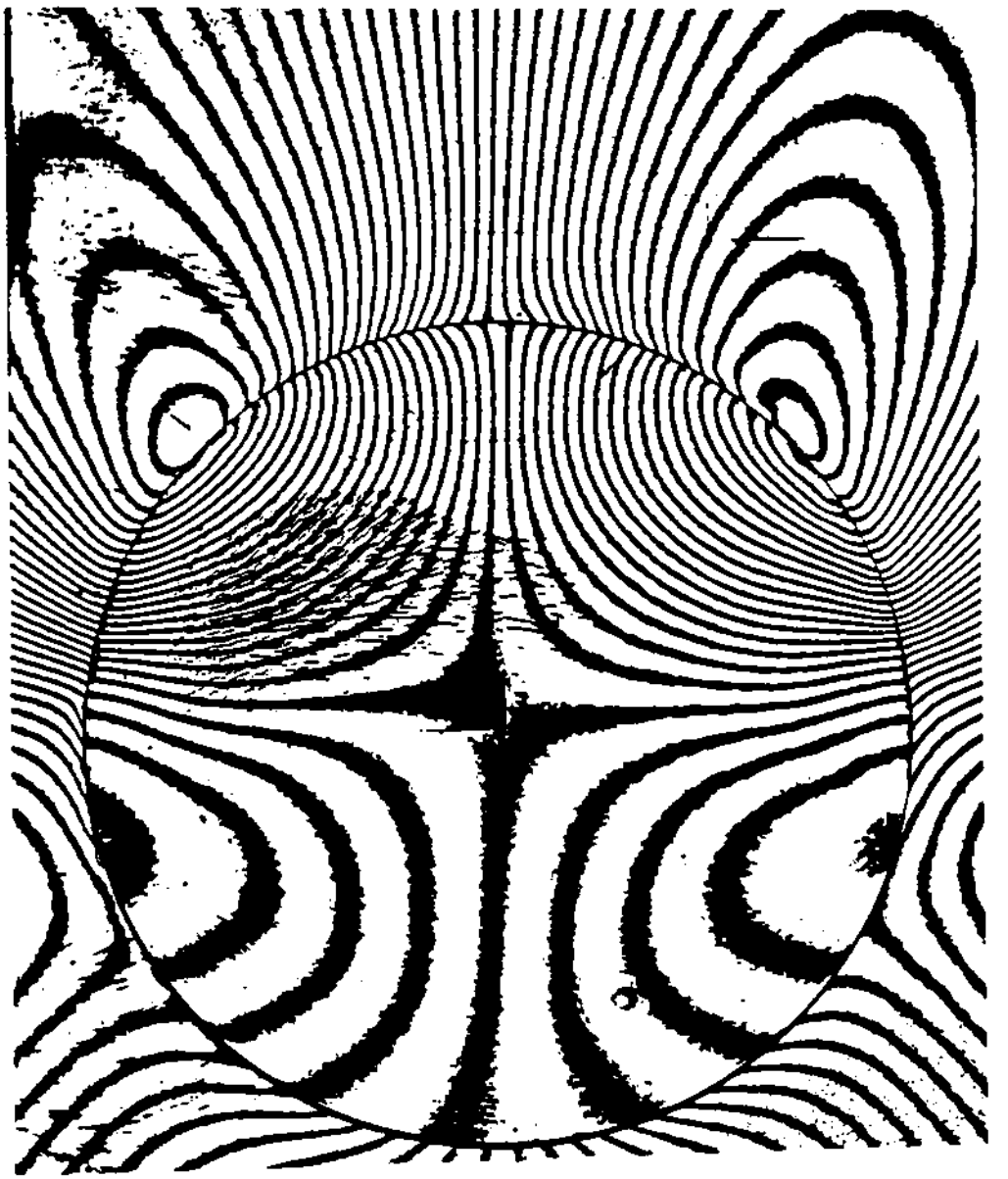

(10) V - 1070 lb

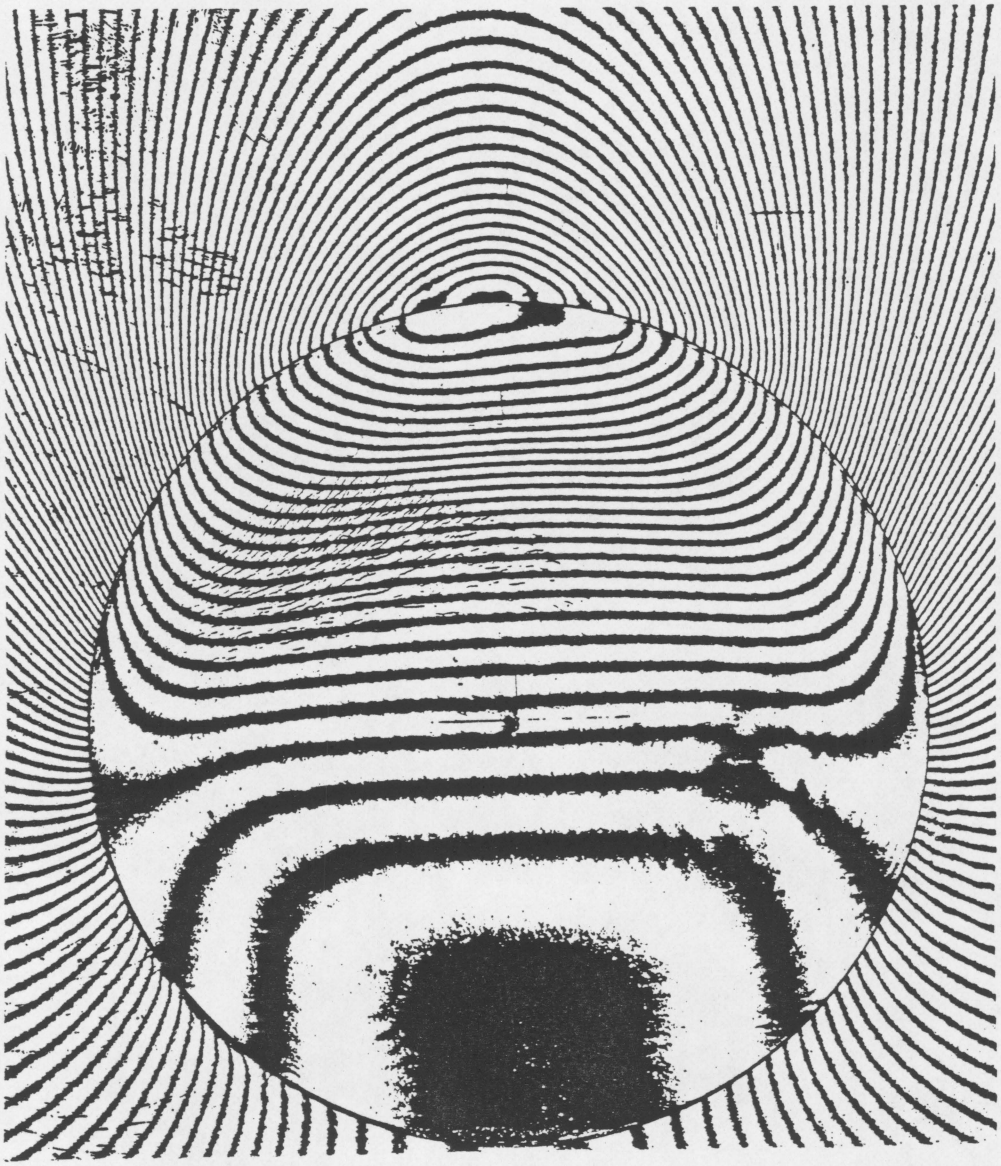

(11) U - 630 lb

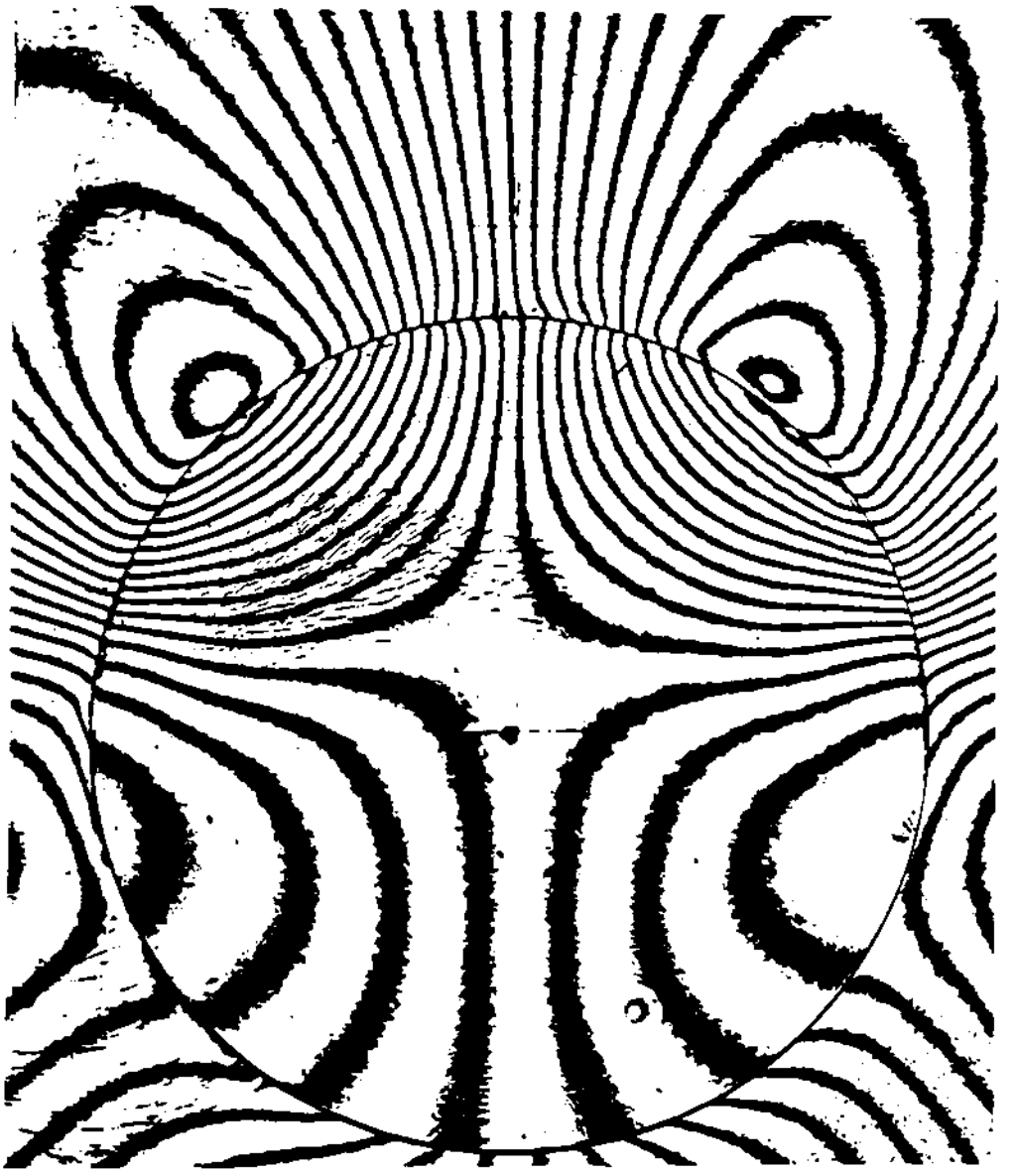

(12) V - 630 lb

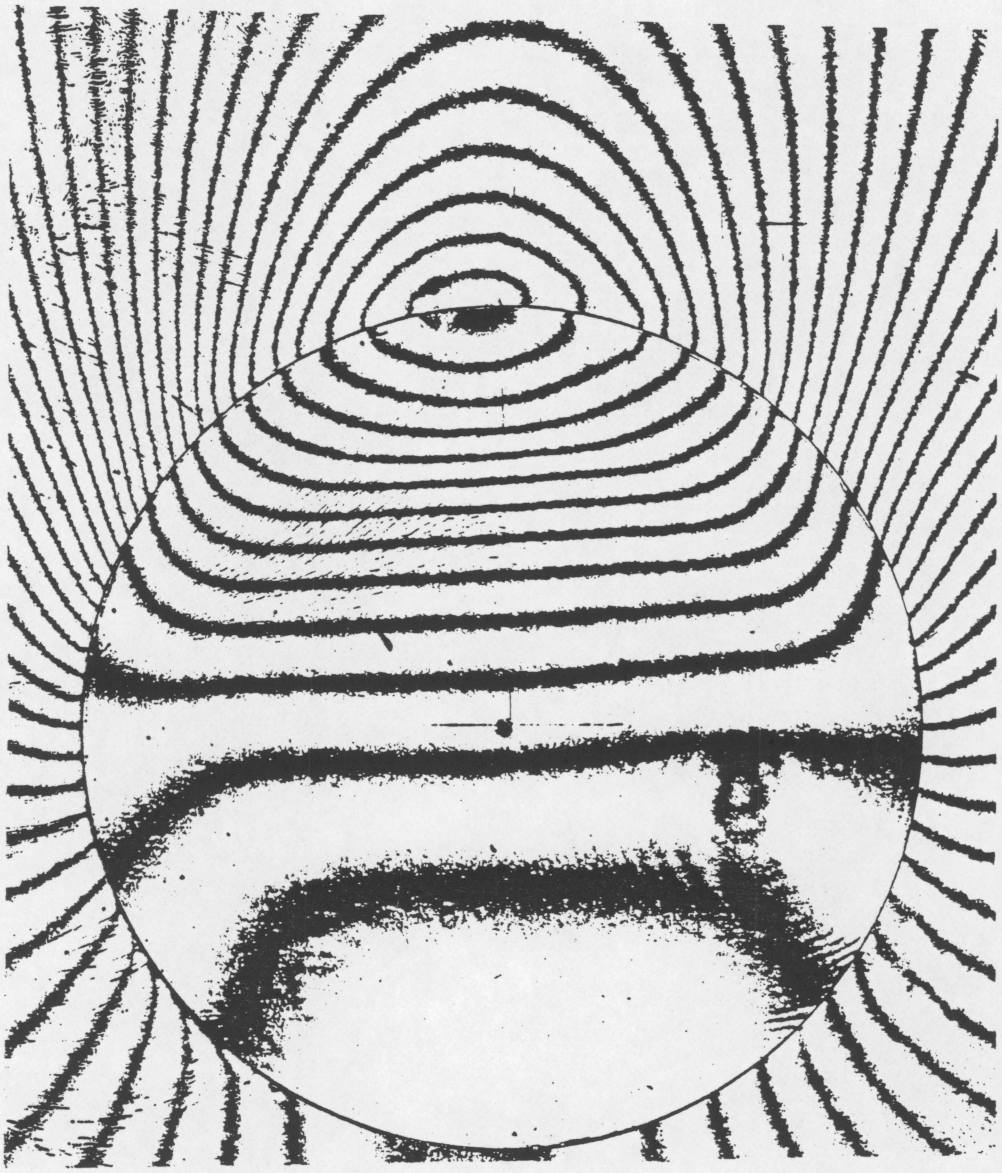

(13) U - 210 1b

(14) V - 210 lb

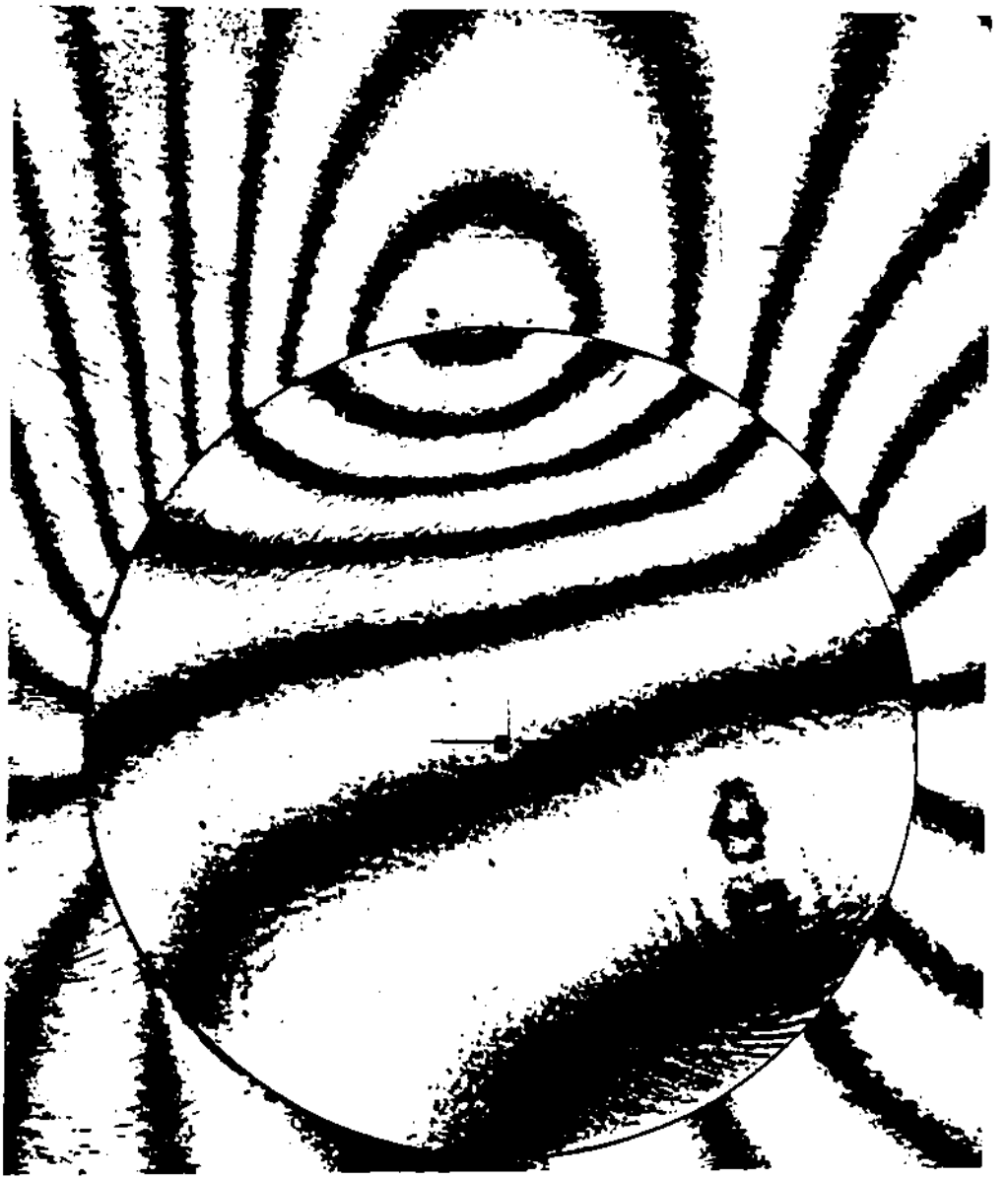

(15) U - 40 lb

(16) V - 40 lb

APPENDIX B

IDENTIFICATION OF SLIP-STICK REGIONS

Representative curves of relative tangential displacements ΔU_θ are shown in Figure B.1 as a function of angle θ. Dashed portions of the curves represent ΔU_θ in the non-contact region, which has no meaning with regard to the slip-stick phenomena under discussion. Points A and B in Figure B.1 are end limits of contact regions at each of the corresponding load levels. The section OA of curve I represents the total ΔU_θ which has occurred from the initial state of zero load whether or not the two bodies have been in contact with each other. That is, in the fringe pattern obtained at this load level, ΔU_θ registered prior to actual contact of the pin and the bore of the hole is included. Therefore, the curves of ΔU_θ in Figure B.1 represent relative tangential dispalcements, including the virtual slip occurred before actual contact of pin and bore of the hole which must be subtracted from the total ΔU_θ to obtain the actual slip. However, the common sections of the curves, OC and OD, definitely correspond to no-slip regions caused by sticking of the contact surfaces. Points C and D lie within the contact region differentiating between the slip and the stick regions at each load level of I and II.

The magnitude of slip, ΔS, is defined as the changes in relative tangential displacements of the two contacting points, which occurred after they came into contact with each other. That is,

$$\Delta S = \Delta U_\theta^{II} - \Delta U_\theta^{I} \qquad (B.1)$$

A,B: Outer limits of contact zones at load levels I and II

C,D: Points between slip and stick regions

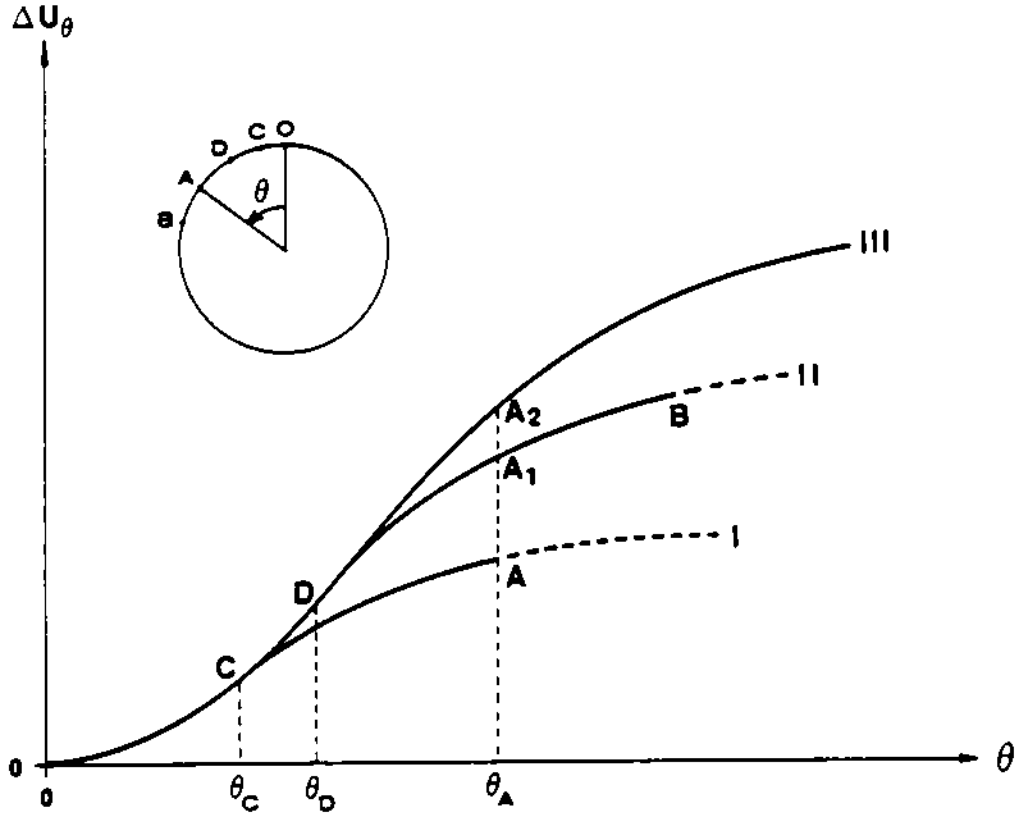

Figure B.1 Graphical scheme to identify slip-stick regions.

while the two surfaces remain in contact.

It is rather complicated to demonstrate the amplitude of slip by a graphical scheme, since slip and stick regions change their sizes and locations according to the loads. To find the magnitude of slip, ΔU_θ curves at different load levels are compared with one another. Point A in Figure B.1 may be taken, for example, which is an end limit of the contact region at load level I. $\Delta U_\theta{}^A$ is interpreted as the relative tangential displacement accumulated by the deformed pin and the plate until the two points at angle θ_A make the first contact. No net slip has occurred at point A so far. An additional increase of load to level II gives rise to the increase of contact region from OA to OB in Figure B.1, while the relative tangential displacement at angle θ_A attains $\Delta U_\theta{}^{A1}$. Then the magnitude of net slip of the points at angle θ_A can be determined to be $(\Delta U_\theta{}^{A1} - \Delta U_\theta{}^{A})$ at the load level II. At other points on the curve section OA, however, net slip cannot be obtained, since ΔU_θ at the state of initial contact is yet to be known for reference. Now, by the increased load of level III, slip is advanced to $(\Delta U_\theta{}^{A2} - \Delta U_\theta{}^{A})$.

A more descriptive graph can be brought forth, as shown in Figure B.2. Figure B.2 illustrates a band of slip amplitudes developed with the phase of load increase in an arbitrary loading cycle. The slip initiation curve consists of the points of ΔU_θ measured at the outer limits of the contact regions which extends with every load increment. The distribution of ΔU_θ registered in the fringe pattern of the maximum load constitutes the slip termination curve in Figure B.2. The slip amplitude at any point within the contact region can be

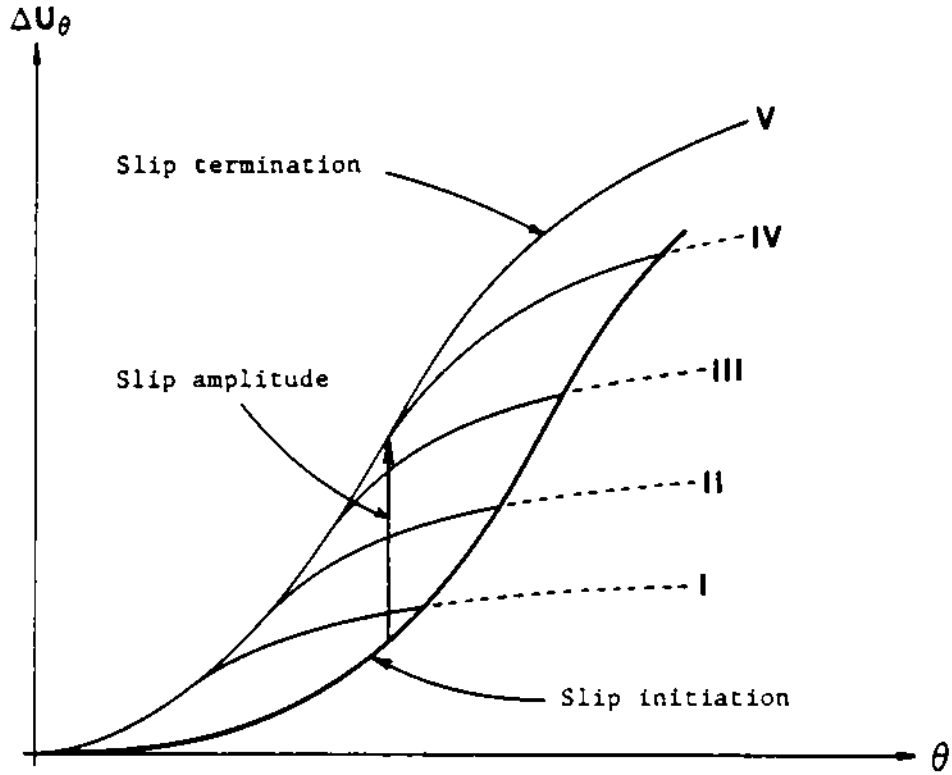

Figure B.2 Graphical scheme to measure the amplitude of slip. Slip-amplitude band is enclosed by two curves, slip initiation curve and slip-termination curve.

determined by the vertical distance between these two curves at the corresponding contact angles of the points. The assessment of load at any point in the slip band can be done by the interpolation of the curves of load levels obtained.

During the load-decreasing phase the curve of the maximum load level becomes the slip initiation curve. In this case the direction of slip is reversed in its sense. Slip will terminate when the two points in contact are separated. Thus the curve formed by the end limits of contact region becomes the slip-termination curve. As shown in Chapter IV the two contact regions of the same load levels for the two phases in loading cycle do not coincide.

The two page vita has been removed from the scanned document. Page 1 of 2

The two page vita has been removed from the scanned document. Page 2 of 2